

# Carnegie Mellon University

CARNEGIE INSTITUTE OF TECHNOLOGY

## THESIS

SUBMITTED IN PARTIAL FULFILLMENT OF THE REQUIREMENTS

FOR THE DEGREE OF Doctor of Philosophy

TITLE Arsenic Dissolution from Sedimentary Formations Under  
Geologic Carbon Dioxide Storage Conditions

PRESENTED BY Hariprasad Parthasarathy

ACCEPTED BY THE DEPARTMENTS OF

Civil and Environmental Engineering

Athanasios Karamalidis December 16, 2014  
CO-ADVISOR, MAJOR PROFESSOR DATE

David A. Dzombak December 16, 2014  
CO-ADVISOR, MAJOR PROFESSOR DATE

David A. Dzombak December 16, 2014  
DEPARTMENT HEAD DATE

APPROVED BY THE COLLEGE COUNCIL

Vijayakumar Bhagavatula December 17, 2014  
DEAN DATE

**Arsenic Dissolution from Sedimentary Formations under Geologic Carbon  
Dioxide Storage Conditions**

Submitted in partial fulfillment of the requirements for  
the degree of

**Doctor of Philosophy**

**in**

**Civil and Environmental Engineering**

Hariprasad Parthasarathy

B.Tech. Industrial Biotechnology, Anna University  
M.S. Civil and Environmental Engineering, Carnegie Mellon University

Carnegie Mellon University  
Pittsburgh, PA

December 2014

## **Acknowledgments**

This work was performed as part of the National Energy Technology Laboratory's Regional University Alliance (NETL-RUA) under the RES contract DE-FE0004000. Additional support for tuition and research was provided by the Carnegie Mellon University (CMU) Dean's Fellowship (2011/12) and the Bertucci Graduate Fellowship (2012/13).

I would like to thank my advisors Dr. Athanasios Karamalidis and Dr. David Dzombak for their constant support and encouragement through the course of my graduate studies at CMU. I have had the liberty of dropping by their offices for brainstorming sessions or to clear questions that I've had. From them I've learnt the importance of being organized, committed, and professional in research, teaching, and professional service. I hope to carry forward these lessons for the rest of my career. I would also like to thank my committee members- Dr. Gregory Lowry and Dr. Alexandra Hakala for their insightful comments, ideas, and suggestions on my work. Despite their busy schedules, they've always made time to meet and discuss my work, which has been of enormous help in designing and conducting experiments.

A part of the work presented in this thesis was conducted in collaboration with scientists at NETL. I would like to thank Dr. John P. Baltrus for conducting XPS analysis (Chapter 4), Dr. Sittichai Natesakhawat for performing B.E.T analysis, and Dr. Christina Lopano and Dr. Mengling Stuckman for the XANES and XRD analyses performed for Chapter 7. I would also like to thank Dr. Andy Wall for his help with ICP-OES analysis when I started my Ph.D.

I am extremely grateful to my colleagues at CMU for their help during various stages of my Ph.D.-Hao Liu for his help with conducting experiments, John Stegmeier for his assistance in XRD analysis of solid samples, and Clint Noack for his patience and willingness to help me with a number of things including statistics, ICP-MS data analysis, and computational modeling. I would also like to thank Aniela Burant and the CCUS-Shale gas group, and Joe Moore and the 207 C-Journal Club, for their encouragement and suggestions. I am also grateful to CEE alumni Dr. Arvind Muralimohan, Dr. Brian Reinsch, Dr. Djuna Gulliver, and Ms. Meghna Nooyi for their support and assistance at various instances.

I would like to express my gratitude to Ron Ripper, Laboratory Manager, Hauck Environmental Engineering Labs at CMU. Ron has been extremely helpful in sourcing parts, reagents, and equipment required for my experiments and has played an integral part in the smooth completion of my Ph.D.

Apart from those mentioned above, I would like to thank Maxine Leffard and the CEE staff. Their hard work and effort has made international students like me, feel right at home at CEE. I will always be grateful for their support.

I have met a lot of interesting people over the past 5 years and have learnt something of value from each of them. I am grateful to all my friends in Pittsburgh, and India who've made this experience special. I am thankful to my friends from high school and college who are now in various parts of the U.S- they have given me sound advice in my professional and personal life.

Finally, I would like to thank my family - my aunt and uncle in Canada, my grand mom, my brother, and my parents, Anitha and Parthasarathy who have made every effort possible to ensure my well being.

Hariprasad Parthasarathy  
Carnegie Mellon University  
Pittsburgh, Pennsylvania  
November 2014

## Abstract

The overall goal of this Ph.D. study was to investigate the mobilization of arsenic (As) from sedimentary formations under conditions representative of geologic carbon dioxide storage (GCS) i.e., high pressure, temperature, and salinity. GCS is a promising technology for the mitigation of increasing CO<sub>2</sub> emissions in the atmosphere. It primarily involves the capture of CO<sub>2</sub> from point sources, followed by transport and injection into deep subsurface formations for long-term storage. Of the potential subsurface formations under consideration in the United States, saline formations, characterized by the presence of high salinity brines, are estimated to have the largest storage capacity. Potential for leakage of injected CO<sub>2</sub>, native brines, and CO<sub>2</sub>-saturated brines from these reservoirs exists and may lead to an increase in mineral dissolution from reservoir formations, and leakage pathways. Of particular interest in the risk assessment of GCS is the dissolution and mobilization of toxic metals such as arsenic (As) and lead.

The primary mineral source of As in high and low permeability sedimentary formations is arsenopyrite (FeAsS (s)). While the oxidative dissolution of FeAsS (s) has been reported in the literature, the dissolution of FeAsS (s) under anoxic, high salinity conditions of GCS remains unexplored.

To conduct dissolution experiments at high pressure, temperature, and salinity, a small-scale plug-flow system capable of measuring dissolution rates without mass transfer limitations was designed and constructed. The capacity of the system in measuring dissolution rates under GCS conditions was validated. The plug-flow system is capable of accurate and rapid measurement of

dissolution rates for minerals with slow and moderate dissolution rates, with a maximum rate limitation of  $5 \times 10^{-5}$  mol/m<sup>2</sup>s at a flow rate of 10 ml/min.

To enable accurate determination of reaction rates, a method for preparation of uniformly sized arsenopyrite particles free of surface oxides was developed. The method involves sonication of crushed minerals with ethanol, washing with 12N HCl, and 50% ethanol, followed by drying in N<sub>2</sub>. Analysis of the arsenopyrite surface with X-ray photoelectron spectroscopy revealed that the method was successful in removing all the oxides of As and S on the surface, while only 12% of Fe was left oxidized.

Subsequently, the dissolution of arsenopyrite, galena, and pyrite in low-concentration alkali and alkaline metal chloride solutions under anoxic conditions was investigated. Further, the effect of Na-Ca-Cl brines on the release of arsenic was determined under ambient as well as GCS conditions. The result of these experiments revealed that electrolytes traditionally considered inert, such as NaCl, CaCl<sub>2</sub>, and MgCl<sub>2</sub> are capable of effecting sulfide mineral dissolution. In particular, the dissolution of As increased with increasing cation activity, and the dissolution of sulfur decreased with an increase in chloride ion activity in solution. Dissolution experiments with 1.5M Na-Ca-Cl brines resulted in arsenic dissolution rates in the range of  $10^{-10}$  to  $10^{-11}$  mol/m<sup>2</sup> s under anoxic conditions. The rate of As release was found to be dependent on the CaCl<sub>2</sub> content of these Na-Ca-Cl brines. Upon the introduction of CO<sub>2</sub> into the system, the dissolution rate of As decreased and was determined to be in the range of  $10^{-11}$  to  $10^{-12}$  mol/m<sup>2</sup>s. For comparison, the rate of As release from arsenopyrite under oxic conditions is in the range of X to Y mol/m<sup>2</sup> s.

Finally, dissolution experiments aimed at understanding the release of As from naturally occurring seal rocks of a GCS formation were conducted. A primary seal rock and two secondary seal rocks were obtained from the Cranfield oil field CO<sub>2</sub>- EOR site in Mississippi. The rock samples were characterized by micro Xray adsorption near edge structure analysis, which revealed that multiple sources of As exist in the reservoir seal rocks studied. Dissolution experiments with seal rocks and anoxic brines of 105g/L NaCl resulted in the dissolution of arsenic in concentrations of 70 to 80 ppb at steady state. Dissolution of CO<sub>2</sub> in the brine had no discernible effect on the steady state release concentration of As.

## Table of Contents

Acknowledgements	ii
Abstract	v
Table of Contents	viii
List of Tables	xii
List of Figures	xvi
Chapter 1. Introduction	1
1.1. Introduction	2
1.2. Problem Identification	4
1.3. Research Objectives and Thesis Structure	4
1.4. References	9
Chapter 2. Sources of Arsenic in Sedimentary Geologic Formations	10
2.1. Abstract	11
2.2. Introduction	12
2.2.1. CO <sub>2</sub> Storage	12
2.2.2. Arsenic Release	13
2.3. Approach	15
2.4. Results and Discussion	15
2.4.1. Arsenic parent mineral	15
2.4.2. Concentration of As in sedimentary formations	16
2.5. Summary and Conclusions	18
2.6. References	19
Chapter 3. A Small-Scale Flow-Through Column System to Determine the Rates of Mineral Dissolution at High Temperature and Pressure	20
3.1. Abstract	21
3.2. Introduction	22
3.3. Materials and Methods	25
3.3.1. Mineral preparation	26
3.3.2. Experimental apparatus	26
3.3.3. Cleaning the system prior to experiments, and setup	29
3.3.4. Sampling and analysis	29
3.4. Modeling and Calculations	30
3.4.1. Pressure drop across the column	30

3.4.2. Data interpretation- obtaining dissolution rates from effluent concentrations	31
3.4.3. Managing mass transfer limitations within the column	34
3.5. Results and Discussion	39
3.5.1. Effect of flow rates on dissolution	39
3.5.2. Reproducibility and high pressure experiments	41
3.5.3. Arsenopyrite dissolution mechanism	43
3.5.4. Comparison with observed rates	43
3.5.5. Limitations	45
3.6. Summary and Conclusions	46
3.7. References	47
Chapter 4. A Method for Preparation and Cleaning of Uniformly Sized Arsenopyrite Particles.	50
4.1. Abstract	51
4.2. Introduction	52
4.3. Materials and Methods	54
4.3.1. Mineral preparation and reagents	54
4.3.2. Surface cleaning	55
4.3.3. Particle size distribution	58
4.3.4. XPS	58
4.3.5. SEM-EDS	58
4.4. Results and Discussion	59
4.4.1. Particle size analysis	59
4.4.2. XPS	60
4.4.3. SEM-EDS	64
4.5. Conclusions	67
4.6. References	68
Chapter 5. Alkali and Alkaline Earth Metals as Reactants in Sulfide Mineral Dissolution	69
5.1. Abstract	70
5.2. Introduction	71
5.3. Materials and Methods	72
5.4. Results and Discussion	74
5.5. References	86

Chapter 6. The Effect of Na-Ca-Cl Brines on the Dissolution of Arsenic from Arsenopyrite	88
6.1. Abstract	89
6.2. Introduction	90
6.3. Materials and Methods	92
6.3.1. Mineral preparation and characterization	92
6.3.2. Experimental setup	93
6.3.3. Reagents	94
6.3.4. Dissolution experiments	94
6.3.5. Analysis	96
6.3.6. Data analysis	96
6.4. Results and Discussion	98
6.4.1. The effect of brine composition	98
6.4.2. The effect of CO <sub>2</sub> injection	104
6.4.3. Effect of high temperature and pressure	107
6.4.4. Limitation	110
6.5. References	112
 Chapter 7. Dissolution of Arsenic and Iron from the Lower Tuscaloosa Formation of the Cranfield Field CO <sub>2</sub> Sequestration Site	 114
7.1. Abstract	115
7.2. Introduction	116
7.3. Materials and Methods	118
7.3.1. Sample preparation and characterization	118
7.3.2. Dissolution experiments	119
7.3.3. Micro- Xray- Adsorption Near Edge Structure	121
7.4. Results	122
7.4.1. Material characterization	122
7.4.2. Dissolution experiments	123
7.4.3. Micro XANES analysis and linear combination fitting	127
7.5. Summary	132
7.6. References	133
 Chapter 8. Conclusions and recommendations for future work	 135
8.1. Conclusions	136
8.2. Recommendations for Future Work	140
8.3. References	143
Appendix A. Supporting Information for Chapter 2	144
 Appendix B. Supporting Information for Chapter 3	 162

Appendix C. Supporting Information for Chapter 5	166
Appendix D. Supporting Information for Chapter 6	181
Appendix E. Supporting Information for Chapter 7	192
Appendix F. Data Tables	204

## List of Figures

- Figure 1.1** Schematic of the geologic CO<sub>2</sub> storage process, depicting different storage formations
- Figure 2.1** Schematic representatio of CO<sub>2</sub> release and potential impacts on groundwater
- Figure 2.2** Arsenic parent material in high permeability sedimentary formations
- Figure 2.3** Arsenic parent material in low permeability sedimentary formations
- Figure 2.4** Arsenic concentration ranges in high and low permeability sedimentary formations
- Figure 3.1** Schematic of the flow-through column reactor system for studying mineral dissolution under a range of temperature, pressure and solution conditions
- Figure 3.2** Schematic of a cylindrical flow-through reactor of length L, radius r<sub>c</sub> and volume V. Mass balance across elemental length dX
- Figure 3.3**  $\left(\frac{C}{C_0}\right)$  vs. Damköhler number
- Figure 3.4** Flow pattern around a spherical mineral particle and mass transfer processes
- Figure 3.5** Comparison between  $k_c$  Fe<sup>3+</sup> and  $k_r$ , for different flow rates.
- Figure 3.6** Effect of flowrate on dissolution-(A) Oxidative dissoluton of arsenopyrite with 10<sup>-4</sup> M Fe<sup>3+</sup> at pH 2, T=25 °C, P= 1 bar -Effluent arsenic concentration from arsenopyrite dissolution vs pore Volume. (B) The effect of influent flow rate on overall reaction rate
- Figure 3.7** Arsenic concentration (mmol/L) vs. number of pore volumes. Experiments at 1 bar were conducted in triplicate to show the reproducibility of the system and compared to that conducted at 100 bar to show the pressure effect on arsenopyrite dissolution. Experimental conditions: Flow rate = 0.8 mL/min; Temperature = 293 K; pH = 2; [Fe<sup>3+</sup>] = 0.1 mM.
- Figure 4.1** Schematic of the flow-through column reactor system for studying mineral dissolution under a range of temperature, pressure and solution conditions

**Figure 4.2** Schematic of a cylindrical flow-through reactor of length  $L$ , radius  $r_c$  and volume  $V$ . Mass balance across elemental length  $dX$

**Figure 4.3**  $3 \left( \frac{C}{C_0} \right)$  vs. Damköhler number

**Figure 4.4** Flow pattern around a spherical mineral particle and mass transfer processes

**Figure 5.1** Galena and pyrite dissolution by alkali metal chloride electrolytes. pH 2.55,  $T=25^\circ\text{C}$ ,  $P = 1$  bar: (A) Steady state S concentration ( $\mu\text{M}$ ) from galena vs. anion activity; (B) Steady state Pb concentration ( $\mu\text{M}$ ) from galena vs. anion activity; (C) Steady state S concentration ( $\mu\text{M}$ ) from pyrite vs. anion activity; (D) Steady state Fe concentration ( $\mu\text{M}$ ) from pyrite vs. anion activity

**Figure 5.2** Arsenopyrite dissolution by alkali metal chloride electrolytes. pH 2.55,  $T=25^\circ\text{C}$ ,  $P = 1$  bar: (A) Steady state As concentration ( $\mu\text{M}$ ) vs. cation activity; (B) Steady state Fe concentration ( $\mu\text{M}$ ) vs. cation activity; (C) Steady state S concentration ( $\mu\text{M}$ ) vs. anion activity

**Figure 5.3** Schematic of the dissolution of sulfide minerals under anoxic conditions with alkaline metal chlorides in solution. Three kinds of nucleophilic anions on sulfide minerals are depicted – (A) Monosulfides; (B) Disulfides/Polysulfides; and (C) Sulfur-Arsenic polyanion. The high proton affinity of S anions enables reaction with  $\text{H}^+$ , while the higher nucleophilic reactivity of  $\text{As}^-$  facilitates interaction with electrophilic cations in solution.

**Figure 6.1** The effect of brine composition on the rate of arsenic release from arsenopyrite at  $T=25^\circ\text{C}$ ,  $P= 1$  bar,  $I=1.54\text{M}$ ; (A) As effluent concentration normalized to mineral surface area as a function of time; (B) Rate of As release as a function of %  $\text{CaCl}_2$  (by moles) in the brine solutions.

**Figure 6.2** The effect of chloride activity on release rates of arsenic from arsenopyrite. (A) Chloride ion activity in brines as a function of %  $\text{CaCl}_2$  content. (B) The effect of chloride ion activity on the rates of As release from arsenopyrite by  $\text{CaCl}_2$  containing brines.

- Figure 6.3** The effect of CO<sub>2</sub> dissolution in brines on the rate of arsenic release at T=25°C, 1 bar, I=1.54M. R represents molar ratio of CaCl<sub>2</sub> to NaCl (R<sub>CaCl<sub>2</sub>/NaCl</sub>). (A) As effluent concentration normalized to mineral surface area as a function of time. CO<sub>2</sub> injection at 15h is depicted by a solid line. (B) Average brine pH as a function of time before and after CO<sub>2</sub> injection. (C) As release rate as a function of % CaCl<sub>2</sub> content in brines. Closed markers represent experiments without CO<sub>2</sub>
- Figure 6.4** The effect of chloride ion activity on the dissolution of arsenic from arsenopyrite by brines containing CaCl<sub>2</sub> after CO<sub>2</sub> injection. Closed markers represent dissolution rates in the absence of CO<sub>2</sub>.
- Figure 6.5** The effect of temperature and pressure on arsenic release from arsenopyrite with Na-Ca-Cl brine of R<sub>CaCl<sub>2</sub>/NaCl</sub>=0.11. (A) As effluent concentration normalized to mineral surface area, at 298K, 1 bar and 333K and 100 bars. (B) The effect of temperature on arsenic release rate.
- Figure 7.1** Elemental compositions of primary and secondary seal rocks.
- Figure 7.2** Effluent concentration of (A) Fe, and (B) As, as a function of time. CO<sub>2</sub> injection at 20 hours; T =60 °C; P= 100 bars. Influent = 105 g/L NaCl.
- Figure 7.3** XRD Patterns: sample from 10,193 ft. – Pre (red) and Post (blue) reaction. Inset: Enlarged image of a section of the spectra (yellow box), revealing potential clay precipitation or swelling.  
(Source: Lopano, C. and Stuckman, M.)
- Figure 7.4** Effect of CO<sub>2</sub> injection (closed markers) vs. chemical pH adjustment (open markers) on the effluent concentration of (A) Fe, and (B) As, as a function of time, CO<sub>2</sub> injection at 20 hours; T =60 °C; P= 100 bars. Influent = 105 g/L NaCl.
- Figure 7.5** XANES spectra for (A) 14 As references and (B) all measured micro-spots in different samples. Dash vertical lines from right to left display energies at 11868.8eV, 11871.26eV, 11875eV, representing white line peaks for AsV-FeOxide group, AsIII-FeOxide group and AsIII in Sulfide group, respectively.  
(Source: Lopano, C. and Stuckman, M.)
- Figure B1** Modeled effluent tracer concentration with respect to pore volume

- Figure C1** XRD Spectra for (A) Arsenopyrite, (B) Galena, and (C) Pyrite are shown in red with the standard reference peaks in blue.
- Figure C2** Dissolution of arsenopyrite with 10mM NaCl, CaCl<sub>2</sub>, and MgCl<sub>2</sub> at T= 25°C, P= 1 bar, pH = 2.55: (A) Concentration of Fe (μM) vs. time; (B) Concentration of As (μM) vs. time; (C) Concentration of S (μM) vs. time
- Figure C3** Dissolution of arsenopyrite at equal cation activity.  $\{Na^+\} = \{Ca^{2+}\} = \{Mg^{2+}\} = 0.0051$  at T= 25°C, P= 1 bar, pH = 2.55: (A) Concentration of Fe (μM) vs. time; (B) Concentration of As (μM) vs. time; (C) Concentration of S (μM) vs. time
- Figure C4** Dissolution of galena with 10mM NaCl, CaCl<sub>2</sub>, and MgCl<sub>2</sub> at T= 25°C, P= 1 bar, pH = 2.55: (A) Concentration of Pb (μM) vs. time; (B) Concentration of S (μM) vs. time
- Figure C5** Dissolution of pyrite with 10mM NaCl, CaCl<sub>2</sub>, and MgCl<sub>2</sub> at T= 25°C, P= 1 bar, pH = 2.55: (A) Concentration of Fe (μM) vs. time; (B) Concentration of S (μM) vs. time
- Figure D1** XRD Spectra for Arsenopyrite sample is shown in red with the standard reference peaks in blue.
- Figure D2** System validation (A) Influent and Effluent Temperature over time (B) Pressure stability over time
- Figure D3** Flowrate stability over time. (A) Set flowrate vs measured flowrate; (B) Flowrate vs pressure.
- Figure E1** XANES spectra for (A) 14 As references and (B) all measured micro-spots in different samples. Dash vertical lines from right to left display energies at 11868.8eV, 11871.26eV, 11875eV, representing white line peaks for AsV-FeOxide group, AsIII-FeOxide group and AsIII in Sulfide group, respectively. (Source: Lopano, C. and Stuckman, M.)

## List of Tables

- Table 3.1** Comparison of rate of arsenopyrite dissolution reported in literature
- Table 4.1** Methods for cleaning surface oxides on arsenopyrite particles
- Table 4.2** The effect of drying method on surface oxidation of arsenopyrite
- Table 4.3** Summary of arsenopyrite preparation method
- Table 6.1** Average brine composition data from the U.S. Brine Well database
- Table 6.2** Composition of synthetic brines used in studying dissolution of arsenic from arsenopyrite.
- Table 7.1** List of experiments conducted to investigate Fe and As release from seal rock samples of the lower Tuscaloosa formation.
- Table 7.2** Qualitative XRD results for Mudstone Starting Materials Where Major ~ > 25%; Minor ~ 5-25%, and Trace ~ <5%; ND = not detected.  
(*Source: Lopano, C. and Stuckman, M.*)
- Table 7.3** Sample IDs for  $\mu$ -XANES analysis
- Table 7.4** Relative abundance of As reference groups from LCF analyses of  $\mu$ -XANES spectra of all samples.  $E_0$  shift of all phases were restrained to  $\pm 0.5\text{eV}$ . R factor is defined as  $\frac{\sum [(data-fit)^2]}{\sum (data^2)}$ . (*Source: Lopano, C. and Stuckman, M.*)
- Table A1** Arsenic in High Permeable Sedimentary Formations
- Table A2** Arsenic in Low Permeable Sedimentary Formations
- Table B1** Summary of reactor properties for studying dissolution at high temperature, pressure and salinity
- Table C1** Solid phase characterization of mineral samples for dissolution experiments
- Table C2** List of experiments for each mineral at equal electrolyte concentrations
- Table C3** Equal cation activity experiments for arsenopyrite dissolution

<b>Table C4</b>	Method detection limits for sulfate using ion chromatography
<b>Table D1</b>	Solid phase characterization of arsenopyrite samples for dissolution experiments
<b>Table D2</b>	Complete list of experiments conducted to investigate the effect of brines on arsenic dissolution from arsenopyrite
<b>Table D3</b>	Column Characteristics
<b>Table D4</b>	Ion Specific Calculations of surface saturation assuming hydrated ions
<b>Table D5</b>	Ion Specific Calculations of surface saturation assuming dehydrated ions
<b>Table E1</b>	Absorption edge positions and white-line peaks of reference spectra used in XANES data analysis. Edge position is defined as the maximum in the first-derivative of the energy vs. absorption function. White line position is defined as the maximum in the energy vs. absorption function.
<b>Table F1</b>	Data for Figure 3.6
<b>Table F2</b>	Data for Figure 3.7
<b>Table F3</b>	Data for Figure 4.3
<b>Table F4</b>	Data for Figure 5.1
<b>Table F5</b>	Data for Figure 5.2
<b>Table F6</b>	Data for Figure 6.1
<b>Table F7</b>	Data for Figure 6.3
<b>Table F8</b>	Data for Figure 6.5
<b>Table F9</b>	Data for Figure 7.2
<b>Table F10</b>	Data for Figure 7.4

## **CHAPTER 1**

### **INTRODUCTION, PROBLEM IDENTIFICATION, AND RESEARCH OBJECTIVES**

## 1.1 Introduction

Geologic carbon dioxide storage (GCS) is the most promising mitigation technology for reducing CO<sub>2</sub> emissions into the atmosphere. It involves the capture of CO<sub>2</sub> from point sources (such as coal fired power plants, cement and steel refineries, and electricity generators), transport, and permanent injection of compressed CO<sub>2</sub> into subsurface geologic formations, overlain by competent sealing formations and geologic traps (NETL, 2012).

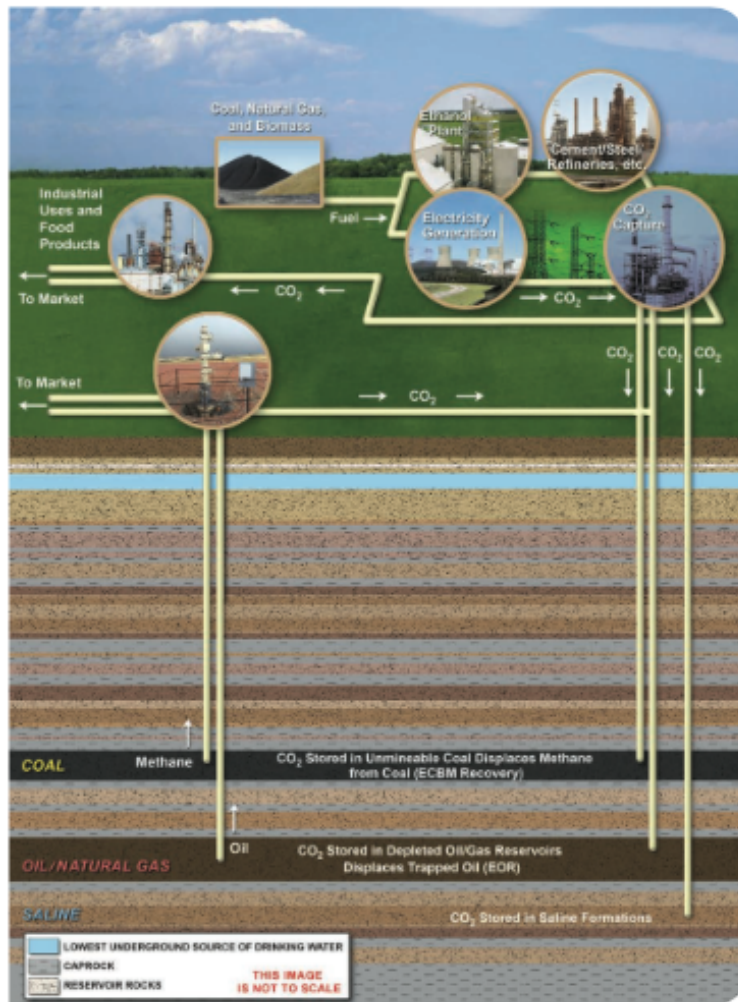


**Figure 1.** Schematic of the geologic CO<sub>2</sub> storage process, depicting different storage formations.

(NETL, 2012)

Geologic formations under consideration for carbon storage (Figure 1.1) include (1) oil and gas reservoirs, (2) unmineable coal, (3) saline formations, (4) organic rich shales, and (5) basalt formations (NETL, 2012).

The physical state, density, and viscosity of CO<sub>2</sub> are dependent on pressure and temperature. At temperatures and pressures higher than the critical point (31.1 °C and 72.9 bars) CO<sub>2</sub> is said to be in a supercritical state (IPCC, 2005). Storage of CO<sub>2</sub> in the supercritical state is advantageous, as it requires substantially lower storage volumes. At depths below 800 m (2600 ft.), natural temperatures and fluid pressures are in excess of the critical point of CO<sub>2</sub>, thus making formations below 800m, ideal for geologic storage (NETL, 2012).

Saline sedimentary formations are widespread and offer much larger storage capacities than oil and natural gas reservoirs (NETL, 2012). While not all saline formations in the United States have been examined, the U.S. Department of Energy (DOE) has documented estimates of storage capacities range from 2,000 to 20,000Gt. of CO<sub>2</sub> (NETL, 2010). Ranges of temperature, pressure and salinity representative of a typical saline reservoir are (NETL, 2003) –temperature: 304-403 K, pressure: 74- 500 bar, and salt concentration (NaCl equivalent): 0-7 molal.

Injected CO<sub>2</sub> is trapped by four main mechanisms- (1) structural trapping where CO<sub>2</sub> is sealed by the presence of impermeable rock layer, (2) residual trapping where it is left behind as droplets in pore spaces of the formations, (3) solubility trapping where CO<sub>2</sub> dissolves into formation water or brines in the case of saline formations, and (4) mineral trapping where over a long time, CO<sub>2</sub> is converted to carbonate rock (IPCC, 2005).

## **1.2 Problem Identification**

One of the concerns of GCS is the dissolution of injected CO<sub>2</sub> in pore water and brines leading to a decrease in pH, which may cause increased mobilization of toxic metals from formation rocks (Xu et al., 2003; 2005; Kharaka et al., 2006; Zheng et al., 2009). Potential leakage of CO<sub>2</sub>, displaced brines, or CO<sub>2</sub> saturated-brines may impact drinking water by causing elevated concentrations of metals including arsenic (As) and lead (Pb), dissolved from formation minerals, or from leakage pathways. Preliminary studies conducted by the U.S DOE on the dissolution of carbonate reservoir rocks under GCS environments showed release of As in concentrations higher than the U.S. Environment Protection Agency's Maximum contaminant levels (Karamalidis et al., 2012).

To predict the impact of geologically stored CO<sub>2</sub> on arsenic concentrations in water, it is important to assess the potential for arsenic release from sedimentary geologic formations under physical and chemical conditions representative of GCS. While the oxidative dissolution of As bearing minerals has been studied in detail (Corkhill and Vaughan, 2009), the dissolution of As under conditions representative of GCS has largely remained unexplored.

## **1.3 Research Objectives and Thesis Structure**

The overall motivation of this dissertation was to understand the mobilization of As from subsurface sedimentary formations under conditions representative of GCS. Investigating As mobility under these conditions will enable the prediction the risks associated with GCS on groundwater quality.

The specific objectives were- (1) to determine the sources of As in sedimentary geologic formations, (2) to design, construct, and validate a small scale system for conducting dissolution experiments at high pressure, temperature, and salinity, (3) to investigate the dissolution of As from arsenopyrite (FeAsS) in saline brines under anoxic conditions, and (4) to study the dissolution of As from natural rock samples, under conditions representative of GCS. These objectives were met through six specific tasks.

### **Objective 1**

*Task 1 (Chapter 2): Determine the sources of arsenic in sedimentary geologic formations*

Potential reservoirs for GCS are characterized by the presence of high permeability formations (reservoir) surrounded by impermeable formations (seal rocks) that prevent the leakage of CO<sub>2</sub>. To identify potential source of As that are of relevance to GCS, formations were segregated based on their permeability as high and low. Most common sources and typical concentrations of As were identified based on their frequency of reporting in the literature.

### **Objective 2**

*Task 2 (Chapter 3): Design, construct, and validate a small-scale, inexpensive reactor system for studying mineral dissolution at high temperature, pressure, and salinity*

In order to study mineral dissolution under GCS conditions, a robust system capable of withstanding high pressure, temperature, and high salinity was required. Existing systems for such studies are expensive as they are made of titanium or Teflon. A small-scale plug flow column system was constructed, designed, and validated for the study of mineral dissolution under GCS conditions, without complications arising from mass transfer limitation.

### **Objective 3**

*Task 3 (Chapter 4): Develop a method for preparation of arsenopyrite to enable accurate determination of dissolution rates*

The results of Task 1 revealed that the most common pure phase mineral source of arsenic in sedimentary geologic formations is arsenopyrite. A review of arsenopyrite dissolution rates under comparable conditions revealed a large variability of reported rates. One possible reason for this variability is the lack of a consistent method for mineral preparation, which would result in variations in mineral surface area and extent of surface oxidation. To enable accurate determination of arsenopyrite dissolution, a standard mineral preparation method was developed that ensures uniformly sized particles that are free of surface oxides. Particle size distribution and X-ray photoelectron spectroscopy were utilized to verify the quality of mineral preparation.

*Task 4 (Chapter 5): Investigate the effect of alkali and alkaline metal chlorides on the dissolution of sulfide minerals*

Saline sedimentary formations are potential reservoirs of GCS, and are characterized by the presence of high salinity brines. These brines may have salinities up to 7m NaCl-equivalent and typically have large concentrations of Na, Ca, and Cl. Typically, alkali and alkaline earth metal chlorides such as NaCl, and CaCl<sub>2</sub> have been used to maintain ionic strength while studying sulfide mineral dissolution by strong oxidants such as dissolved O<sub>2</sub>. Prior to investigating the effect of high salinity brines (electrolyte mixtures), the effect of individual chloride salt solutions on arsenopyrite (and other sulfide minerals) dissolution needs to be understood. The effect of 10mM NaCl, CaCl<sub>2</sub>, and MgCl<sub>2</sub> on the dissolution of pyrite (FeS<sub>2</sub>), galena (PbS), and

arsenopyrite (FeAsS) was determined in this task. Further, a hypothesis that explains observed dissolution trends based on the aqueous chemistry of the salt solutions was developed.

*Task 5 (Chapter 6): Determine the effect of Na-Ca-Cl brines on As release rates from arsenopyrite under anoxic conditions.*

The objective of task 5 was to investigate the potential effects of high salinity binary electrolyte mixtures on arsenic release from arsenopyrite under anoxic conditions. For this purpose, synthetic brines of ionic strength 1.5M, with varying molar ratios of CaCl<sub>2</sub>/NaCl were used as influents to determine the effect of brine composition on arsenic release rates in the presence and absence of CO<sub>2</sub> under anoxic conditions. Further, the effect of high temperature and pressure on the rate of arsenic release was investigated.

#### **Objective 4**

*Task 6 (Chapter 7): Investigate the dissolution of As and Fe from seal rocks of the lower Tuscaloosa formation of the Cranfield Field CO<sub>2</sub> sequestration site*

Tasks 3, 4, and 5 were primarily concerned with the dissolution of arsenic from arsenopyrite. However, actual geologic formations contain multiple sources of arsenic and other secondary minerals and hence, the objective of Task 6 was to understand the dissolution of arsenic from natural samples from an actual GCS reservoir. The Cranfield oil field CO<sub>2</sub>-EOR site in Mississippi is a field test site to analyze the effects of long-term storage of CO<sub>2</sub> in subsurface formations. While field and laboratory dissolution studies on the reservoir rock of the lower Tuscaloosa formation of the Cranfield oil field site have been reported in the literature, the dissolution of seal rock samples has not been explored. The dissolution of As and Fe from

primary and secondary seal rocks of the formation by 105 g/L NaCl brine at 60°C and 100 bars was investigated. Micro- Xray- Adsorption Near Edge Structure ( $\mu$ -XANES) was used to determine the speciation of As on the rock samples before and after dissolution experiments.

Chapter 8 summarizes the key conclusions from each task, as well as overall conclusions of this thesis, with suggestions for future work arising from the findings. Supporting information for each chapter including data tables for all graphs are presented in Appendices A-E

## 1.4 References

Corkhill, C., Vaughan, D.J., 2009. Arsenopyrite oxidation- A review. *Applied Geochemistry* 24, 2342-2361

IPCC (2005) *Carbon dioxide Capture and Storage*. [report]. Intergovernmental Panel on Climate Change (IPCC)- Bert Metz, Ogunlade Davidson, Heleen de Coninck, Manuela Loos and Leo Meyer (Eds.) Cambridge, England: Cambridge University Press, UK.

Karamalidis, A., Torres, S., Hakala, J., Shao, H., Cantrell, K. and Carroll, S. (2013) Trace Metal Source Terms in Carbon Sequestration Environments. *Environmental Science and Technology*, 47 (1), p.322-329.

Kharaka, Y., Cole, D., Hovorka, S., Gunter, W., Knauss, K. and Friefeld, B. 2006. Gas–water–rock interactions in Frio Formation following CO<sub>2</sub> injection: implications for the storage of greenhouse gases in sedimentary basins. *Geology*, 34 pp.577-580.

NETL (2003) *U.S. Brine Wells Database*, DOE/NETL-2003/119 National Energy Technology Laboratory, U.S. Department of Energy. Morgantown, WV

NETL (2010) *Carbon Utilization and Storage Atlas of the United States and Canada, 3rd ed.* National Energy Technology Laboratory, U.S. Department of Energy. Morgantown, WV

NETL (2012) *Carbon Utilization and Storage Atlas of the United States and Canada, 4th ed.* National Energy Technology Laboratory, U.S. Department of Energy. Morgantown, WV

Xu, T., Apps, J. and Pruess, K. 2003. Reactive geochemical transport simulation to study mineral trapping for CO<sub>2</sub> disposal in deep arenaceous formations. *Journal of Geophysical Research*, 108 p.2071.

Xu, T., Apps, J. and Pruess, K. 2005. Mineral sequestration of carbon dioxide in a sandstone-shale system. *Chemical Geology*, 217 pp.295-318.

Zheng, L., Apps, J., Zhang, Y., Xu, T. and Birkholzer, J. 2009. On mobilization of lead and arsenic in groundwater in response to CO<sub>2</sub> leakage from deep geological storage. *Chemical Geology*.

## CHAPTER 2

### **SOURCES OF ARSENIC IN SEDIMENTARY GEOLOGIC FORMATIONS**

The information presented in this chapter was prepared along with Ms. Kazi Tasneem, who was a graduate student in the Department of Civil and Environmental Engineering at CMU (2009/10) and submitted as an internal report.

## **2.1 Abstract**

Geologic carbon dioxide storage in subsurface sedimentary formations may have an impact on groundwater quality. Potential leakage of CO<sub>2</sub>, brines, and brines saturated with CO<sub>2</sub> could lead to the increase in dissolution of trace metals such as arsenic (As). A literature review on the occurrence of arsenic in sedimentary formations was performed to identify the most common sources of arsenic in such formations. Sedimentary formations were classified based on their permeability as high and low and literature reports were perused to identify reported sources. The results of the review revealed that the major sources of arsenic are arsenian pyrite, arsenopyrite (FeAsS (s)), and iron oxy hydroxides (as a secondary source) in both high and low permeable sedimentary formations. Concentration of arsenic in sedimentary rocks was most commonly reported in the range of 0-50 mg/Kg, with some reports of concentrations exceeding 500 mg/Kg.

## **2.2 Introduction**

The mobilization of toxic metals due to potential leakage of CO<sub>2</sub>, and brines from geological storage reservoirs is of interest for risk assessment related to carbon capture and storage. Arsenic occurs commonly in sedimentary formations and is of particular interest due to its toxicity. A literature review was performed to identify the parent materials of arsenic (primary and secondary sources) and their relative abundance in sedimentary geological formations.

### **2.2.1 CO<sub>2</sub> Storage**

Geologic carbon dioxide storage (GCS) has been proposed as a means to mitigate increasing greenhouse gas emissions. In geologic storage, carbon dioxide is captured from large point sources (such as power plants or other industrial sources), transported to the injection site, pressurized and injected into deep geological formations for storage (Newmark et al., 2010). CO<sub>2</sub> injection into deep geological formation may potentially alter the geochemical environment and cause mineral specific metal dissolution, which could result in contamination of groundwater. A schematic showing release of CO<sub>2</sub> from storage and potential impacts on aquifers is given in Figure 2.1.

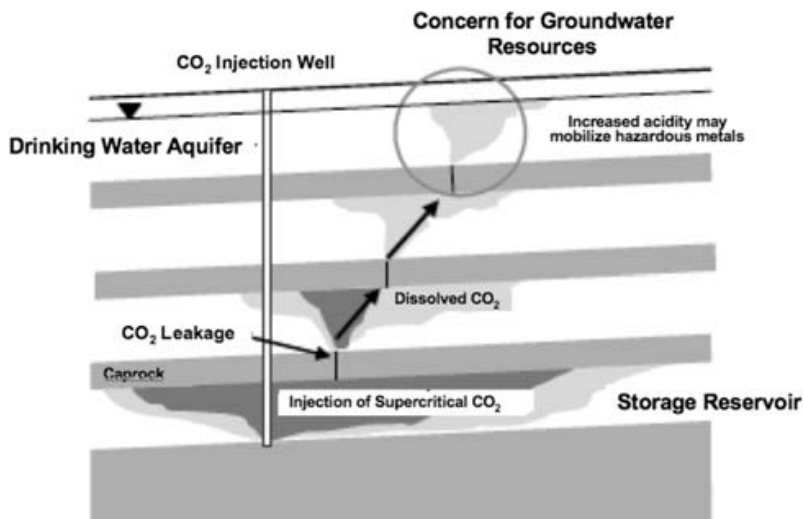


**Figure 2.1:** Schematic representation of CO<sub>2</sub> release and potential impacts on groundwater  
(Newmark et al., 2010)

### 2.2.2 Arsenic Release

Dissolution of CO<sub>2</sub> in deep saline brines could result in a reduction of pH and increase the dissolution of metals from reservoir formations. Experiments have indicated that the acidity associated with CO<sub>2</sub>-rich brines dissolves trace metals from sandstone and shale at rates similar to the dissolution of major silicate phases (Carroll, 2010). Concentrations of several trace metals could exceed the U.S. Environmental Protection Agency's (EPA) primary Maximum Contaminant Level (MCL). One trace element of concern is arsenic as it is toxic even at low concentrations and has many health and environmental impacts. Significant clusters of chronic illness associated with ingestion of arsenic contaminated groundwater have been reported from Bangladesh, India, Taiwan, Chile and Argentina due to exposures to elevated concentrations of naturally occurring arsenic in drinking water (Henke, 2009). Therefore, World Health Organization (WHO) recommended a maximum concentration of arsenic of 10 µg/L in drinking

water and the U.S. EPA has established a maximum contamination level of 10  $\mu\text{g/L}$  in drinking water (US EPA, 2001).

The majority of arsenic problems are caused by naturally occurring inorganic arsenic. It is associated with igneous and sedimentary rocks. Pyrite rocks, particularly contain appreciable amounts of arsenic (up to 6 wt. %) in solid solution (Welch et al, 2000).

The fate and the mobility of arsenic is mainly controlled by five categories of processes in surface water and groundwater (Cheng et al., 2009):

1. Redox Reactions
2. Adsorption and Desorption
3. Competitive Adsorption
4. Solid Phase Precipitation and Dissolution
5. Biological Activity

Factors such as redox potential (Eh), pH, alkalinity/acidity, chemical composition of the system (redox pairs, competing anions, aquifer minerals, etc.) and reaction kinetics play an important part in these processes (Cheng et al., 2009).

Several geochemical mechanisms, including reductive dissolution of iron (oxy) hydroxides, release of sorbed arsenic from mineral surfaces, and oxidation of arsenic bearing sulfide minerals, have been identified as the primary sources of arsenic contamination in ground water (Henke, 2009). Furthermore, the release of arsenic involves several transport mechanisms that make the identification of the parent source of arsenic complicated. Thus, it is of interest to

investigate arsenic sources and solid phase concentrations in sedimentary geological formations in which CO<sub>2</sub> maybe stored, to assess the risk associated with CO<sub>2</sub> storage.

### **2.3 Approach**

A literature review was performed and data on source materials for arsenic and typical arsenic solid phase concentrations were extracted. Sedimentary formations were classified based on their permeability as high (sand, gravel, alluvial, sand stone, unconsolidated deposit, glacial tilt) and low permeability (shale, clay stone, mudstone, clay minerals) formations. The solid phase arsenic concentrations in these rocks were tabulated and compared graphically. An attempt was made to classify formations based on depth, but reported values indicated that arsenic concentrations in sedimentary rocks did not vary with depth. It must be noted that much of the data acquired on high permeability sedimentary formations was from the Bengal Basin.

### **2.4 Results and Discussion**

#### **2.4.1 Arsenic parent mineral**

Literature was reviewed for high and low permeability sedimentary formations and the results were tabulated (Appendix A: Table A1 and A2 respectively). Based on these tables, graphs depicting the most common source of arsenic for both high and low permeability formations (Figure 2.2 and Figure 2.3).

### 2.4.2 Concentration of As in sedimentary formations

Literature reports were also analyzed for reported concentrations of arsenic in sedimentary formations. Figure 2.4 depicts the most commonly reported concentration ranges.

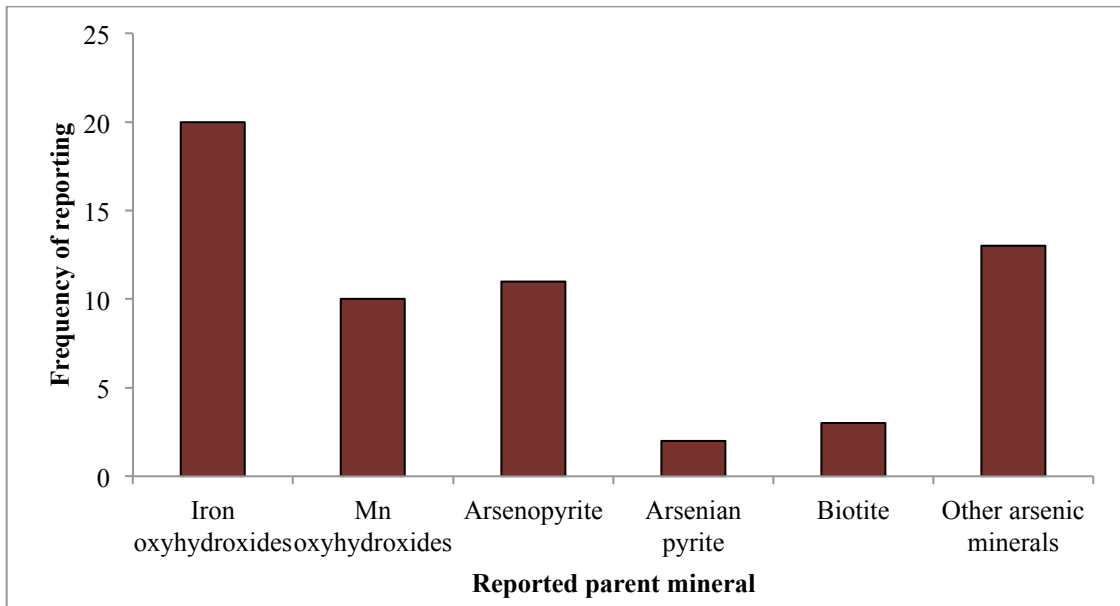


**Figure 2.2:** Arsenic parent material in high permeability sedimentary formations

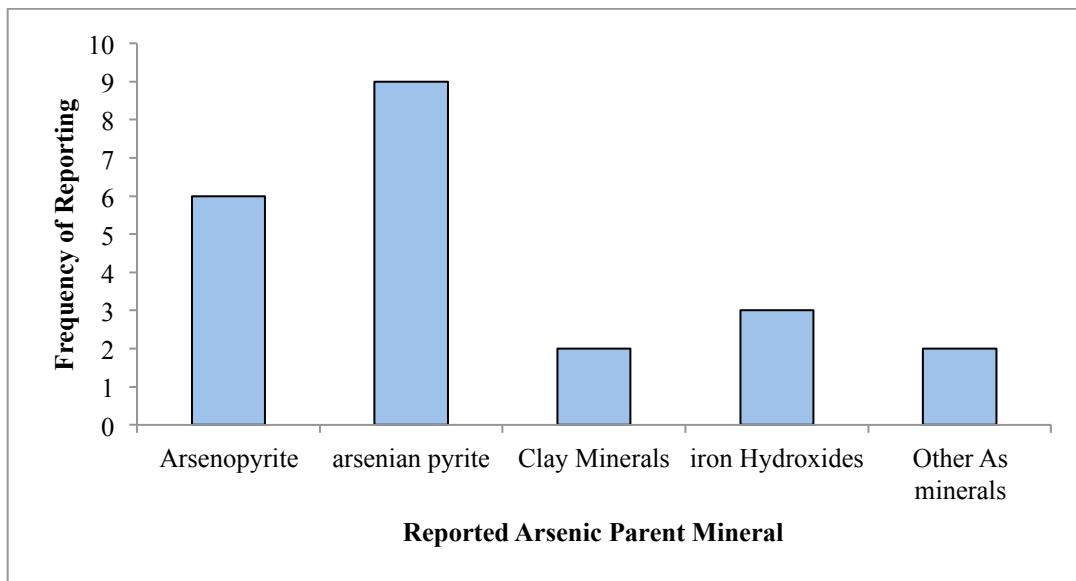


**Figure 2.3:** Arsenic parent material in low permeability sedimentary formations

As can be seen from Figure 2.2 the most common sources of arsenic in high permeability sedimentary formations were iron and manganese oxyhydroxides (Fe or Mn(O(OH))) and arsenopyrite (FeAsS). Since, mobilized arsenic gets adsorbed onto the surfaces of iron and manganese hydroxides, these were considered as secondary sources. Arsenopyrite and arsenian pyrite are the major sources of arsenic in low permeability sedimentary formations (Figure 2.3). Arsenian pyrite is pyrite in which some sulfur atoms are substituted with arsenic as opposed to arsenopyrite, which has a fixed stoichiometry. Other arsenic minerals include minerals such as realgar (As<sub>4</sub>S<sub>4</sub>), orpiment (As<sub>2</sub>S<sub>3</sub>) and scorodite (FeAsO<sub>4</sub> · 2H<sub>2</sub>O).

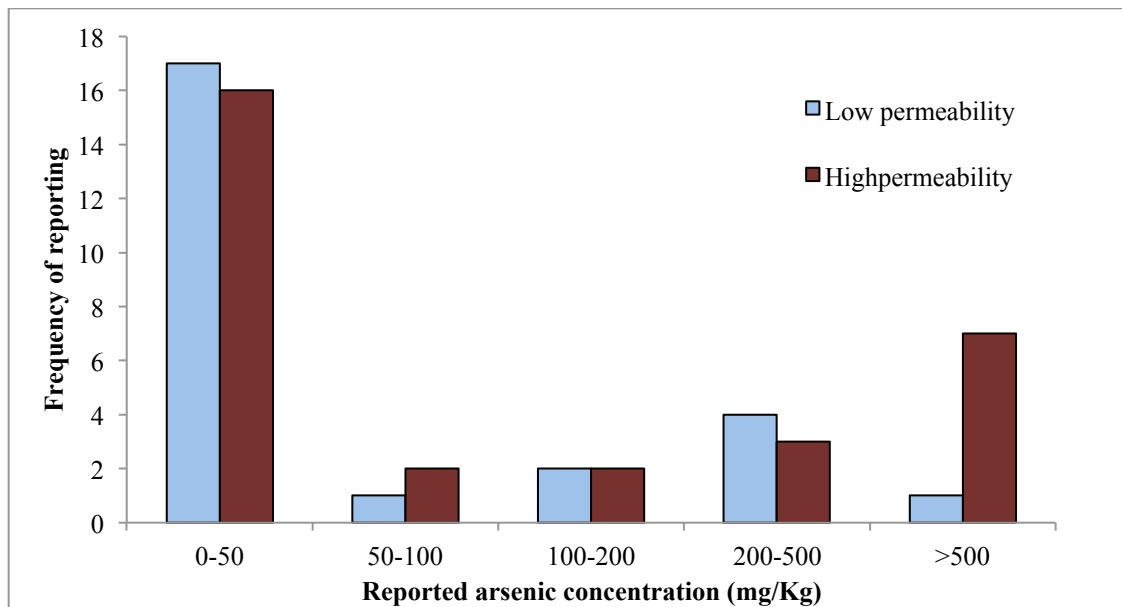


**Figure 2.4:** Arsenic concentration ranges in high and low permeability sedimentary formations

Figure 2.4 shows the reported concentration ranges of arsenic in high and low permeability sedimentary formations. The 0-50 mg/Kg range has the highest frequency of occurrence in the

literature. Very high concentrations of arsenic (>500 mg/Kg) for high permeability sedimentary formations were also reported.

## **2.5 Summary and Conclusions**

A review of the literature on the occurrence of arsenic in sedimentary formations was performed to identify the most common sources of arsenic in such formations and the ranges of arsenic concentrations reported. The principal findings from this review are as follows:

- a. In both high permeable and low permeable sedimentary formations, the major sources of arsenic are arsenian pyrite, arsenopyrite (FeAsS), and iron oxy hydroxides (as a secondary source.)
- b. Concentration of arsenic in sedimentary rock is most commonly reported in the range of 0-50 mg/Kg although concentrations greater than 500 mg/Kg have been reported.

## 2.6 References

Carroll, S.A. (2010). Trace metal geochemistry in carbon sequestration environments. *Environmental and Geochemical Aspects of Carbon Sequestration*, March 22, 2010.

Cheng, H., Hu, Y., Luo J., Xu, B. and Zhao, J. (2009). Geochemical processes controlling fate and transport of arsenic in acid mine drainage (AMD) and natural systems. *Journal of Hazardous Materials*, 165(1-3), 13-26.

Henke, K.R., ed. (2009). *Arsenic: Environmental Chemistry, Health Threats and Waste Treatment*, John Wiley & Sons, New York.

Newmark, R.L., Freidmann, S.J. and Carroll, S.A. (2000). Water Challenges for Geologic Carbon Capture and Sequestration. *Environmental Management*, 45, 651-661.

Welch A.H., Westjohn D.B., Helsel, D.R. and Wanty, R.B. (2000). Arsenic in Ground Water of the United States: Occurrence and Geochemistry. *Ground Water*, 38(4), 589-604.

U.S. Environmental Protection Agency. (2001). National primary drinking water regulations; Arsenic and Clarifications to compliance and new source contaminants monitoring: final rule: Federal Register 66, no. 14, 6976-7066.

## CHAPTER 3

### **A SMALL-SCALE FLOW-THROUGH COLUMN SYSTEM TO DETERMINE THE RATES OF MINERAL DISSOLUTION AT HIGH TEMPERATURE AND PRESSURE**

The information presented in this chapter was published in *Chemical Geology*, 354, 65-72 (2013). The co-authors of this paper were: David A. Dzombak, Athanasios K. Karamalidis.

### 3.1 Abstract

Mineral dissolution is a critical phenomenon in many geochemical systems, including those of geologic CO<sub>2</sub> storage. It affects the mobilization, fate and transport of toxic metals in subsurface waters. A small-scale plug-flow system was designed and demonstrated for use in determining dissolution rates and simulating mineral-water interactions under a wide range of conditions, including high pressure (P, up to 300 bar) and temperature (T, up to 120 °C). The system enables rapid achievement of steady-state rates, and minimizes the experimental time to study such mineral-water systems. The performance of the system was evaluated through study of the oxidative dissolution of arsenopyrite (FeAsS (s)). Rates of arsenic release induced by dissolved Fe<sup>3+</sup> (10<sup>-4</sup> M) in anoxic systems at 25 °C and pressures of 1 bar and 100 bars were measured. The performance testing confirmed the ability to obtain reproducible results under the wide range of conditions tested, and to obtain similar results to certain benchmark cases, e.g., the FeAsS (s) dissolution rate of 10<sup>-8.09</sup> mol As/m<sup>2</sup>s at 25 °C and 1 bar was comparable to previously reported values. Potential mass-transfer limitations associated with the system were studied and results indicate such limitations can be avoided at flow-rates higher than 0.8 mL/min (interstitial velocity of 0.13 cm/s).

### **3.2 Introduction**

Mineral dissolution contributes to processes controlling soil fertility, porosity in aquifers and oil reservoirs, transport and sequestration of chemical constituents, cycling of metals and formation of ore deposits, and many other geochemical characteristics and phenomena (Brantley et al., 2008). Understanding of mineral dissolution rates under a wide range of physical and chemical conditions is important, especially for effective and environmentally safe operation of geologic CO<sub>2</sub> storage in deep saline sedimentary formations.

Numerical models have shown that as CO<sub>2</sub> is injected into a saline reservoir, the pH of the reservoir water, close to the injection zone, could reduce to as low as pH 3 (Kharaka et al., 2007; Xu et al., 2007), which may initiate or increase mineral dissolution from formation and cap rocks. The implications for such dissolution are many, including release of toxic metals (Wang and Jaffe, 2004) like arsenic (As), and transport to overlying aquifers via potential reservoir leakage. Understanding the mechanism and kinetics of release of such metals is important to be able to predict and calculate the risks associated with metal dissolution in geologic CO<sub>2</sub> storage.

While aqueous dissolution rates of many minerals at moderate temperatures and pressures, including calcite, kaolinite, quartz, pyrite and arsenopyrite have been reported in the literature (e.g., Sjoberg and Rickard, 1984; Wieland and Stumm, 1992; Knauss and Wolery, 1988; Papangelakis and Demopoulos, 1992; McKibben et al., 2007), kinetics of dissolution under the unusual physical and chemical conditions associated with geologic storage of CO<sub>2</sub> remains unexplored. Mineral dissolution experiments spanning wide ranges of temperatures and solution conditions have been performed but measurements at pressures other than 1 atm are quite

limited. Although the effect of pressure on activation volumes and hence the dissolution rates of minerals is limited (Drljaca et al., 1998), higher pressures as seen in geologic reservoirs could affect other phases in the system including the physical state of CO<sub>2</sub>.

The majority of experiments measuring the dissolution rate of minerals use three basic types of reactor systems: batch reactors, mixed-flow reactors and flow-through reactor systems (Levenspeil, 1972; Hill, 1977; Rimstidt and Dove, 1986), with batch reactors employed most commonly owing to their simplicity (Rimstidt and Dove, 1986) and adaptability to high pressure and temperatures. The mineral is placed inside the reactor, which is then filled with the solution of interest. The temperature of the system is maintained through a water jacket or other means. The solution is mixed continuously, and samples of the solution are extracted at regular time intervals to determine the dissolved concentrations of elemental components of the mineral, which are used to determine dissolution rates. Since these systems rely on change in concentration of analytes to determine rates, a challenge in interpreting the data is the buildup of reaction products in solution (Paschka and Dzombak, 2004). This is apparent with iron releasing reactions, which tend to be limited by iron oxy-hydroxide saturation, especially at high pH values (McKibben et al., 2007). Batch systems are not ideal for studying oxidative/reductive dissolution processes as product accumulation during experiments can change the redox conditions in the system.

Some of the drawbacks of batch systems can be overcome by using mixed flow and plug flow reactors. Mixed flow systems are configured like batch reactors but with continuous flow of solution. The mineral is held in a holder in the middle of the reactor, the reactor is filled with

solution and mixed continuously, an influent solution is continuously added, and an effluent stream is withdrawn from the reactor at the same rate as the influent flow. Once steady-state concentration of the target dissolution product is attained in the effluent stream, the rate of dissolution is determined by multiplying the difference in concentration of the analyte (mol/L) in the influent and effluent by the flow-through rate (L/s) (Rimstidt and Dove, 1986). These systems have been widely used to study dissolution rates at ambient pressures and temperature (Yunmei et al., 2004; 2007; Walker et al., 2006). Past studies of kinetics at high temperatures and pressure, however, have been hindered by experimental difficulties and labor intensive processes required with producing reliable results (Dove and Crerar, 1990). This is overcome by using hydrothermal mixed flow reactors, constructed from industrial grade titanium which forms a non reactive oxide layer (passivated TiO<sub>2</sub>) on its surface and can hence be used at temperatures up to 300 °C and pressures up to 124 bar (Dove and Crerar, 1990; Berger et al., 1994; Carroll et al., 2005). Hydrothermal mixed flow systems are expensive to construct, however, and tedious to assemble and operate.

Plug flow reactors are an alternative to batch and mixed-flow systems for studying dissolution rates (Knauss and Wolery, 1988; Rimstidt and Newcomb, 1993; Tester et al., 1994). These reactors typically consist of a column maintained at a constant temperature and pressure through which, the solution moves as slugs without mixing in the forward or reverse direction and without the addition or loss of fluid along the flow path (Rimstidt and Newcomb, 1993). Influent solution at a constant rate is supplied to the column and the effluent is analyzed for concentration of dissolved mineral components to determine rates. Plug flow reactors are usually operated under steady state conditions and can be used to measure long-term dissolution rates. Non-

steady state phenomena, such as preferential dissolution or rapid surface dissolution, may occur during the start-up period (Rimstidt and Dove, 1986) and such data are usually not considered representative. Since the dissolution within the column is not constant, data generated from plug flow systems are difficult to analyze. Hence, these systems are not ideal for initial rate determination. Plug flow systems can be used under a wide range of pressures, temperatures, solution compositions, and with different minerals without significant design changes. The advantages and disadvantages of the three types of systems are tabulated in Appendix B.

In this work, we designed, constructed and operated a small-scale flow-through column system for use in rapid determination of long-term dissolution rates of minerals under a range of pressure, temperature and solution conditions, which are representative of deep geologic formations. The specific design objectives were to (i) be able to operate at high temperatures and pressure, (ii) eliminate mass transfer limitations within the system and (iii) maintain a constant rate of dissolution within the reactor to eliminate mathematical difficulties. The performance of the system was analyzed for the oxidative dissolution of arsenopyrite induced by a  $10^{-4}$  M  $\text{Fe}^{3+}$  as the oxidizing agent.

### **3.3 Materials and Methods**

A small-scale flow-through system for studying mineral dissolution under a range of temperature and pressure conditions was assembled and evaluated by study of the oxidative dissolution of arsenopyrite ( $\text{FeAsS}$  (s)). Evaluation of the system involved the following experiments: 1) A blank experiment, with deionized water adjusted to a pH of 2 with HCl to ensure that the system hardware did not release any arsenic or iron; 2) measurement of the rate of arsenic release from

arsenopyrite at pH 2, temperatures of 25 °C and pressures of 1.0 bar and 100 bar, with an influent solution containing  $10^{-4}$  M  $\text{Fe}^{3+}$ , in the absence of oxygen; and 3) measurement of rate of arsenic release from arsenopyrite at temperatures of 25 °C and pressures of 1.0 bar, with an influent solution containing  $10^{-4}$  M  $\text{Fe}^{3+}$  (pH =2) and at different influent flow rates to determine the effects of fluid velocity on the dissolution rate. The system was also checked for its ability to maintain constant temperature and pressure within the column for extended periods of time.

### **3.3.1 Mineral Preparation**

Arsenopyrite samples were obtained from Wards Natural Science Inc. (Rochester, NY) in 10 g batches. They were crushed in ethanol and wet sieved to obtain a uniform size fraction of 150-250  $\mu\text{m}$  (Wolfe et al., 2007), which was reported as the optimal particle size range for dissolution (McKibben et al., 2007). The particles were dried at 105 °C and stored in crimp-top vials under nitrogen gas. Samples required for each run were pre-treated to remove fines and surface oxide layers using the method developed by McKibben et al. (2007). The method entails cleaning the mineral with ultrasonication in methanol for 2 minutes, then rinsing it with 1.8 M  $\text{HNO}_3$  for 1 minute, followed by rinse with deionized water, rinse with ethanol and drying at 105 °C. The BET surface area of the cleaned arsenopyrite particles was measured in triplicate using a 5-point Kr absorption isotherm and was found to be  $0.04 \pm 2\%$   $\text{m}^2/\text{g}$ .

### **3.3.2 Experimental Apparatus**

The flow-through reactor consisted of six main parts, as shown in Figure 3.1: a thermally controlled influent tank, a pump (Isocratic piston pump: model P-1010; Chromtech, USA), a column, a pressure controller, a sampling port, and an effluent tank (waste). For the purpose of

the arsenopyrite dissolution study, a Pyrex glass bottle (2 L) with screw cap having three ports was used as an influent tank. The tank was chosen based on the ability to withstand heat and maintain constant temperature, be chemically resistant, have low potential for cross contamination with the mineral sample, and allow for gas sparging. The temperature of the influent solution was maintained by heating the influent bottle using a Corning heat plate. The P-1010 piston pump was capable of supplying the system with influent solution at a constant rate (0.01- 10 mL/min) for a range of pressures up to 6000 Psi (Figure 3.1).

A PEEK (Poly Ether Ether Ketone) column from BioChrom Labs, Inc. (Indiana, USA) usually employed for high-performance liquid chromatography, was chosen for studying the dissolution of minerals under various conditions. PEEK is a high-performance thermoplastic with a high degree of mechanical and chemical resistance. PEEK is capable of withstanding pressures up to 300 bar and has a glass transition temperature of 140 °C. The low thermal conductivity of the material ensures that very little heat is lost to the surroundings, thereby maintaining the constant temperature conditions required for the experiments. PEEK is chemically inert and can be used in saline environments as well as under a wide range of pH values.

Downstream of the column (Figure 3.1), a pressure regulation system consisting of an adjustable backpressure regulator (Swagelok KHB series high pressure backpressure regulator) and a pressure reducer (Swagelok KHP series) was used to maintain the pressure inside the column. The backpressure regulator allows flow only if a particular pressure is reached upstream of the regulator and the pressure reducer down-regulates the pressure for sampling. The pressure regulators were rated for 6000 Psi (414 bar).

An effluent tank was used to collect the discharge from the system, and a sampling port consisting of a 3-way valve (Hamilton Inc., USA) was provided. All connections in the system were made using PEEK tubing (I.D 3.2 mm and 1.6 mm; Sigma Aldrich, USA) and high-pressure Swagelok fittings. The entire system was placed in a zipper locked, plastic glove bag (Sigma Aldrich, USA), which was filled with nitrogen, to maintain anoxic conditions. The dissolved oxygen content in the influent solutions and in the glove bag was measured using an Accumet XL 60 dissolved oxygen meter (Fisher Scientific, USA).

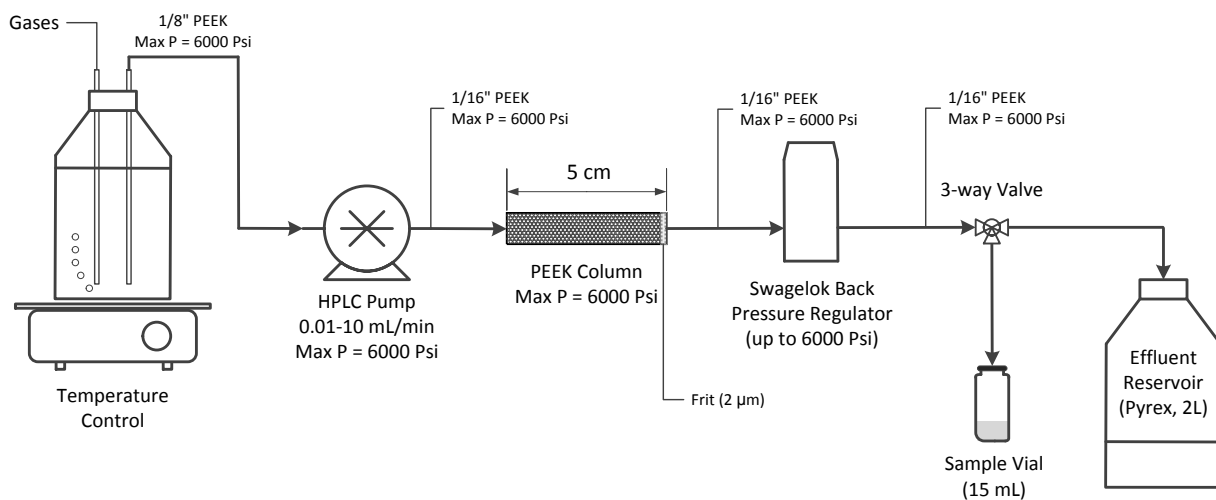


**Figure 3.1.** Schematic of the flow-through column reactor system for studying mineral dissolution under a range of temperature, pressure and solution conditions

### **3.3.3 Cleaning the system prior to experiments and setup**

Prior to every experiment the system was cleaned by flowing a 10 % HNO<sub>3</sub> (w/v) solution through the apparatus for 30 minutes to remove any residual trace metals in the column and tubing or residual trace metals from previous experiments, followed by a rinse with deionized water for 30 minutes. A blank experiment was run with each influent solution and tested to check for background concentration of arsenic and iron. The packed column was connected to the pump, the pressure was adjusted to the required value (1 bar or 100 bar) and influent solution pump started.

### **3.3.4 Sampling and analysis**

Samples of the effluent solution were collected in 15 mL centrifuge tubes every 180 minutes for a flow rate of 0.4 mL/min, every 120-180 minutes for a flow rate 0.8 mL/min and every 45 minutes for a flow rate of 1.1 mL/min. Samples were collected by diverting the flow from the effluent tank to the sampling container using the 3-way valve which was allowed to bleed for a few minutes to remove residual liquid in the tubing. This sampling strategy enabled samples to be collected at regular pore volume intervals. Sampling was started after one hour of operation to ensure that any fine particles were removed from the packed bed of mineral particles. The effluent end of the column was fitted with a PEEK frit to prevent mineral particles from escaping. In addition, the absence of fines was confirmed by filtering effluent sample with a 0.2 µm PTFE membrane syringe filter.

The collected samples were preserved in 2% trace metal grade HNO<sub>3</sub> and analyzed for arsenic and iron using an Agilent 7700x ICP-MS. The detection limits were 5 ng/L for Fe and 1 ng/L for As.

Each experiment was conducted until a steady state effluent concentration was achieved. Steady state was defined as when the difference in arsenic concentrations was within  $\pm 10\%$  for a period of 500 pore volumes. At the end of each run, arsenopyrite samples were collected and analyzed for reactive surface areas using BET analysis.

### **3.4 Modeling and Calculations**

To determine the column design ensuring negligible pressure buildup, and no mass transfer effects and to develop the method for data interpretation, a model was developed for mineral dissolution in the plug flow reactor.

#### **3.4.1 Pressure drop across the column**

The pressure drop across the column was calculated using the Kozeny-Carman equation (McCabe et al.,2005).

$$\frac{\Delta p}{L} = \frac{180V_0\mu(1-\varepsilon)^2}{\Phi_s^2 D_p^2 \varepsilon^3} \quad (3-1)$$

where  $\Delta p$  is the pressure drop (psi),  $L$  is the total height of the bed (cm),  $V_0$  is the velocity (cm/s),  $\mu$  is the viscosity of the fluid (g/cms),  $\varepsilon$  is the porosity of the bed,  $\Phi_s$  is the sphericity of the particles in the packed bed, and  $D_p$  is the diameter (cm) of the related spherical particle. For

the system under consideration the pressure drop was calculated for different flow rates. Results ranged from 0.1- 0.4 psi for flow rates of 0.5- 2 mL/min. These results indicate that the pressure drop within the column was very small.

### 3.4.2 Data Interpretation- obtaining dissolution rates from effluent concentrations

In order to interpret the effluent dissolution constituent concentrations measured in the flow-through reactor dissolution experiments, a reactive transport model was developed. For a flow-through reactor packed with mineral, the following assumptions were made: the flow in the reactor was assumed to be ideal plug flow, and all mineral particles were assumed perfect spheres. For an unopposed reaction of order  $n$ , the rate expression can be expressed as (Eq. 3-2):

$$r = \frac{dC}{dt} = -kC^n \quad (3-2)$$

Where  $r$ , is the rate of the reaction (mol/L.s), which is determined by  $k$ . the rate constant of the reaction and  $C$ , the concentration of reactant (mol/L).

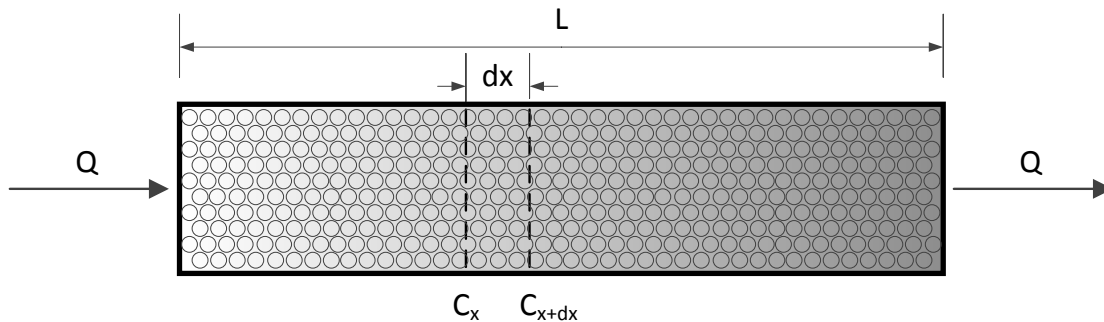


**Figure 3.2** Schematic of a cylindrical flow-through reactor of length  $L$ , radius  $r_c$  and volume  $V$ .

Mass balance across elemental length  $dX$

The conceptual model for the flow-through reactor is shown in Figure 3.2, having a dry packed column of length  $L$  (cm), radius  $r_c$  (cm) and volume  $V$  (L). Consider an influent solution pumped at a flow rate of  $Q$  (L/s).

The mass balance on an elemental volume  $dv$ , is given by equation 3-3:

$$Q \cdot C_v - k \cdot C^n \cdot dv = Q \cdot C_{v+dv} \quad (3-3)$$

As shown by Rimstidt and Newcomb (1993), the above equation can be simplified to yield the integrated form of the rate law (for  $n \neq 1$ )

$$\left( \frac{C}{C_0} \right)^{-n+1} = - \frac{(-n+1) \cdot k \cdot t}{C_0^{-n+1}} + 1 \quad (3-4)$$

where  $C$  is the concentration at the effluent end of the reactor,  $C_0$  is the influent concentration and  $t$  is the residence time of the fluid in the reactor given by  $\frac{V}{Q}$ .

Traditionally the plug flow equation (Eq. 3-4) can be solved using either binomial or logarithmic expansion (Rimstidt and Newcomb, 1993). These manipulations result in final equations relating the effluent concentrations with the residence time of the solution. As a consequence, multiple experiments at different flow rates have to be conducted to determine the reaction rate under a particular condition. Therefore, analysis and interpretation of results from plug flow reactors is mathematically tedious.

Under certain conditions, however, these difficulties can be overcome to measure reaction rates directly as shown below:

The plug flow equation (3-4) can be re-written as

$$\left(\frac{C}{C_0}\right)^{-n+1} = -(-n+1) \cdot D_a + 1 \quad (3-5)$$

where  $D_a$  is the Damköhler's number defined (Fogler et al., 2006) as

$$D_a = k \cdot C_0^{n-1} \cdot t \quad (3-6)$$

The Damköhler number represents the ratio between the rate of reaction and the rate of convective mass transport.  $\left(\frac{C}{C_0}\right)$  was plotted for a range of Damköhler numbers, for different reaction orders (Figure 3.3).

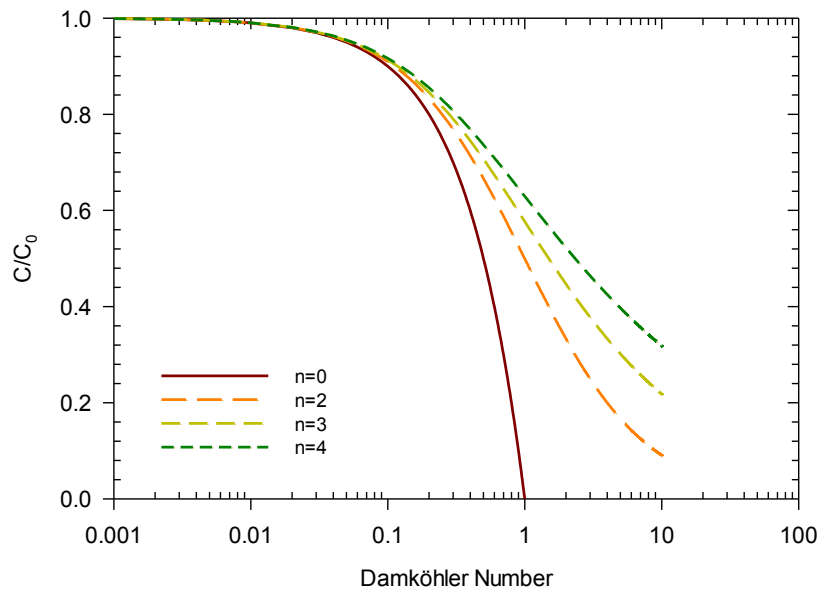


**Figure 3.3**  $\left(\frac{C}{C_0}\right)$  vs. Damköhler number

As seen in the figure, for low values of Damköhler number ( $D_a < 0.01$ ), the value of  $\left(\frac{C}{C_0}\right)$

becomes independent of reaction order, since the mass flux of reactant lost by reaction is very

small as compared to the influent mass flux through convection. This implies that irrespective of the rate law, the reaction behaves like a pseudo-0<sup>th</sup> order reaction.

For a 0<sup>th</sup> order reaction, the plug flow equation (Eq. 3-4) simplifies to

$$k = \frac{C_0 - C}{t} \quad (3-7)$$

Thus for  $D_a < 0.01$ , the plug flow reactor can be used to measure reaction rates directly.

To enable comparison of rates between experiments that differ in the starting material, the rate obtained from Eq 3-7, is normalized for surface area of the crushed minerals. This is achieved by multiplying it with the ratio of the surface area of solid (A) to the mass of liquid (M), in the reactor. The rate law can then be determined by fitting reaction rates obtained using different influent reactant concentrations.

### **3.4.3 Managing mass transfer limitations within the column**

To measure the maximum rate of dissolution governed by chemical reaction of the mineral with the flowing aqueous solution, the column must be free of physical mass transfer limitations including dispersive effects and mass transfer resistance between the mineral particles and the bulk fluid. Longitudinal dispersion can lead to non-uniform reactant concentrations and dissolution rates within the column. The effective dispersivity is proportional to the fluid velocity in the column, and at very high flow rates could lead to erroneous rate data. Effective

dispersivity modeled for this particular column system at flow rates as high as 10 ml/min showed the absence of dispersive effects after 50 pore volumes (appendix B).

Mass transfer resistance between the fluid moving through the column and the surface of mineral particles across a boundary layer, and buildup of dissolution product in the boundary layer can decrease the driving force for dissolution and lead to dissolution rates controlled by mass transport and not surface reaction. To examine the transport of mass through a packed column, we consider a perfectly spherical, non-porous particle. The flow pattern around this particle is shown in Figure 3.4. The particle is surrounded by a thin boundary layer as shown. The concentrations of reactant (R) and product (P) inside the boundary layer (denoted by 's') and in the bulk fluid (denoted by 'b') are also shown.

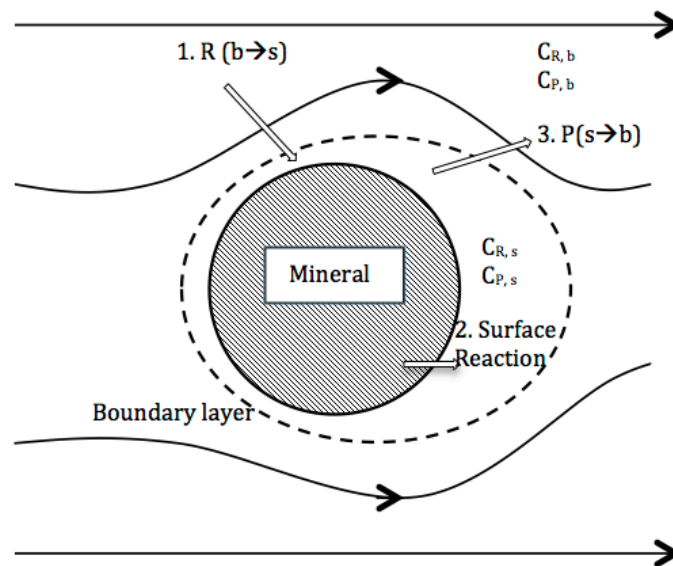


**Figure 3.4.** Flow pattern around a spherical mineral particle and mass transfer processes.

The transfer of mass to and from the particle involves three processes (Figure 3.4): 1) Flux of the reactant from the bulk solution to the surface of the particles, 2) dissolution reaction at the surface of the mineral particles and 3) flux of products from the surface to the bulk fluid. The overall rate of reaction can be limited by any of these three processes. If processes 1 or 3 are the slowest, the overall reaction is mass transfer limited. Conversely if process 2 is the slowest, the overall reaction rate is limited only by chemical reaction rate, which is the desired condition for dissolution experiments.

Mathematically, these three processes can be expressed as:

The molar flux of reactant from the bulk fluid to the surface of the particle is given by

$$W_R = k_{c,R} \cdot (C_{R,b} - C_{R,s}) \quad (3-8)$$

where  $W_R$  is the molar flux (mol/m<sup>2</sup>s) of the reactant from the bulk fluid to the boundary layer,  $k_{c,R}$  is the mass transfer coefficient (m/s),  $C_{R,b}$  is the concentration (M) of reactant in the bulk, and  $C_{R,s}$  is the reactant concentration (M) inside the boundary layer near the particle surface.

The value of  $k_{c,R}$  can be calculated by the Ranz-Marshall correlation (Fogler, 2006) shown in Eq.3- 9

$$Sh = \frac{k_c d_p}{D_A} = 2.0 + 0.6 Re^{0.5} Sc^{0.33} \quad (3-9)$$

where  $Sh$  is the Sherwood number,  $Re$  is Reynolds number,  $Sc$  is the Schmidt number,  $d_p$  is the particle diameter (m), and  $D_A$  is the diffusion coefficient (m<sup>2</sup>/s).

The rate of dissolution at the surface can be expressed as –

$$r_s = -k_r C_{R,s}^n \quad (3-10)$$

where,  $r_s$  is the surface rate of reaction (mol/m<sup>2</sup>s) , and  $k_r$  is the specific rate of reaction (m/s).

The molar flux of products from the surface to the bulk can be expressed as-

$$W_p = k_{c,p} \cdot (C_{P,s} - C_{P,b}) \quad (3-11)$$

where,  $W_p$  is the molar flux (mol/m<sup>2</sup>s) of products from the bulk fluid to the boundary layer,  $k_{c,p}$  is the mass transfer coefficient (m/s),  $C_{P,b}$  (M) is the concentration of products in the bulk, and  $C_{P,s}$  is the product concentration (M) inside the boundary layer near the particle surface.

At the limit of boundary layer, the rate of reactants utilized in the reaction is equal to the molar flux of reactant from the bulk to the surface. From equations 3-8 and 3-10, the rate of the reaction can be derived for different orders of reaction. For all values of  $n$ , it can be shown that if the mass transfer coefficient is much greater than the surface reaction rate ( $k_{cR} \gg k_r$ ) the overall reaction rate becomes surface reaction rate limited. Conversely if  $k_{cR} \ll k_r$  , then the reaction becomes dependent on the rate of mass transfer and is said to be mass transfer limited.

The mass transfer coefficient  $k_{cR}$  has been shown to be proportional to the velocity inside the column (Dutta, 2007). At low velocities, the boundary layer on the surface of the particle is large and the overall reaction is limited by the rate of diffusion across the boundary layer. At higher velocities, the boundary layer becomes small and the rate of dissolution on the surface limits the

overall rate of the reaction. Thus when the observed reaction rate no longer increases with increasing velocity, the system is said to be free of mass transfer limitations.

For arsenopyrite dissolution studies, the value of  $k_{c_{Fe^{3+}}}$  was calculated for a variety of flow rates and compared with the value of  $k_r$  obtained from the study by McKibben et al. (2007). The comparison plot (Figure 3.5) shows that the value of  $k_{c_{Fe^{3+}}}$  is much higher than  $k_r$ , thereby making the system free from mass transfer resistance across the boundary layer.

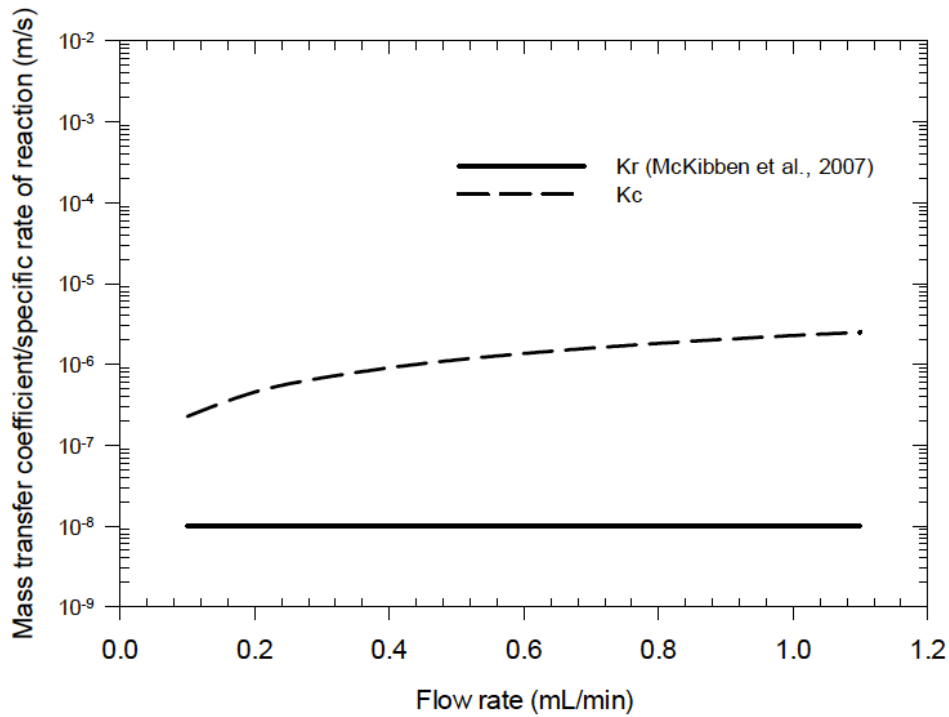


**Figure 3.5.** Comparison between  $k_{c_{Fe^{3+}}}$  and  $k_r$ , for different flow rates.

### 3.5 Results and Discussion

#### 3.5.1 Effect of flow rates on dissolution

The blank experiments conducted with deionized water at pH 2 exhibited concentrations of iron and arsenic below the detection limit.

**Table 3.1.** Results of arsenopyrite dissolution experiments with  $\text{Fe}^{3+} 10^{-4} \text{ M}$  at pH 2,  $P = 1 \text{ bar}$ ,

$T = 25 \text{ }^\circ\text{C}$

Flow Rate (ml/min)	Q (L/s)	Residence Time (s)	Concentration Steady State (mol/L)	Surface area of solid/mass of liquid (A/M) ( $\text{m}^2/\text{kg}$ )
1.1	$1.83 \times 10^{-05}$	26.73	$4.45 \times 10^{-05}$	213.06
0.8	$1.33 \times 10^{-05}$	36.75	$6.51 \times 10^{-05}$	210.61
0.4	$6.67 \times 10^{-06}$	73.50	$9.30 \times 10^{-05}$	203.27
0.2	$3.33 \times 10^{-06}$	147	N/A	206.43

Table 3.1 summarizes the experiments and the results obtained. Experiments with an influent Fe concentration of  $10^{-4} \text{ M}$  were conducted at four different flow rates (0.2 mL/min, 0.4 mL/min, 0.8 mL/min and 1.1 mL/min) to determine the effect of flow rate on arsenic release rate. Experiments were conducted until a steady state was reached; the duration varied from 1000 to 1500 pore volumes. Steady state was defined achieved if the difference in effluent arsenic concentration was less than 10 % for a period of 500 pore volumes. Effluent arsenic concentrations were plotted with respect to pore volumes for the different flow rates as shown in

Figure 3.6A. The dependence of overall reaction rate on the influent flow rate is shown in Figure 3.6B.

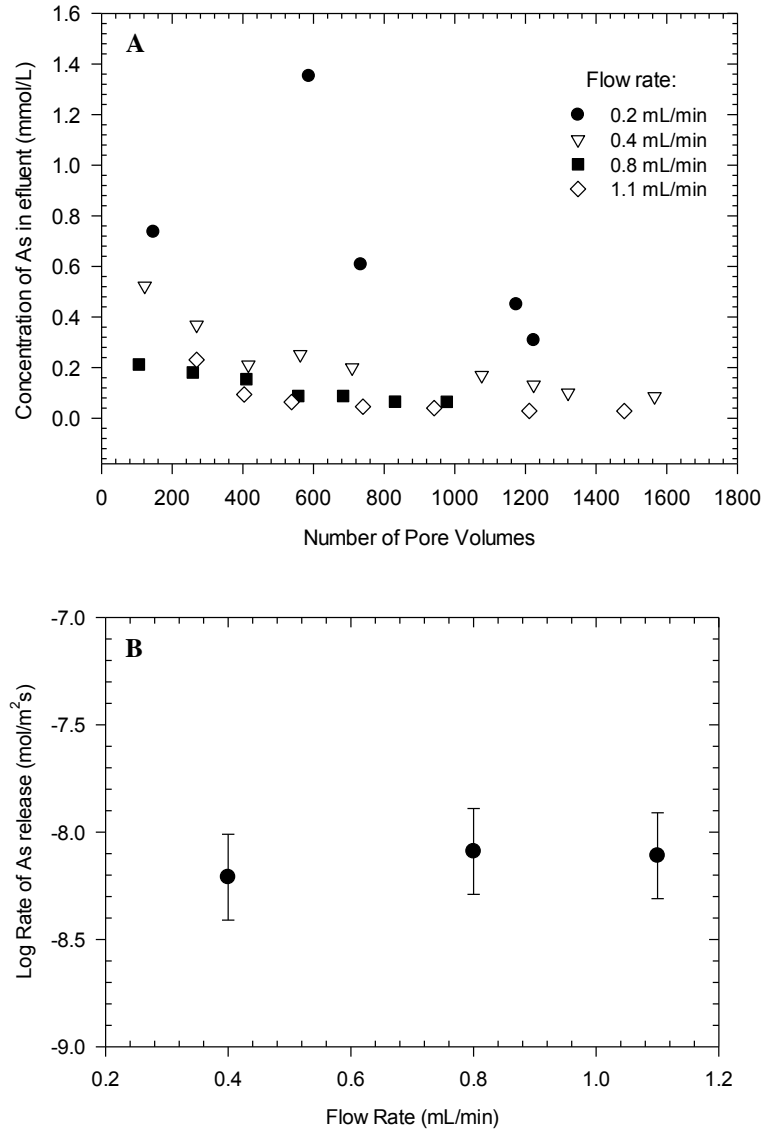


**Figure 3.6** Effect of flowrate on dissolution-(A) Oxidative dissolution of arsenopyrite with  $10^{-4}$  M  $\text{Fe}^{3+}$  at pH 2,  $T=25^\circ\text{C}$ ,  $P=1$  bar -Effluent arsenic concentration from arsenopyrite dissolution vs pore Volume. (B) The effect of influent flow rate on overall reaction rate

The concentration of arsenic in the effluent decreased with increasing flow rates (Figure 3.6A) due to decreased retention times of the liquid phase inside the reactor. While the higher flow rate experiments (0.8 mL/min; 1.1 mL/min) reached a steady state at around 500 pore volumes, the experiments at 0.2 mL/min and 0.4 mL/min did not attain steady state effluent concentration for the entire duration of the experiment. The rate of arsenic release is slower at 0.4 mL/min than at 0.8 mL/min (Figure 3.6B), which suggests that there is a mass transfer limitation at lower flow rates. This limitation is overcome at flow rates higher than 0.8 mL/min as there is no discernible difference between the reaction rates at 0.8 mL/min and 1.1 mL/min (Figure 3.6B).

The effluent concentrations were used to compute reaction rates (Equation 3-7). The steady state reaction rates obtained at flow rates of 0.8 mL/min and 1.1 mL/min were calculated to be  $10^{-8.09}$  mol/m<sup>2</sup>s and represent the maximum steady state rate of arsenic release from arsenopyrite under the conditions studied. The estimated reaction rates for the experiments at 0.2 mL/min and 0.4 mL/min did not correspond to steady state effluent conditions and were lower than the rates obtained by using higher flow rates. These experiments also showed a high initial rate of dissolution, which decreased with the progress of the experiment. This could have been caused by preferential dissolution through defects on the surface of the arsenopyrite particles, as observed by Walker et al. (2007), amplified by the longer contact times at the slower flow rate.

### **3.5.2 Reproducibility and high-pressure experiments**

The reproducibility of the system was tested at 1 bar, 25 °C and pH =2 for a Fe<sup>3+</sup> solution of concentration 10<sup>-4</sup> M. The results are shown in Figure 3.7.

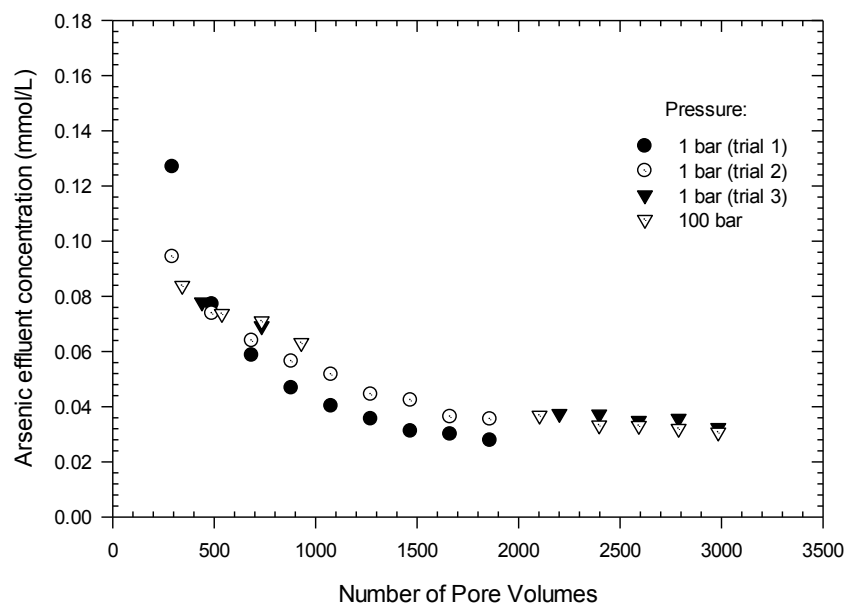


**Figure 3.7** Arsenic concentration (mmol/L) vs. number of pore volumes. Experiments at 1 bar were conducted in triplicate to show the reproducibility of the system and compared to that conducted at 100 bar to show the pressure effect on arsenopyrite dissolution. Experimental conditions: Flow rate = 0.8 mL/min; Temperature = 293 K; pH = 2;  $[\text{Fe}^{3+}] = 0.1 \text{ mM}$ .

The figure depicts three trials of arsenopyrite dissolution from the same sample, which were repeated under the same conditions of temperature, pressure, iron concentration, pH, and flow rate. Trials 1, 2, 3 at 1 bar show close similarity. Two more sets of replicates that were conducted to check for reproducibility showed similar results. The graph for 100 bars suggests that pressure does not have a discernible effect in the rate of dissolution under these conditions. The temperature of the influent solution was increased to 60 °C and the system was able to maintain this temperature for a period of 30 hours. This was confirmed by measuring the effluent and influent solution temperatures.

### **3.5.3 Arsenopyrite dissolution mechanism**

The decrease in As concentration at higher pore volumes at all flow rates can be attributed to the mechanism of arsenopyrite dissolution. The fate of Fe, As and S species on the surface of arsenopyrite and the preferential enrichment of any of these species could potentially impact the overall mechanism as well rates of oxidation. The scientific consensus on the S species on the surface varies significantly, depending mainly on the technique used to examine the surface. While many research groups (e.g. Fernandez et al., 1996; McGuire et al., 2001) have detected elemental S on the surface using Raman spectroscopy, the majority of authors (e.g. Nesbitt et al., 1995; Corkhill et al., 2008) who use vacuum and x-ray based techniques did not detect elemental sulfur (Corkhill and Vaughan, 2009). Asta et al., (2010) detected three possible sulfur species on the surface using XPS and a peak corresponding to elemental sulfur species at acidic pH by using Raman spectroscopy. They argued that the precipitation of elemental S is unlikely considering that the system is under saturated. Some authors (Fernandez et al., 1996; Cruz et al., 1997) suggested that the accumulation of elemental sulfur could result in a decrease in oxidation by forming a passivating layer. The latter is indicative of the decrease in As concentrations at large pore volumes for all flow rates seen in Figure 3.6A. The question on the exact mechanism of dissolution and its effects at large pore volumes remains. The proposed small-scale flow-through system can be used to elucidate dissolution for much longer time scales to observe the evolution of the arsenopyrite surface and its relation to As effluent concentrations.

### **3.5.4. Comparison with observed rates**

The rate of arsenic release from arsenopyrite caused by oxidative dissolution using  $\text{Fe}^{3+}$  at low pH under ambient conditions has been determined by multiple groups using various systems.

Yunmei et al. (2004, 2007) used a mixed-flow reactor, while McKibben et al. (2007) used batch systems to derive the rate expression. Table 3.2 shows the rates of arsenopyrite dissolution obtained in various experiments using different oxidants. The rate obtained in this study of  $10^{-8.09}$  mol/m<sup>2</sup>s, using a flow-through system is within the range of previously established values for arsenopyrite dissolution by Fe<sup>3+</sup> ( $10^{-4}$  M) at pH 2. The reaction mechanisms of arsenopyrite dissolution are not well understood. The presence of different reaction pathways in different systems and the significant differences in B.E.T surface areas between the studies contribute to the large scatter in dissolution rates.

**Table 3.2.** Comparison of rate of arsenopyrite dissolution reported in literature

Study	System Type	Oxidant	Surface Area (m <sup>2</sup> /g)	Log (Rate) (mol mineral/m <sup>2</sup> s)	Rate Measuring Variable
Rimstidt et al., 1994	Batch	Fe <sup>3+</sup> ( $10^{-4.10}$ M) (pH 1.8)	0.066	-6.93	Total As released
Yunmei et al., 2004	Mixed Flow	Fe <sup>3+</sup> ( $10^{-4}$ M) (pH 2)	0.031	-7.52	Total As released
Walker et al., 2006	Mixed Flow	Dissolved Oxygen ( $10^{-4.8}$ M) (pH 6.3 - 6.7)	0.0388	-10.14	Steady state As release
McKibben et al., 2007	Batch	Fe <sup>3+</sup> ( $10^{-4}$ M) (pH 2)	0.103	-9.19	Fe (III) release
Asta et al., 2010	Mixed-Flow	Dissolved oxygen ( $10^{-4.8}$ M) (pH 2)	0.3- 0.7	-10.82	As release
This study	Plug Flow	Fe <sup>3+</sup> ( $10^{-4}$ M) (pH 2)	0.04	-8.09	Total As released

### 3.5.5 Limitations

As seen earlier the Damköhler number is controlled by the reaction rate, the flow rate, as well as influent concentration of reactant. As a result, for minerals that have rapid dissolution rates, the flow rates required can be extremely high, which could cause undesirable turbulent flow inside the reactor.

The maximum flow rate at which laminar flow limit is still maintained in this current system is 10 mL/min, which limits the range of dissolution rates that can be studied. The ideal flow rates to study the dissolution rates of minerals for an influent reactant concentration range of 0.1 mM to 1 M were calculated for different orders of reaction rates and the maximum dissolution rate that can be studied in this system was determined to be  $5 \times 10^{-05}$  mol/m<sup>2</sup>s at a reactant concentration of 0.1 mM (which corresponds to a pH of 4).

A similar approach can be used for those reactions whose rate is controlled by the dissolved product species, but to achieve uniform rates for rapidly dissolving minerals, very high velocities would be required. For example, the surface reaction rate of gypsum dissolution, far from equilibrium as reported by Jeschke et al. (2000), was 1.1 mol/m<sup>2</sup>s, which is in the realm of mixed-kinetics where surface reaction and mass transfer control the overall reaction rate. The presence of mass transfer limitations leads to non-uniform reaction rates within the column. To make the analysis of such a system easier, very high velocities would be required to maintain the desired Damköhler number conditions. This system is not ideal for the study of minerals with such high rates of dissolution, but is till capable of accurately determining surface reaction rates of minerals with moderate and slow rates of dissolution.

### 3.6 Summary and Conclusions

A small-scale flow-through column system involving a plug flow reactor was developed for study of mineral dissolution at high temperature and pressure. The plug flow reactor is capable of measuring dissolution rates directly for minerals with moderate and low dissolution rates. The maximum rate of dissolution that can be studied with this setup was found to be  $5 \times 10^{-05}$  mol/m<sup>2</sup>s, for a maximum flow rate of 10 ml/min (interstitial velocity of 1.6 cm/s). The performance of the flow-through system for determining reaction rates of minerals under ambient conditions and high-pressure conditions was demonstrated through study of arsenopyrite dissolution. The system was demonstrated to be capable of functioning at high temperature and pressure and to be free of mass transfer limitation at flow rates higher than 0.8 mL/min. Dissolution rates for arsenopyrite in contact with an aqueous solution at pH 2 and with  $10^{-4}$  M Fe<sup>3+</sup> as oxidizing agent were analyzed for four different flow rates and a steady state was achieved at flow-rates of 0.8 ml/min and 1.1 mL/min at 500 pore volumes. The experiments were conducted at both 1 bar and 100 bar of pressure. The steady state dissolution rate obtained under ambient conditions (T=25 °C, P=1 bar) was within the range of arsenopyrite dissolution rates previously reported for such conditions.

### 3.7 References

- Asta, M., Cama, J., Ayora, C., Acero, P., Giovanni de Giudici. (2010). Arsenopyrite dissolution rates in O<sub>2</sub>-bearing solutions. *Chemical Geology* 273, 272-285.
- Berger, G., Cadore, E. (1994). Dissolution rate of quartz in lead and sodium electrolyte solutions between 25 and 300°C: Effect of the nature of surface complexes and reaction affinity. *Geochimica et Cosmochimica Acta* 58 (2), 541-551.
- Brantley, S.L., Kubicki, J.D., White, A.F. (2008). *Kinetics Of water-rock interaction*. Chapter 5: Kinetic of Mineral dissolution, New York, Springer.
- Carroll, S., Knauss, K. (2005). Dependence of labradorite dissolution kinetics on CO<sub>2(aq)</sub>, Al<sub>(aq)</sub>, and temperature. *Chemical Geology* 217, 213-225.
- Corkhill, C., Vaughan, D.J. (2009). Arsenopyrite oxidation- A review. *Applied Geochemistry* 24, 2342-2361.
- Corkhill, C., Wincott, P., Lloyd, J.R., Vaughan, D.J. (2008). The oxidative dissolution of arsenopyrite (FeAsS) and enargite (Cu<sub>3</sub>AsS<sub>4</sub>) by leptospirillum ferrooxidans. *Geochimica et Cosmochimica Acta* 72, 5616-5633.
- Craw, D., Falconer, D., Youngson, J.H. (2003). Environmental arsenopyrite stability and dissolution: theory, experiment and field observation. *Chemical Geology* 199, 71-82.
- Cruz, R., Lazaro, I., Rodriguez, J.M., Monroy, M., Gonzalez, I. (1997). Surface characterization of arsenopyrite in acidic medium by triangular scan voltammetry on carbon paste electrodes. *Hydrometallurgy* 46, 303-319.
- Dove, P., Crerar, D. (1990). Kinetics of quartz dissolution in electrolyte solutions using a hydrothermal mixed flow reactor. *Geochimica et Cosmochimica Acta* 54 (4), 955-969.
- Drljaca, A., Hubbard, C.D., van Eldik, R., Asano, T., Masilevsky, M.V., le Noble, W.J. (1998). Activation and reaction volumes in solution 3. *Chemical Reviews* 98 (6), 2167-2290.
- Dutta, B.K. (2007). *Principles of mass transfer and separation processes*. New Delhi, Prentice-Hall of India.
- Fogler, H.S. (2006). *Elements of chemical reaction engineering*. Upper Saddle River, NJ, Prentice Hall PTR.
- Fernandez, P., Linge, H., Willing, M.J. (1996). Oxidation of arsenopyrite (FeAsS) in acid part I: stoichiometry and reaction scheme. *Journal of Applied Electrochemistry* 26, 585-591.
- Karamalidis, A.K., Parthasarathy, H., Dzombak, D. (2012). Methods, Apparatuses, and Systems for Mineral Dissolution Assays. Provisional patent application, Docket No. 2012-146.

- Kharaka, Y.K., Hanor, J.S., Heinrich, D.H., Karl, K.T. (2007). Deep fluids in the continents: I. Sedimentary basins. In *Treatise on Geochemistry*, Pergamon: Oxford, 1-48.
- Knauss, K., Wolery, T. (1988). The dissolution kinetics of quartz as a function of pH and time at 70°C. *Geochimica et Cosmochimica Acta* 52 (1), 43-53.
- Levenspiel, O. (1972). *Chemical Reaction Engineering*, 2<sup>nd</sup> ed., John Wiley and Sons, New York, 578.
- McCabe, W.L., Smith, J.C., Harriott, P. (2005). *Unit operations of chemical engineering*. Boston, McGraw-Hill.
- McGuire, M., Banfield, J., Hammers, R.J. (2001). Quantitative determination of elemental sulfur at the arsenopyrite surface after oxidation by ferric iron: mechanistic implications. *Geochemical Transactions* 2, 25.
- McKibben, M., Tallant B.A., del Angel, J.K. (2007). Kinetics of inorganic arsenopyrite oxidation in acidic aqueous solutions. *Applied Geochemistry* 23, 121-135.
- Nesbitt, H., Muir, I., Pratt, A.R. (1995). Oxidation of arsenopyrite by air and air-saturated distilled water and implications for mechanism of oxidation. *Geochimica et Cosmochimica Acta* 59, 1773-1786.
- Papangelakis, V., Dempoulos, G. (1991). Acid pressure oxidation of pyrite: reaction kinetics. *Hydrometallurgy* 26 (3), 309-325.
- Paschka, M.G., Dzombak, D.A. (2004). Use of Dissolved Sulfur Species to Measure Pyrite Dissolution in Water at pH 3 and 6. *Environmental Engineering Science* 21(4), 411-420.
- Perovich, R. (1981a). Kinetics of dissolution of mechanically comminuted rock-forming oxides and silicates—I Deformation and dissolution of quartz under laboratory conditions. *Geochimica et Cosmochimica Acta* 45, 1665-1674.
- Perovich, R. (1981b). Kinetics of dissolution of mechanically comminuted rock-forming oxides and silicates—II Deformation and dissolution of oxides and silicates under laboratory conditions, and at the Earth's surface. *Geochimica et Cosmochimica Acta* 45, 1676-1686.
- Rimstidt, J.D., Barnes, H.L. (1980). The kinetics of silica-water interactions. *Geochimica et Cosmochimica Acta* 44, 1683-1699.
- Rimstidt, J.D., Dove, P.M. (1986). Mineral/solution reaction rates in a mixed flow reactor: Wollastonite hydrolysis. *Geochimica et Cosmochimica Acta* 50, 2509-2516.
- Rimstidt, J.D., Newcomb, W.D. (1993). Measurement and analysis of rate data: The rate of reaction of ferric iron with pyrite. *Geochimica et Cosmochimica Acta* 57, 1919-1934.

- Sjoberg, E., Rickard, D. (1984). Temperature dependence of calcite dissolution kinetics between 1 and 62°C at pH 2.7 to 8.4 in aqueous solutions. *Geochimica et Cosmochimica Acta* 48 (3), 485-493.
- Tester, W.J, Worley, G.W., Robinson, B.A, Grigsey, C.O., Feerer, J.L. (1994). Correlating quartz dissolution kinetics in pure water from 25 to 625°C. *Geochimica et Cosmochimica Acta* 58 (11), 2407-2420.
- Walker, F., Schreiber, M.E., Rimstidt, J.D. (2006). Kinetics of arsenopyrite oxidative dissolution by oxygen. *Geochimica et Cosmochimica Acta* 70 (7), 1668-1676.
- Wang, S., Jaffe, P.R. (2004). Dissolution of a mineral phase in potable aquifers due to CO<sub>2</sub> releases from deep formations; effect of dissolution kinetics. *Energy Conversion and Management* 45 (18-19), 2833-2848.
- Wieland, E., Stumm, W. (1992). Dissolution kinetics of kaolinite in acidic aqueous solutions at 25°C. *Geochimica et Cosmochimica Acta* 56 (9), 3339-3355.
- Wolfe, A.L., Liu, R., Stewart, B.W., Capo, R.C., Dzombak, D.A. (2007). A method for generating uniform size-segregated pyrite particle fractions. *Geochemical Transactions* 8, 9.
- Xu, T., Apps, J.A., Pruess, K., Yamamoto, H. (2007). Numerical modeling of injection and mineral trapping of CO<sub>2</sub> with H<sub>2</sub>S and SO<sub>2</sub> in a sandstone formation. *Chemical Geology* 242 (3-4), 319-346.
- Yunmei, Y., Yongxuan Z., Willams-Jones, A.E., Zhenmin, G., Dexian, L. (2004). A kinetic study of the oxidation of arsenopyrite in acidic solutions: implications for the environment. *Applied Geochemistry* 19, 435-444.
- Yunmei Y., Yongxuan, Z., Zhenmin, G., Gammons, C.H., Li, D. (2007). Rates of arsenopyrite oxidation by Oxygen and Fe (III) at pH 1.8-12.6 and 15-45°C. *Environmental Science and Technology* 41, 6460-6464.

## CHAPTER 4

### **A METHOD FOR PREPARATION AND CLEANING OF UNIFORMLY SIZED ARSENOPYRITE PARTICLES**

The information presented in this chapter was published in *Geochemical Transactions*, 15.1, 1-7 on October 2014. The co-authors of this paper were: John P. Baltrus, David A. Dzombak, Athanasios K. Karamalidis

#### **4.1 Abstract**

The oxidative dissolution of sulfide minerals, such as arsenopyrite (FeAsS), is of critical importance in many geochemical systems. A comprehensive understanding of their dissolution rates entails careful preparation of the mineral surface. Measurements of dissolution rates of arsenic from arsenopyrite are dependent on the size and degree of oxidation of its particles, among other factors. In this work, a method was developed for preparation and cleaning of arsenopyrite particles with size range of 150-250  $\mu\text{m}$ . Four different cleaning methods were evaluated for effectiveness based on the removal of oxidized species of iron (Fe), arsenic (As) and sulfur (S) from the surface. The percentage oxidation of the surface was determined using X-ray photoelectron spectroscopy (XPS), and surface stoichiometry was measured using scanning electron microscopy – energy dispersive X-ray spectroscopy (SEM-EDS). Results indicate that sonicating the arsenopyrite particles and then cleaning them with 12N HCl followed by 50% ethanol, and drying in nitrogen was the most effective method. This method was successful in greatly reducing the oxide species of Fe while completely removing oxides of As and S from the arsenopyrite surface. Although sonication and acid cleaning have been widely used for mineral preparation, the method described in this study can significantly reduce grain size heterogeneity as well as surface oxidation, which enable greater control in surface and dissolution experiments.

## 4.2 Introduction

Arsenopyrite ( $\text{FeAsS}$  (s)) is the most common arsenic (As) bearing pure phase mineral in the earth's crust. It is present in a variety of deposits such as hydrothermal, and magmatic systems and is an important reservoir of arsenic in the subsurface. Due to its common association with gold, it is often discarded as solid waste after gold extraction. The oxidation of arsenopyrite can release As into the environment which has potential environmental and health impacts (Corkhill and Vaughan 2009).

A number of studies (Walker et al. 2006; McKibben et al. 2008; Yunmei et al. 2004; Asta et al. 2010) have been conducted that investigate the kinetics of arsenopyrite dissolution with oxidants such as dissolved oxygen and iron, but there is significant variation in reported rates. One of the possible sources of this variation is the lack of a consistent mineral preparation procedure. Differences in mineral preparation can significantly affect grain size distribution as well as affect the extent of oxidation on the surface prior to conducting dissolution studies.

Previous research (McKibben et al. 2008) indicates that grain sizes can exert significant control over oxidation and dissolution rates. McKibben et al. (2008) determined that 150-250  $\mu\text{m}$  was the most convenient grain size for arsenopyrite dissolution. Arsenopyrite is typically prepared by homogenous grinding of the sample in a mortar and pestle, and then dry sieved to obtain required size fractions. Fine particles have high specific surface areas and their presence in these fractions can cause exaggerated dissolution rates (McKibben and Barnes 1986), as well as affect reproducibility of dissolution experiments. Typically, sonication of crushed mineral in ethanol or

acetone has been used to remove fines from the surface of sulfide minerals (McKibben et al 2008; Yunmei et al. 2007; Wolfe et al. 2007).

Dissolution studies can be further complicated by the presence of oxidized species on the mineral surface, which can lead to erroneous initial rates (Walker et al. 2006). Since the dissolution of arsenopyrite is oxidative in nature, oxidized species on the surface could drive subsequent dissolution of arsenopyrite. Acid cleaning has been used extensively in the literature as a method of cleaning sulfide minerals such as pyrite and arsenopyrite, but rely on indirect methods such as initial sulfate release to determine the extent of surface oxidation. Moses et al. (1987) reported the use of a combination of boiling 6 N HCl and acetone for surface cleaning of pyrite. The extent of oxidation was determined by monitoring the immediate release of  $\text{SO}_4^{2-}$  into solution. In the case of arsenopyrite, McKibben et al. (2008) reported the use of 1.8 N  $\text{HNO}_3$  for cleaning, while other groups (Walker et al. 2006; Asta et al. 2010) did not report methods for surface oxide removal. Oxidized iron and arsenic were observed to be removed from the surface of arsenopyrite when it was immersed in an air-saturated acetic acid solution (Buckley and Walker 1998). However, studies on the relative rates of elemental oxidation of arsenopyrite upon exposure to air have shown that As and Fe oxidize at rates faster than S (Nesbitt et al. 1995; Costa et al. 2002), suggesting that measurement of immediate release of sulfate into solution might not accurately reflect the extent of surface oxidation. As a result, there exists a need for direct evaluation of acid cleaning as a viable method for surface oxide removal on arsenopyrite prior to dissolution experiments. Typically, X-ray photoelectron spectroscopy (XPS) has been used to study surface oxidation on many minerals, but studies on arsenopyrite have been limited to vacuum fractured pristine surfaces and surfaces exposed to oxidants.

The objective of this study was to develop a reproducible and effective procedure to generate arsenopyrite particles of a uniform size fraction, free of surface oxides. The specific objectives were to (i) obtain arsenopyrite particles of the size fraction 150-250  $\mu\text{m}$  by removing fines adhering to the surface, and (ii) clean the surface of crushed particles to remove oxide species of Fe, As and S, without altering the stoichiometry of the mineral. The effectiveness of HCl and acetic acid for cleaning the surface of arsenopyrite was evaluated, based on their reported use for this purpose in the literature. The resulting method developed for cleaning the arsenopyrite surface was verified through XPS, particle size distribution analysis, and scanning electron microscopy – energy dispersive X-ray spectroscopy (SEM-EDS).

### **4.3 Materials and Methods**

#### **4.3.1 Mineral preparation and reagents**

Arsenopyrite from Hunan province in China was obtained from Wards Science Inc. (Rochester, NY) in 10g batches. Each batch was ground to powder using a porcelain mortar and pestle. The mortar and pestle were soaked with 10%  $\text{HNO}_3$  (w/v) overnight prior to being used for the first time. The powdered arsenopyrite was then dry sieved using 250  $\mu\text{m}$  and 150  $\mu\text{m}$  nylon sieves, which were also soaked in 10%  $\text{HNO}_3$  (w/v) overnight. The fraction of particles between 150-250  $\mu\text{m}$  was collected and transferred into a plastic tube. From every 10g batch of mineral, 5g in the 150-250  $\mu\text{m}$  fraction was obtained in this manner.

ACS reagent grade acids (HCl, acetic acid) were used in all cleaning experiments. All aqueous solutions were prepared using ultra-pure water (18.2 M $\Omega$ .cm, Barnstead Nanopure purifying

system). Laboratory grade nitrogen (99.9 % purity) was used in all experiments for mineral drying.

#### **4.3.2 Surface Cleaning**

Surface cleaning of arsenopyrite consisted of two steps -

1. Removal of fine particles adhered to the surface: particles significantly smaller than the sieved range can be electrostatically bound to the surface of larger particles. Such fines could result in exaggerated measurement of dissolution rates and hence need to be removed.

To remove fines, the particles were sonicated with 50 % (v/v) ethanol for 3 minutes using a Branson 5200 sonicator (Branson Inc., Connecticut, USA). Upon sonication, the ethanol phase turned black in color indicating suspended fine particles, and was subsequently decanted. This process was repeated three times and the particles were transferred to a petri dish and dried. Since drying the particles could affect the extent of surface oxidation, two different methods of drying were evaluated: a) drying the particles in air at 105 °C for 15 minutes and b) drying the particles in air for 1 hour at room temperature (25°C). The dried arsenopyrite particles were then subjected to XPS analysis and a method for drying was chosen based on the extent of surface oxidation. Limiting the extent of initial surface oxidation enables easier removal of oxidized layers from the surface.

2. Removal of oxide layers – limited surface oxidation can occur during crushing, sieving, and drying of arsenopyrite. This can impact initial dissolution rate determination, as the rate of oxide phase dissolution can be significantly different from that of arsenopyrite. Further, arsenopyrite dissolution being oxidative in nature could be affected by dissolved oxidized species. Removal

of oxides to the largest possible extent aids in accurate initial rate measurements. Oxides on the surface were removed by washing the arsenopyrite particles with acid.

Four methods for surface oxide removal were evaluated to identify an effective protocol for surface cleaning. These methods are shown in Table 4.1. As indicated there, the methods were similar except for the acid employed in the first rinse step, which involved either HCl (1N or 12N) or 50% v/v acetic acid.

After cleaning the particles, samples intended for XPS analysis were placed in glass vials, flushed with N<sub>2</sub>, crimped, and transported in vacuum containers capable of maintaining vacuum of 14.7" Hg for over 24h, (Desi-Vac 700 mL containers, Cole palmer, USA). All samples were analyzed the same day that the cleaning method was applied.

**Table 4.1.** Methods for cleaning surface oxides on arsenopyrite particles

<b>Method</b>	<b>Particle size</b>	<b>1<sup>st</sup> Rinse</b>	<b>2<sup>nd</sup> Rinse</b>	<b>3<sup>rd</sup> Rinse</b>	<b>Drying environment</b>	<b>Drying duration</b>	<b>Temp.</b>
1	150-250 µm	1N HCl (5 mins)	DI <sup>a</sup> water (3 mins)	50 % (v/v) ethanol (1 min)	N <sub>2</sub>	1 h	25°C
2	150-250 µm	12N HCl (5 mins)	DI water (3 mins)	50 % (v/v) ethanol (1 min)	N <sub>2</sub>	1 h	25°C
3	150-250 µm	50% (v/v) acetic acid (10 mins)	DI water (3 mins)	50 % (v/v) ethanol (1 min)	N <sub>2</sub>	1 h	25°C
4	150-250 µm	50% (v/v) acetic acid (20 mins)	DI water (3 mins)	50 % (v/v) ethanol (1 min)	N <sub>2</sub>	1 h	25°C

<sup>a</sup>DI: Deionized

### **4.3.3 Particle Size Distribution**

The effectiveness of sonication in removing fines was analyzed by measuring the average diameter of the particles by laser diffraction at Particle Tech Labs (Illinois, USA). Ten grams of sonicated and dried arsenopyrite were shipped in a 15 mL centrifuge tube (Corning USA) for analysis. The particle diameter distribution was calculated on a % volume basis.

### **4.3.4 XPS**

XPS measurements were carried out using a PHI 5600ci instrument. The XPS instrument employed monochromatic Al K $\alpha$  X-rays and the pass energy of the analyzer was 23.5 eV. The arsenopyrite powders were attached to the sample holder using double-sided adhesive, electrically conductive tape. Percentages of elemental oxidation were calculated from the relative areas of component peaks after the overall peak envelope for a given XPS peak was fitted with the component peaks due to oxidized and unoxidized forms of the element. Elemental concentrations were calculated using sensitivity factors provided by the instrument manufacturer. XPS peak fitting analyses were accomplished using CasaXPS data processing software. Binding energies were referenced to the C 1s peak for adventitious carbon at 284.6 eV.

### **4.3.5 SEM- EDS**

SEM was used for visual confirmation of arsenopyrite particle size and to evaluate surface composition of the particles. Once a suitable method for cleaning was chosen based on XPS data, arsenopyrite was prepared fresh, stored under vacuum, as previously described, and subjected to analysis within 2 hours of cleaning. The SEM was performed using a Philips XL30 FEG scanning microscope equipped with an SE Everhart Thornley detector and an Oxford INCA EDS

with full quantitative composition analysis. The operating conditions were, accelerating voltage 10 kV, spot size 3, and a working distance of 10 mm. The SEM-EDS had a detection limit of 1% by weight.

## 4.4 Results and Discussion

### 4.4.1 Particle Size Analysis

The results of the particle size distribution are shown in Figure 4.1. The particles were normally distributed with a mean diameter of 208.9  $\mu\text{m}$  and a standard deviation of 1.764  $\mu\text{m}$ , and the median was 219.2  $\mu\text{m}$ . This suggests that while the distribution was not entirely symmetric, a large fraction of particles was within the size range of 150-250  $\mu\text{m}$ .

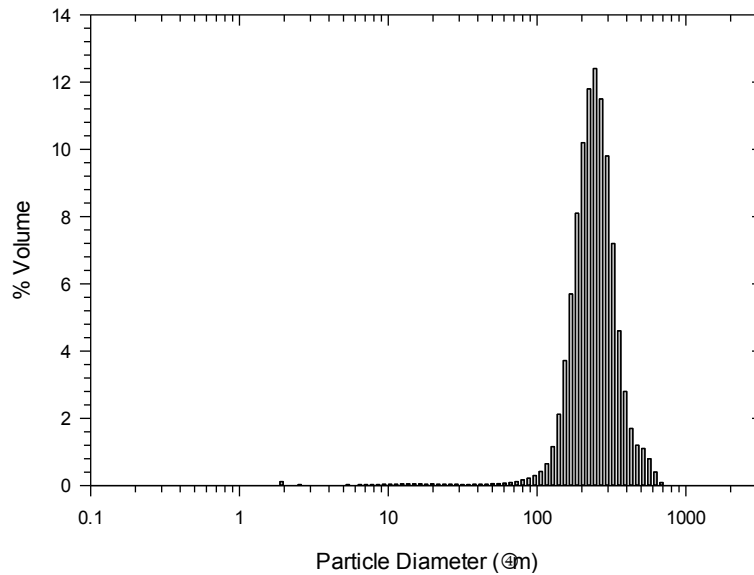


**Figure 4.1.** Particle size distribution of prepared arsenopyrite particles expressed as volume %.

## 4.4.2 XPS

### Drying

The effects of two different drying protocols on the extent of arsenopyrite surface oxidation can be seen by examining the results of curve fitting the three elemental regions: As 3d, Fe 2p<sub>3/2</sub>, and S 2p in Table 4.2.

**Table 4.2.** The effect of drying method on surface oxidation of arsenopyrite

Drying method	% Oxidation on the surface		
	Fe	As	S
In air, 105 °C	93.9	92.0	63.7
In air, 25 °C	43.8	42.9	11.9

Representative curve-fitted XPS spectra for a sample prior to treatment are shown in Figure 4.2 (A-C). Excellent fits of the overall As 3d spectra (Figure 4.2A) could be obtained using a minimum of three peak doublets (3d<sub>5/2</sub> and 3d<sub>3/2</sub> separated by 0.64 eV) corresponding to two types of oxidized arsenic species along with unoxidized arsenic. The oxidized species with 3d<sub>5/2</sub> binding energy 45.1 eV is most likely As<sup>5+</sup>, while the smaller doublet with a 3d<sub>5/2</sub> binding energy of 43.9 eV is between the values typically reported for As<sup>1+</sup> and As<sup>3+</sup> (Corkhill and Vaughan 2009). The Fe 2p<sub>3/2</sub> spectra were also fitted with 2 peaks, corresponding to oxidized and unoxidized Fe (Figure 4.2B). No attempt was made to resolve the broad peak assigned to oxidized Fe into components that could be attributed to individual oxidation states since our only concern was the relative amounts of oxidized and unoxidized Fe. The S 2p spectra were resolved into three sets of doublets (Figure 4.2C) corresponding to the unoxidized sulfide (S 2p<sub>3/2</sub> = 162.0

eV), a metal-deficient sulfide ( $S\ 2p_{3/2} = 163.2 - 163.7\ eV$ ), and oxidized sulfur in the form of sulfate ( $S\ 2p_{3/2} = 167.7\ eV$ ).

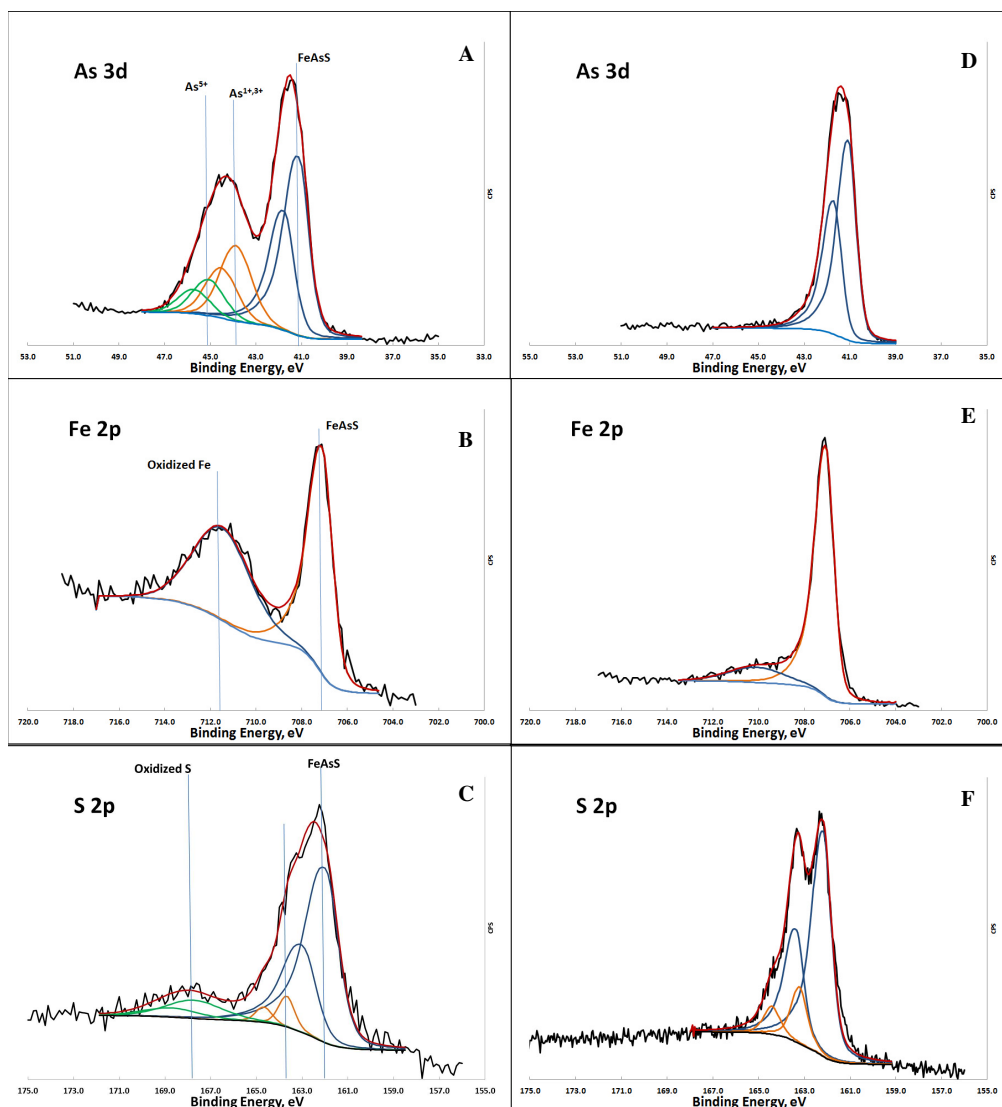


**Figure 4.2.** XPS spectra depicting speciation of As, Fe, and S on arsenopyrite. Representative curve fitted XPS spectra for (A) arsenic – As 3d, (B) iron- Fe 2p, and (C) sulfur – S 2p, for a sample of arsenopyrite prior to any treatments to remove surface oxidation. (D) Arsenic- As 3d, (E) iron- Fe 2p, and (F) sulfur- S 2p, for a sample of arsenopyrite treated with 12N HCl to remove surface oxides.

The reported percentages of oxidation were calculated based solely on the fraction of each element that is bound to oxygen. While the extents of oxidation measured from the Fe 2p<sub>3/2</sub> and As 3d spectra for a given sample agreed within experimental error, the degree of sulfur oxidized to sulfate measured from the S 2p spectra for the same sample was much less. This has been commonly attributed to the formation of a metal-deficient sulfide species in other studies of the oxidation of pyrite and arsenopyrite surfaces (Buckley and Walker 1998; Buckley and Woods 1987; Schaufuss et al. 2000). Further, sulfur on the arsenopyrite surface, oxidizes at a rate much lower than iron and arsenic (Nesbitt et al. 1995; Nesbitt and Muir 1998), thereby resulting in a lower extent of sulfur oxidation on the surface.

The results in Table 4.2 clearly indicate that the drying procedure at room temperature is preferable to drying at 105°C as it limits the extent of surface oxidation. Thus, this procedure was implemented for drying the samples prior to applying various treatments to remove surface oxidation.

#### Removal of surface oxide species

The percentages of oxidation of each element determined from peak fitting the XPS spectra of the arsenopyrite samples after the application of various cleaning methods being tested to remove oxidized surface species are shown in Figure 4.3. The corresponding XPS spectra for the sample cleaned with HCl are shown in Figures 4.2D-4.2F.

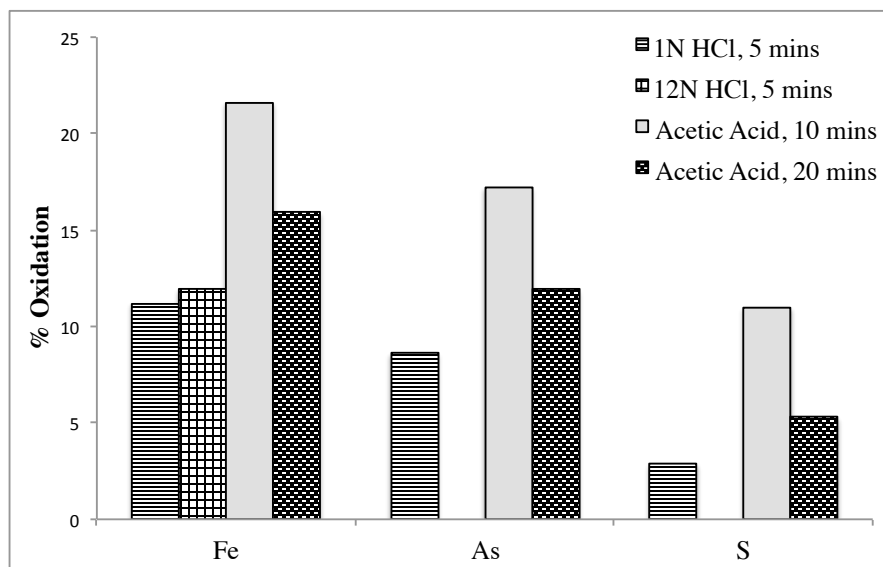


**Figure 4.3.** Percentages of Fe, As, and S oxidation determined from XPS spectra of arsenopyrite after various cleaning procedures.

The results indicate that treatment with the strong acid HCl was more effective in removing surface oxidation than treatment with the weak acid, acetic acid. A higher concentration of HCl was more effective in removing the last traces of surface oxidation over the given treatment time. Within the acetic acid treatments, increasing the treatment time resulted in increased removal of oxidized surface species, but even a treatment time of 20 minutes was insufficient for complete removal of oxidized species.

Only 12N HCl removed all oxidized species of sulfur and arsenic over the given treatment time. However, all four methods failed to remove oxidized iron completely, with 12N HCl being the most effective. For the case of 12N HCl, fitting of the Fe  $2p_{3/2}$  spectra still indicated some residual surface oxidation. The presence of oxidized iron species has also been observed on vacuum fractured surfaces of arsenopyrite by Nesbitt et al. (Nesbitt et al. 1995), who reported

that ~17% of the Fe on the surface could be attributed to Fe (III)-(As-S) species. Moreover, the overall higher surface sensitivity of the XPS measurement to the Fe 2p level compared to As 3d and S 2p and/or some small amount of preferential reoxidation of Fe during the sample's exposure to air during its transfer to the XPS instrument could have also resulted in the detection of oxidized iron species, even after cleaning the surface. Comparing the S 2p spectra before and after the HCl treatment, one can see that while all the sulfur oxidized to sulfate has been completely removed by the treatment, the relative percent of metal-deficient polysulfide increased from 5% to 17% of the non oxygen-bound sulfur species. Although metal deficient polysulfide species have been reported in vacuum fractured arsenopyrite (Corkhill and Vaughan 2009), oxidation of samples during procurement and grinding could have resulted in the formation of polysulfides on the surface (Buckley and Walker 1998; Buckley and Woods 1987; Schaufuss et al. 2000).

While the 12N HCl cleaning method can be used for other sulfide minerals, using 12N HCl might not be appropriate for acid volatile sulfides (AVS) such as galena (PbS), which dissolve in concentrated HCl (Cooper and Morse 1998).

#### **4.4.3 SEM-EDS**

SEM images of freshly prepared arsenopyrite particles, cleaned with 12N HCl and 50% ethanol are shown in Figure 4.4. The ground mineral particles are uniformly sized and the surfaces do not show the presence of any fine particles (Figure 4.4A). The arsenopyrite particles were analyzed for iron, arsenic and sulfur using EDS (Figure 4.4B) and the measured weight percentages were converted to stoichiometric quantities. The prepared arsenopyrite sample was

divided into ten batches and five measurements (Figure 4.4B) were made per batch. The average stoichiometry was found to be  $\text{Fe}_{1.04\pm 0.08}\text{As}_{0.96\pm 0.05}\text{S}_{1.03\pm 0.04}$ . Considering that sulfur on arsenopyrite oxidizes at a rate lower than Fe and As (Nesbitt et al. 1995; Nesbitt and Muir 1998), the surface is expected to be sulfur enriched after cleaning with HCl. While XPS measurements indicated some enrichment, the average mineral stoichiometry measured by SEM-EDS was close to the theoretical stoichiometry of FeAsS. Surface sulfur enhancement measured through XPS can be included in dissolution rate calculations while conducting dissolution experiments to ensure accurate measurement of rates of Fe, As, and S release.

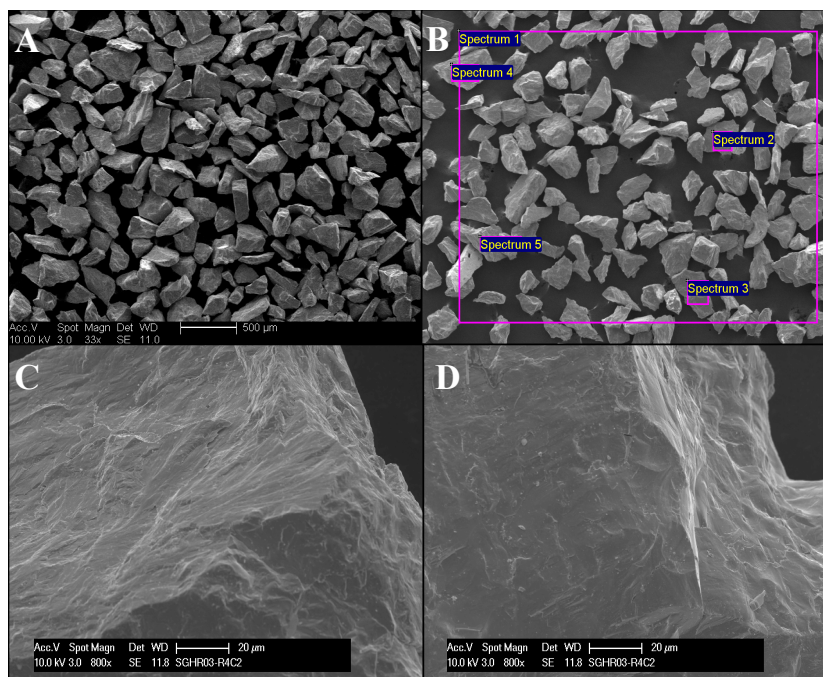


**Figure 4.4.** SEM analysis of arsenopyrite particles. (A) Secondary electron image of clean size segregated arsenopyrite particles (B) Sample surface composition measurements of arsenopyrite using SEM-EDS. Comparison of SEM images between (C) arsenopyrite surface prior to acid treatment and (D) arsenopyrite surface after cleaning with 12N HCl reveals no significant morphological changes to the surface of the mineral.

Further, SEM images of arsenopyrite particles before (Figure 4.4C) and after treatment with 12N HCl (Figure 4.4D) did not reveal any significant morphological changes on the surface suggesting minimal change in the specific surface area of the mineral particles due to acid treatment. A comparison between the images depicts an absence of pitting or etching from acid treatment.

#### 4.5 Conclusions

A method for preparing size-segregated arsenopyrite particles, free of surface oxides for dissolution experiments was developed. A summary of the developed method is shown in Table 4.3. Arsenopyrite particles in the size fraction of 150-250  $\mu\text{m}$  was obtained by sonication of suspensions of crushed particles in 50% v/v ethanol and verified by particle size distribution and SEM analysis. Four methods of cleaning the surface were investigated and the method involving 12N HCl and 50% ethanol was found to be the most effective. XPS analysis revealed the method succeeded in removing all oxide species of S and As on the surface, while only 12% of surface Fe remained oxidized.

**Table 4.3.** Summary of arsenopyrite preparation method

1	Arsenopyrite was crushed in a mortar and pestle. Dry sieved to obtain 150-250 $\mu\text{m}$ size fraction.
2	Sonicated in 50% ethanol and supernatant decanted (thrice).
3	Dried under $\text{N}_2$ at room temperature for 1 hour.
4	Rinsed with 12N HCl for 5 minutes, followed by water (3 minutes) and 50% ethanol (1 minute)
5	Dried under $\text{N}_2$ for 1 hour.

## 4.6 References

- Asta, M.P., Cama, J., Ayora, C., Acero, P., de Giudici, G. (2010). Arsenopyrite dissolution rates in O<sub>2</sub>-bearing solutions. *Chemical Geology* 2010, 273 (3–4): 272-285.
- Buckley AN, Walker GW: The surface composition of arsenopyrite exposed to oxidizing environments. *Applied Surface Science*, 35 (2): 227-240.
- Buckley, A.N., Woods, R. (1987). The surface oxidation of pyrite. *Applied Surface Science*, 27 (4): 437-452.
- Cooper, D.C., Morse, J.W. (1998). Extractability of Metal Sulfide Minerals in Acidic Solutions: Application to Environmental Studies of Trace Metal Contamination within Anoxic Sediments. *Environmental Science & Technology*, 32 (8): 1076-1078
- Corkhill, C., Vaughan, D. (2009). Arsenopyrite oxidation - A review. *Applied Geochemistry*, (12): 2342-2361.
- Costa, M., Botelho do Rego, A., Abrantes, L. (2002). Characterization of a natural and an electro-oxidized arsenopyrite: a study on electrochemical and X-ray photoelectron spectroscopy. *International journal of mineral processing*, 65(2): 83--108.
- Mckibben, M.A., Barnes, H.L. (1986). Oxidation of pyrite in low temperature acidic solutions: Rate laws and surface textures. *Geochimica et Cosmochimica Acta*, 50 (7): 1509-1520.
- Mckibben, M.A., Tallant, B., Del Angel, J. (2008). Kinetics of inorganic arsenopyrite oxidation in acidic aqueous solutions. *Applied Geochemistry*, 23 (2): 121-135.
- Moses, C., Kirk Nordstrom, D., Herman, J., Mills, A. (1987). Aqueous pyrite oxidation by dissolved oxygen and by ferric iron. *Geochimica et Cosmochimica Acta*, 51(6): 1561--1571.
- Nesbitt, H., Muir, I., Prarr, A. (1995). Oxidation of arsenopyrite by air and air-saturated, distilled water, and implications for mechanism of oxidation. *Geochimica et Cosmochimica Acta*, 59 (9): 1773-1786.
- Nesbitt, H., Muir, I. (1998). Oxidation states and speciation of secondary products on pyrite and arsenopyrite reacted with mine wastewaters and air. *Mineralogy and Petrology*, 62 (1-2): 123-144.
- Schaufuss, A.G., Nesbitt, H.W., Scaini, M.J., Hoechst, H., Bancroft, M.G., Szargan, R. (2000). Reactivity of surface sites on fractured arsenopyrite (FeAsS) toward oxygen. *The American Mineralogist*, 85 (11-12): 1754.
- Walker, F.P., Schreiber, M.E., Rimstidt, J.D. (2006). Kinetics of arsenopyrite oxidative dissolution by oxygen. *Geochimica et Cosmochimica Acta*, 70 (7): 1668-1676.
- Wolfe, A.L., Liu, R., Stewart, B.W., Capo, R.C., Dzombak, D.A. (2007). A method for generating uniform size-segregated pyrite particle fractions. *Geochemical Transactions*, 8 (1): 9.
- Yunmei, Y., Yongxuan, Z., Williams-Jones, A., Zhenmin, G., Dexian, L. (2004). A kinetic study

of the oxidation of arsenopyrite in acidic solutions: implications for the environment. *Applied Geochemistry*, 19 (3): 435-444.

Yunmei, Y., Yongxuan, Z., Zhenmin, G., Gammons, C.H., Li, D. (2007). Rates of Arsenopyrite Oxidation by Oxygen and Fe (III) at pH 1.8-12.6 and 15-45 °C. *Environmental Science & Technology*, 41 (18): 6460-6464.

## CHAPTER 5

### **ALKALI AND ALKALINE EARTH METAL CHLORIDE SOLUTIONS AS REACTANTS IN SULFIDE MINERAL DISSOLUTION**

The information presented in this chapter has been submitted for publication. The co-authors of this paper were: David A. Dzombak and Athanasios K. Karamalidis

## 5.1 Abstract

Alkaline metal chlorides have predominantly been used to maintain bulk solution ionic strength in sulfide mineral dissolution studies, especially in the presence of oxidizing agents such as  $O_2$  and  $Fe^{3+}$ . The potential reactivity of these electrolytes has also been neglected under anoxic conditions, as exist in most saline subsurface environments. Arsenopyrite ( $FeAsS(s)$ ), galena ( $PbS(s)$ ), and pyrite ( $FeS_2(s)$ ) are representative sulfide mineral phases, dissolution of which affects many ecosystems. In this study, dissolution experiments with these minerals were conducted under anoxic conditions with 10 mM solutions of  $NaCl$ ,  $CaCl_2$ , and  $MgCl_2$  at constant pH. Results show that these electrolytes affect mineral dissolution: either increasing or decreasing the rate, suggesting that they can no longer be considered inert with respect to sulfide mineral dissolution under anoxic conditions. The extent to which sulfide mineral dissolution was affected is measurable and depends on the anionic species on the mineral and cationic species in solution.

## 5.2 Introduction

Traditionally, alkali and alkaline earth metal chlorides such as NaCl, MgCl<sub>2</sub> and CaCl<sub>2</sub> have been used to control bulk solution ionic strength while studying mineral dissolution with strong reactants. These reagents are considered inert and are not expected to affect dissolution significantly aside from influencing the activity of reactants through ionic strength. This is particularly true with the study of sulfide minerals where dissolution experiments are conducted with oxidants such as Fe<sup>3+</sup> and dissolved oxygen (N'Unez et al. 1990; Awakura et al. 1980; Barrett and Anderson 1982; Ohmoto et al. 1994). In strongly oxidizing environments, any effect of background electrolytes on dissolution could be negligible as compared to that caused by oxidants, and hence not observable. Therefore the effect of these electrolytes as possible reactants for dissolution has not been explored. With the emergence of interest in aqueous environments that are anoxic and have high concentrations of alkali metal chlorides, such as brines in deep saline formations, the potential for these salt solutions to influence mineral dissolution merits examination.

The ability of sulfide minerals to react with waters and contribute to acid mine drainage (AMD) and toxic metal mobilization (As, Pb, Cd, Hg, etc.) has driven study of the factors and conditions controlling their dissolution (Vaughan 2006). The dissolution of sulfide minerals has been studied under varying solution conditions including in the presence of alkaline metal chlorides in solution. Non-oxidative acidic dissolution of sphalerite ((Zn,Fe)S (s)) and galena (PbS(s)) has been studied in the presence of sodium and magnesium chloride solutions. The reported increases in dissolution were attributed to a change in H<sup>+</sup> ion activity, and not determined to be a direct effect of the electrolyte (N'Unez et al. 1990; Awakura et al. 1980; Barrett and Anderson

1982). Limited studies have been conducted on the dissolution of pyrite ( $\text{FeS}_2(\text{s})$ ) in the presence of sodium chloride in solution (Ohmoto et al. 1994), and on oxidative dissolution of pyrite and arsenopyrite ( $\text{FeAsS}(\text{s})$ ) in electrolyte solutions (Walker et al. 2006; Lin and Zheng 1996). These studies assume the only reactants in dissolution to be  $\text{H}^+$  or the oxidant species, and the potential interaction of the chloride salts in solution with the minerals, have not been investigated.

The objective of this study was to determine the effect of  $\text{NaCl}$ ,  $\text{CaCl}_2$ , and  $\text{MgCl}_2$  solutions on the anoxic dissolution of  $\text{FeS}_2(\text{s})$ ,  $\text{FeAsS}(\text{s})$ , and  $\text{PbS}(\text{s})$ . For this purpose, dissolution experiments were conducted in a column plug-flow reactor and anoxic influent solutions, at a low pH to avoid Fe precipitation and mass transfer limitation. Effluent concentrations of constituent elements were measured and compared to the variables in each experiment to determine the parameters that influenced the dissolution of these minerals under anoxic conditions. Although most sulfide mineral dissolution experiments have been conducted in batch or mixed flow reactor systems, assuming that reactions with alkali and alkaline earth metal chlorides are very slow, plug-flow reactors would be ideal systems for dissolution as they have inherently high solid-liquid ratios (Rimstidt and Newcomb 1993).

### **5.3 Materials and Methods**

Dissolution of galena, arsenopyrite, and pyrite was studied with 10 mM concentrations of  $\text{NaCl}$ ,  $\text{MgCl}_2$ , and  $\text{CaCl}_2$  in de-oxygenated, carbonate-free solutions under nitrogen atmosphere. The pH was adjusted to  $2.56 \pm 0.01$  by the addition of  $6 \pm 0.4$  mL of 1N  $\text{HCl}$  to 2L of solution and hence the  $\text{H}^+$  activity was constant. However, the ionic strengths of the  $\text{NaCl}$  solutions were

lower than that of  $\text{MgCl}_2$  and  $\text{CaCl}_2$  solutions resulting in  $\text{Na}^+$  activity being higher than  $\text{Mg}^{2+}$  and  $\text{Ca}^{2+}$  in solution. To provide for a direct comparison between electrolytes, an additional experiment with  $\text{NaCl}$ , with  $\text{Na}^+$  activity similar to that of  $\text{Mg}^{2+}$  and  $\text{Ca}^{2+}$  in 10 mM  $\text{MgCl}_2$  and  $\text{CaCl}_2$  respectively, was conducted for arsenopyrite. The activities in solution were calculated using the Extended Debye-Huckel Equation (Benjamin 2010), and the corresponding concentration of  $\text{NaCl}$  was calculated to be 5.6 mM.

Experiments were conducted in a small-scale plug flow packed column system described by Parthasarathy et al. (2013), under nitrogen atmosphere. The system consisted of a Poly Ether-Ether Ketone (PEEK) column of length 5 cm and internal diameter 0.5 cm. The plug-flow system was shown to be capable of measuring dissolution rates up to  $5 \times 10^{-5} \text{ mol/m}^2\text{s}$  of minerals free of mass transfer limitations by Parthasarathy et al., (2013). At low reaction rates as those observed in this study, the system is reaction rate controlled (Parthasarathy et al. 2013). The reactant solutions were prepared with de-ionized (DI) water (18.2 M $\Omega$ ) and purged with laboratory grade nitrogen for 20 hours prior to the experiments, to remove any dissolved oxygen and carbonate in the system. Nitrogen sparging was continued for the entire duration of each experiment. Further, the minerals were acid washed to remove oxidized layers from the surface prior to experiments based on the method described in Parthasarathy et al. (2014). The column was packed with mineral and influent solution was fed at a constant flow rate of 1ml/min. The average pore volume in the column was found to be  $0.45 \pm 0.05$  ml. The masses of specific solid phase packed were  $2.5 \pm 0.1$  g,  $2.7 \pm 0.05$  g, and  $1.7 \pm 0.1$  g of arsenopyrite, galena, and pyrite respectively. The entire system was placed in a nitrogen filled glove bag and the dissolved oxygen concentration in the influent and inside the bag was constantly monitored using an

Accumet XL 60 D.O. meter and the D.O was maintained at 0.00 mg/L. Control experiments with nitrogen purged deionized water (pH 2.55, HCl) were also conducted. A complete description of the materials and methods is presented in the supporting information section (Appendix C).

## **5.4 Results and Discussion**

Effluent concentrations of S, As, and Fe for arsenopyrite, S and Pb for galena, and S and Fe for pyrite were monitored with respect to time, and steady-state concentrations were obtained for each experiment. Since parameters such as mass of mineral, specific surface area, flow rate, and residence time were constant for experiments with each mineral, the steady state concentrations were used as proxies for reaction rate. Steady state concentrations were determined to be reached after 12 hours of dissolution, if the effluent concentration was within  $\pm 15\%$  of the average over 8 hours. In the case of Fe release from arsenopyrite and pyrite, a large variability in effluent concentration was observed; potentially due to the presence of Fe hotspots or/and amorphous iron phases in natural mineral samples. However, Fe concentrations were averaged over the same time frame as As and S which resulted in large error bars for Fe steady state concentrations. Further, effluent concentrations can be influenced by dissolution mechanisms (such as a shrinking core model for galena dissolution) and hence concentrations were averaged over the same time period to provide comparable steady state concentrations.

The steady state concentrations were then plotted against the different experimental parameters (electrolyte concentration, cation activity, ionic strength, anion activity, and electron affinity of the cation) to determine the variable that dissolution rates were most correlated with. The results

of this analysis revealed that the dissolution of these sulfide minerals was dependent on the activities of cations and anions in solution, suggesting an interaction between the ions in solution and the mineral surface, leading to dissolution. The raw dissolution data are presented in the supplementary section (Appendix C: Figures C2- C5) and plots for galena, pyrite, and arsenopyrite depicting the parameter with strongest correlation to dissolution rates are shown in Figures 5.1 and 5.2. Each point on the plots represents a single experiment, with the error bars depicting  $\pm 1\sigma$  uncertainty in steady state concentrations. Since  $H^+$  activity, temperature and pressure were constant for all experiments, they were not considered in the analysis.

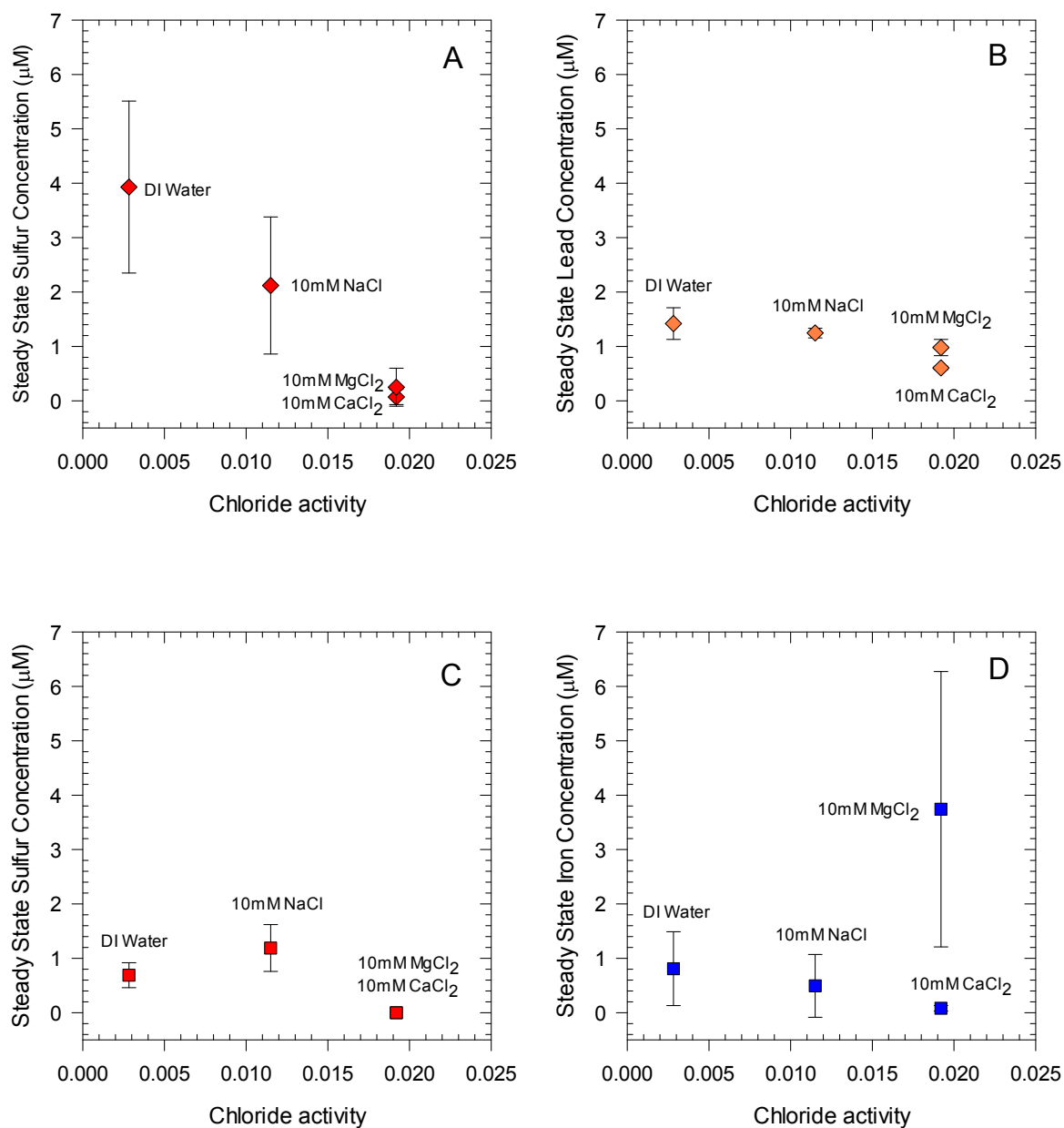


**Figure 5.1.** Galena and pyrite dissolution by alkali metal chloride electrolytes. pH 2.55, T=25 °C, P = 1 bar: **(A)** Steady state S concentration ( $\mu\text{M}$ ) from galena vs. anion activity; **(B)** Steady state Pb concentration ( $\mu\text{M}$ ) from galena vs. anion activity; **(C)** Steady state S concentration ( $\mu\text{M}$ ) from pyrite vs. anion activity; **(D)** Steady state Fe concentration ( $\mu\text{M}$ ) from pyrite vs. anion activity

The results show that dissolution of the three sulfide minerals under anoxic conditions was affected by the presence of alkali and alkaline earth metal chlorides in solution, at constant  $H^+$  activity. In general, the dissolution rates of both  $FeS_2(s)$  and  $PbS(s)$  decreased in the presence of alkaline metal chlorides, but the trends observed for  $FeAsS(s)$  were constituent element specific: a decrease in S dissolution rate was observed while As dissolution rate increased. No discernible trend was observed with Fe release due to the large variability in steady state concentrations.

With  $PbS(s)$ , both sulfur and lead release rates decreased in solutions of alkali metal chlorides. The steady state concentrations were found to be inversely proportional to the chloride ion activity in solution, as depicted in Figures 5.1A and 5.1B. Experiments with 10mM  $MgCl_2$  and 10mM  $CaCl_2$ , with similar chloride ion activities revealed higher dissolution rates of Pb and S with  $MgCl_2$  than  $CaCl_2$ . Dissolution trends similar to galena were observed with Fe and S release from  $FeS_2(s)$ . An increase in chloride activity resulted in a decrease in steady state concentrations of both elements (Figures 5.1C and 5.1D). However, in the case of pyrite, two exceptions were observed: (i) the release rate of sulfur was highest with 10mM  $NaCl$ , (ii) an inordinately high concentration of Fe was observed with 10mM  $MgCl_2$  solution.

The dissolution of  $FeAsS(s)$  was found to follow two distinct trends. The steady state concentrations of As were found to be dependent on cation activity (Figures 5.2A) in solution and not on the  $Cl^-$  activity. In experiments with similar cation activities, ( $Na^+$  in 5.6 mM  $NaCl$ , and  $Mg^{2+}$  and  $Ca^{2+}$  in 10 mM  $MgCl_2$  and  $CaCl_2$  respectively) the steady state concentrations of As were similar. The release rate of sulfur from  $FeAsS(s)$  however, decreased in the presence of

chloride salts in solution and was found to be dependent on  $\text{Cl}^-$  activity in solution (Figure 5.2C), similar to galena and pyrite. Fe release from arsenopyrite did not reveal any discernible trends (Figure 5.2B). The concentrations of Fe released were higher than As effluent concentrations, particularly with the D.I water (pH 2.55) experiment, which is consistent with Fe dissolution from more than one phase in the mineral.

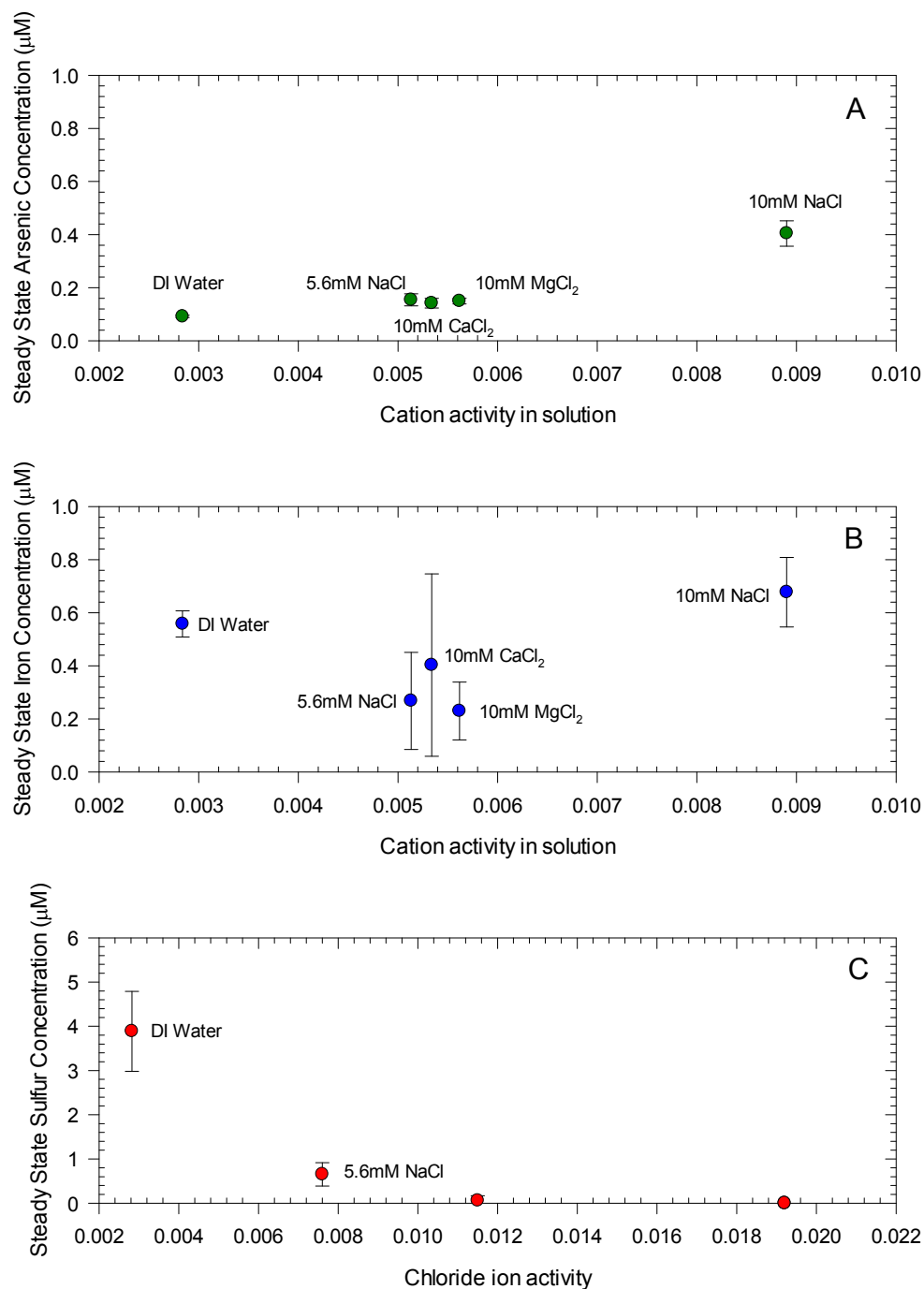


**Figure 5.2.** Arsenopyrite dissolution by alkali metal chloride electrolytes. pH 2.55, T=25 °C, P = 1 bar: (A) Steady state As concentration (μM) vs. cation activity; (B) Steady state Fe concentration (μM) vs. cation activity; (C) Steady state S concentration (μM) vs. anion activity

One approach to interpretation of these dissolution results is to consider the reaction of sulfide minerals with solutions of alkali and alkaline earth metal chlorides as interactions between the anions on the mineral surface and the cations in solution. A schematic depicting these interactions is presented in Figure 5.3. Experiments conducted to determine the isoelectric points ( $\text{pH}_{\text{i.e.p}}$ ) of galena, pyrite, and arsenopyrite under anoxic conditions have revealed a  $\text{pH}_{\text{i.e.p}} < 2$  for all three minerals (Bebie et al. 1998). As a result, at a pH of 2.55 as in this study, the mineral surfaces are negatively charged and would react with cations in solution ( $\text{H}^+$  and  $\text{Na}^+/\text{Ca}^{2+}/\text{Mg}^{2+}$  depending on the alkali metal chloride). Multiple experiments aimed at understanding the speciation on these minerals have revealed the major anionic groups to be sulfide ( $\text{S}^{2-}$ ) on galena (Hernan et al. 1995), disulfide ( $\text{S}_2^{2-}$ ) on pyrite (Nesbitt et al. 1998), and  $\text{As}^-$  and  $\text{S}^-$  as a polyanion ( $[\text{AsS}]^{2-}$ ) on arsenopyrite (Corkhill and Vaughan 2009). These anions ( $\text{S}^{2-}$ ,  $\text{S}_2^{2-}$ ,  $\text{S}^-$ , and  $\text{As}^-$ ) exhibit nucleophilic properties arising from the availability of lone pairs of electrons, while the cations in solution ( $\text{H}^+$ ,  $\text{Na}^+$ ,  $\text{Mg}^{2+}$ ,  $\text{Ca}^{2+}$ ) can act as electrophiles due to their ability to accommodate an electron pair from donor atoms (Pearson 1968). We hypothesize that the dissolution process is based on interactions between nucleophilic anions on the mineral surface and electrophilic cations in solution and depends on three factors: (i) nucleophilic reactivity of the anions on the surface, (ii) activity of other anions in solution that may compete with the surface nucleophiles, and (iii) the electronegativity of cations in solution.

#### **5.4.1 Nucleophilic reactivity of anions on the surface**

One factor that would influence reactions between the mineral and cations in solution is the nature of anions on the mineral surface. The nucleophilic reactivity of a species is measured by

the rate of reaction with a specific electrophilic substrate (Edwards and Pearson 1962). Generally, nucleophilic reactivity is correlated to basicity, or the ability of a species to take up a proton, and the polarizability of the species (Edwards and Pearson 1962). The relationship of nucleophilic reactivity to basicity is implicit in the fact that nucleophile-electrophile interactions are generalized acid-base type reactions (Edwards and Pearson 1962), and hence an increase in basicity is expected to lead to an increase in nucleophilic character. However, the proton is unique in that it does not face any restrictions in its interactions with a nucleophile. Any other electrophile will be restricted by its additional electrons due to the constraints of Pauli's exclusion principle (Edwards and Pearson 1962). This is observed in the S species, which is more reactive to  $H^+$  than to the other cationic species ( $Na^+$ ,  $Ca^{2+}$ ,  $Mg^{2+}$ ). Previous dissolution experiments under anoxic conditions and in the absence of cations other than  $H^+$  report that rates of dissolution of galena, pyrite, and sphalerite are proportional to  $H^+$  activity (Sun et al. 1991; Weerasooriya and Tobschall 2005). Proposed reaction mechanisms involve the protonation of the negatively charged surface resulting in a charged surface complex that subsequently dissociates leading to mineral dissolution (Sun et al. 1991; Weerasooriya and Tobschall 2005). Although the minerals have a common electron donor atom in sulfur, different sulfur groups exhibit slightly different nucleophilic reactivities due to differences in charge of the sulfur atom (-1 in disulfides and -2 in sulfides) and polarizability (Pearson 1968).

The effect of polarizability is also seen in the release of As from  $FeAsS(s)$ . The polarizability of bonding and nonbonding electrons away from the nucleophiles reduces repulsions due to Pauli exclusion and increases nucleophilic character (Edwards and Pearson 1962). Owing to the opposing trends of polarizability and electronegativity in the periodic table (Carey and Sundberg

2007), arsenic is a better nucleophile than the sulfur species. This polarizability of  $\text{As}^-$  enables greater interaction with electrophiles in solution, which results in an increase of As release with an increase in cation activity (Figure 5.2B).

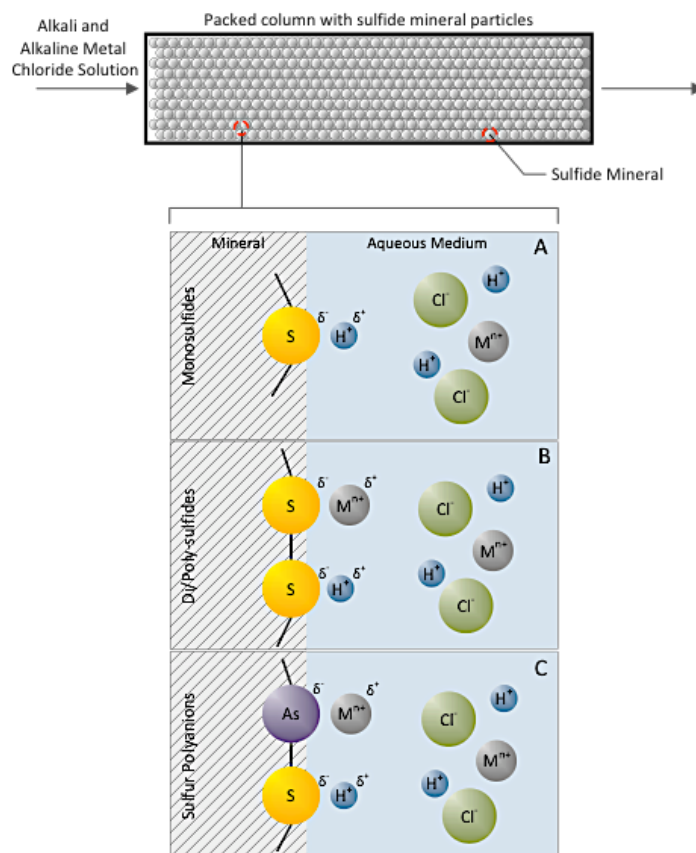


**Figure 5.3.** Schematic of the dissolution of sulfide minerals under anoxic conditions with alkaline metal chlorides in solution. Three kinds of nucleophilic anions on sulfide minerals are depicted – (A) Monosulfides; (B) Disulfides/Polysulfides; and (C) Sulfur-Arsenic polyanion. The high proton affinity of S anions enables reaction with  $\text{H}^+$ , while the higher nucleophilic reactivity of  $\text{As}^-$  facilitates interaction with electrophilic cations in solution.

### 5.4.2 Activity of competing anions in solution

The interactions between electrophilic cations in solution and the anions on the mineral surface are also dependent on other anions present in solution. Given that  $H^+$  activity was constant in the experiments, the dissolution of sulfur was not expected to vary. However, the addition of excess chloride results in interactions between protons and  $Cl^-$  thereby inhibiting proton interactions with the mineral and is reflected as a decrease in dissolution of sulfur with the increase of chloride in solution (Figures 5.1A, 5.1C, and 5.2C). The high electronegativity of  $Cl^-$  limits its nucleophilicity and its effect of inhibiting the interactions between the cations and  $As^-$  is low in the range of concentrations studied. Hence, similar cation activities yield similar steady state dissolution concentrations, even with differences in the activity of  $Cl^-$  (Figure 5.2B). At higher  $Cl^-$  activities, the inhibitory effect on dissolution may be higher.

In this study, only the effect of  $Cl^-$  was observed, but the inhibitory effect may vary depending on the anion and its tendency for interaction with protons and other cations in solution. These interactions are dependent on the basicity and nucleophilicity of the specific electrolyte anion. For instance, with respect to halides, basicity decreases but nucleophilicity increases down the group of the periodic table (Carey and Sundberg 2007). Therefore,  $F^-$  is expected to have a higher inhibitory effect on  $H^+$  while  $I^-$  ion would inhibit other cations to a larger extent.

### 5.4.3 Electronegativity of cations in solution

Although cations affect As release from FeAsS directly, they also affect sulfur release indirectly. The ability of chloride ions to limit  $H^+$  binding to the surface is dependent on other cations in solution, which is observed between experiments with 10mM  $MgCl_2$  and 10mM  $CaCl_2$ . While both solutions have the same activity of  $Cl^-$ , the more electronegative  $Mg^{2+}$  interacts with  $Cl^-$  to a larger extent than  $Ca^{2+}$  causing increased availability of protons leading to higher dissolution with 10mM  $MgCl_2$  as seen with galena (Figures 5.1A and 5.1B).

Based on the trends and properties discussed above, it is clear that  $NaCl$ ,  $MgCl_2$ , and  $CaCl_2$  can no longer be considered inert with respect to reactivity, at least for sulfide minerals. The rate of dissolution of sulfide minerals under anoxic conditions is controlled by the relative activities of the reactive cation(s) ( $H^+$  for galena and pyrite,  $H^+/Na^+/Ca^{2+}/Mg^{2+}$  for arsenopyrite in this study) and the inhibitory anion(s) in solution. The propensity to react with a cation is dependent on the nucleophilicity of the species in the mineral surface and in general, the rate of dissolution of sulfur decreases in the presence of alkali and alkaline earth metal chlorides, as sulfide groups tend to react only with protons. The case of arsenic release from arsenopyrite serves as an exception as  $FeAsS(s)$  contains a second and stronger nucleophilic group in  $As^-$ .

While this study offers an insight into the interaction of electrolytes with sulfide mineral surfaces under low electrolyte concentration conditions, high concentration conditions and long-term dissolution trends remain unexplored. However, certain implications of this work can be extended to geologic systems. The effect of brines on mineral dissolution will be driven by their

compositions. With Na-Ca-Cl brines, the extent to which sulfide mineral dissolution occurs will be dependent on the relative concentrations of  $\text{Cl}^-$ ,  $\text{Na}^+$ , and  $\text{Ca}^{2+}$ . Further, an approach based on electrophile-nucleophile interactions is not necessarily limited to sulfide minerals but could be valid for any solid surface that contains potential donor atoms including but not limited to cyanides, thiocyanides, and carbides

## 5.5 References

- Awakura, Y., Kamei, S., Majima, H. (1980). A kinetic study of nonoxidative dissolution of galena in aqueous acid solution. *Metallurgical Transactions B*, 11, 377-381.
- Barrett, T., Anderson, G. (1982). The solubility of sphalerite and galena in NaCl brines. *Economic Geology*, 77, 1923-1933.
- Bebie, J.; Schoonen, M.; Fuhrmann, M.; Strongin, D. (1998). Surface charge development on transition metal sulfides: an electrokinetic study. *Geochimica et Cosmochimica Acta*, 62, 633-642.
- Benjamin, M. (2010). *Water Chemistry*. Waveland Press, Long Grove, Ill. Ed. 1, pp. 29-30.
- Carey, F., Sundberg, R. (2007). *Advanced organic chemistry*. Springer, New York, NY. Ed. 1.
- Corkhill, C., Vaughan, D. (2009). Arsenopyrite oxidation--A review. *Applied Geochemistry*, 24, 2342-2361.
- Edwards, J., Pearson, R. (1962). The factors determining nucleophilic reactivities. *Journal of the American Chemical Society*, 84, 16-24.
- Hernan, L., Morales, J., Sanchez, L., Tirado, J., Espinos, J. (1995). Diffraction and XPS studies of misfit layer chalcogenides intercalated with cobaltocene. *Chemistry of materials*, 7, 1576-1582.
- Lin, H.; Zheng, Z. (1996). Electrochemical oxidation of arsenopyrite in chloride solutions. *Hydrometallurgy*, 42, 411-424.
- Nesbitt, H., Bancroft, G., Pratt, A., Scaini, M. (1998). Sulfur and iron surface states on fractured pyrite surfaces. *American Mineralogist*, 83, 1067-1076.
- N'UNEZ C., Espiell, F., Garc'ia-Zayas, J. (1990). Kinetics of galena leaching in hydrochloric acid-chloride solutions. *Metallurgical Transactions B*, 21, 11-17.
- Ohmoto, H., Hayashi K., Kajisa Y. (1994). Experimental study of the solubilities of pyrite in NaCl-bearing aqueous solutions at 250--350 C. *Geochimica et cosmochimica acta*, 58, 2169-2185.
- Parthasarathy, H., Dzombak, D.A., Karamalidis, A.K. (2013). A small-scale flow-through column system to determine the rates of mineral dissolution at high temperature and pressure. *Chemical Geology*, 354, 65-72.
- Parthasarathy, H., Baltrus, J.P., Dzombak, D.A., Karamalidis, A.K. (2014). A method for preparation and cleaning of uniformly sized arsenopyrite particles. *Geochemical Transactions*, 15.1, 1-7.
- Pearson, R. (1968). Hard and soft acids and bases, HSAB, part 1: Fundamental principles. *Journal of Chemical Education*, 45, 581.
- Rimstidt, J.D., Newcomb, W. (1993). Measurement and analysis of rate data: The rate of

reaction of ferric iron with pyrite. *Geochimica et Cosmochimica Acta*, 57, 1919-1934 .

Sun, Z., Forsling, W., Ronngren, L., Sjoberg, S. (1991). Surface reactions in aqueous metal sulfide systems. 1. Fundamental surface reactions of hydrous PbS and ZnS. *International journal of mineral processing*, 33, 83-93.

Vaughan, D. (2006). Sulfide mineralogy and geochemistry: introduction and overview. *Reviews in Mineralogy and Geochemistry*, 61, 1-5.

Walker, F., Schreiber, M., Rimstidt, J.D. (2006). Kinetics of arsenopyrite oxidative dissolution by oxygen. *Geochimica et cosmochimica Acta*, 70, 1668-1676.

Weerasooriya, R., Tobschall, J. (2005). Pyrite-water interactions: Effects of pH and pFe on surface charge. *Colloids and surfaces A: Physiochem. Eng. Aspects*. 264, 68-74.

## CHAPTER 6

### **THE EFFECT OF Na-Ca-Cl BRINES ON THE DISSOLUTION OF ARSENIC FROM ARSENOPIRYRITE UNDER GEOLOGIC CARBON DIOXIDE STORAGE CONDITIONS**

The information presented in this chapter has been submitted for publication. The co-authors of this paper were: Hao Liu, David A. Dzombak and Athanasios K. Karamalidis

## 6.1 Abstract

Arsenopyrite (FeAsS) is the most common mineral source of arsenic in sedimentary geologic formations. The dissolution of arsenopyrite releases arsenic, which has potential implications for human and environmental health. With carbon dioxide storage in saline, sedimentary geologic formations being one of the most prominent mitigation strategies for increasing CO<sub>2</sub> emissions, the effect of anoxic brines and injected CO<sub>2</sub> on dissolution of arsenic from arsenopyrite needs to be investigated. Arsenopyrite dissolution was studied using anoxic Na-Ca-Cl brines in the presence and absence of CO<sub>2</sub>, at both ambient and high temperature and pressure conditions. Results revealed that the dissolution rate of arsenic is dependent on brine composition, and that CaCl<sub>2</sub> content of Na-Ca-Cl brines has a strong influence on dissolution. The presence of dissolved CO<sub>2</sub> in brines decreased dissolution rates, even though a reduction in pH to approximately 3.5 was observed. Increase in temperature from 25°C to 60°C and pressure from 1 to 100 bars increased As dissolution rate from arsenopyrite by 1 log unit. Increase in pressure from 1 bar to 100 bars had little effect on arsenic dissolution.

## 6.2 Introduction

Geologic carbon dioxide storage (GCS) involves the capture of CO<sub>2</sub> from points of emission, such as coal fired power plants, and transporting it to deep underground geologic formations for safe and permanent storage (NACAP, 2012). Among the many types of reservoirs considered for CO<sub>2</sub> storage in the United States, deep saline sedimentary formations are estimated to have the largest storage capacity, in the order of 2,000-20,000 Gt of CO<sub>2</sub> per formation (NETL, 2010). CO<sub>2</sub> injection in these formations can induce upward movement of brines (Oldenburg and Rinaldi, 2011), compression of injected and resident fluids, and pore space expansion (Bachu, 2008). Although injected CO<sub>2</sub> is expected to be trapped by many mechanisms, slow leakage of CO<sub>2</sub>, brines, or CO<sub>2</sub>-saturated brines may enhance dissolution of minerals in the subsurface leading to mobilization of naturally occurring toxic metals such as arsenic, lead, and cadmium (Karamalidis et al., 2012). Elevated concentrations of As and Pb have been observed upon CO<sub>2</sub> injection in preliminary dissolution experiments with rock samples from GCS sites (Karamalidis et al., 2012).

Arsenopyrite is found in a range of sedimentary deposits and is the most common mineral source of arsenic (Corkhill and Vaughan, 2009). The release of As in to the environment upon the dissolution of arsenopyrite may impact human and environmental health and therefore, arsenopyrite dissolution under oxidizing conditions has been studied extensively (Corkhill and Vaughan, 2009). These studies have determined the effect of oxidants like dissolved oxygen and Fe<sup>3+</sup> on the rate of arsenic release while also investigating the effects of pH and temperature (Rimstidt et al., 1994; Walker et al., 2006; Yu et al., 2007; McKibben et al., 2008; Asta et al., 2010). The dissolution of arsenopyrite under anoxic, high salinity conditions as those in GCS

reservoirs, however, remains unexplored. With increasing interest in CO<sub>2</sub> storage in the subsurface, the effect of brines under anoxic conditions on the release of arsenic from arsenopyrite merits examination. Aside from GCS, understanding the effects of concentrated salt solutions on arsenic release from arsenopyrite is applicable to other systems where high salinity anoxic solutions may be encountered such as shale gas exploration.

Saline sedimentary formations are layers of porous sedimentary rock containing pore waters with total dissolved solids exceeding 10,000 mg/L (NACAP, 2012). Typical conditions reported for CO<sub>2</sub> storage reservoirs span in the range of 74-500 bars for pressure, salinity of 0-7m in NaCl equivalents, and temperature of 304-433K (NETL, 2003). Multiple ionic species such as Na<sup>+</sup>, Ca<sup>2+</sup>, K<sup>+</sup>, Mg<sup>2+</sup>, Cl<sup>-</sup>, and SO<sub>4</sub><sup>2-</sup> are often present in high concentrations and show substantial variability among different storage formations (Wang et al., 2013). An analysis of data from the U.S. brine well database (NETL, 2003), which provides water chemistry parameters for nearly 65,000 wells, assimilated from different sources, depicts this large variability (Table 6.1). As seen in Table 6.1, the three most abundant ions of these brines are Na<sup>+</sup>, Ca<sup>2+</sup> and Cl<sup>-</sup>, with a wide range of relative sodium and calcium concentrations.

**Table 6.1.** Average brine composition data from the U.S. Brine Well database (NETL, 2003)

	<b>pH</b> <b>(units)</b>	<b>[HCO<sub>3</sub><sup>-</sup>]</b> <b>(ppm)</b>	<b>[Ca]</b> <b>(ppm)</b>	<b>[Cl]</b> <b>(ppm)</b>	<b>[Mg]</b> <b>(ppm)</b>	<b>[Na]</b> <b>(ppm)</b>	<b>[SO<sub>4</sub><sup>2-</sup>]</b> <b>(ppm)</b>
<b>Average</b>	7.08	649	5240	55,569	1056	26,147	1064
<b>St. Dev.</b>	0.98	974	7763	55,629	1621	27,681	1679

In this work, arsenopyrite dissolution experiments with synthetic Na-Ca-Cl brines, at a fixed ionic strength of  $1.54 \pm 0.01\text{M}$ , were conducted under anoxic conditions to examine the effect of brines on the rate of release of arsenic from arsenopyrite. The effect of  $\text{CO}_2$  dissolution in brines on arsenic release rates was studied at ambient, and high pressure and temperature conditions. The specific objectives were (1) to examine the effect of relative concentrations of NaCl and  $\text{CaCl}_2$  on arsenic release under anoxic conditions, (2) to investigate the effect of  $\text{CO}_2$  dissolution in deoxygenated brines (and the subsequent decrease in pH) on the rate of arsenic release, and (3) to determine the effect of GCS physical conditions on the dissolution of arsenopyrite by brines.

## **6.3 Materials and Methods**

### **6.3.1 Mineral preparation and characterization**

Arsenopyrite was obtained from Wards Sci. Inc. (Rochester, NY), crushed in a porcelain mortar and pestle, and size separated using nylon sieves to a range of 150- 250  $\mu\text{m}$ . The mortar, pestle, and sieves were soaked overnight in 10% (w/V)  $\text{HNO}_3$  prior to use. Crushed samples required for each dissolution experiment were pre-treated to remove fines and surface oxides based on the method developed by Parthasarathy et al., (2014). The method involves sonication of ground particles in 50% ethanol, followed by rinsing with 12N HCl and 50% ethanol, and finally drying in  $\text{N}_2$  atmosphere.

X-ray diffraction (XRD) analysis of the prepared mineral confirmed arsenopyrite as the primary crystalline phase, with no major secondary phases detected. Scanning electron microscopy-energy dispersive X-ray spectroscopy (SEM-EDS) analysis revealed the stoichiometry of the

prepared mineral to be  $\text{Fe}_{1.03\pm 0.05}\text{As}_{1.01\pm 0.05}\text{S}_{0.87\pm 0.05}$ . The specific surface area was measured in triplicate using BET analysis with a Kr adsorption isotherm and was found to be  $0.125\pm 0.005$   $\text{m}^2/\text{g}$ . Details of the XRD and SEM-EDS analyses can be found in the supporting information section (Appendix D).

### 6.3.2 Experimental system

All dissolution experiments in this study were conducted using a small-scale plug flow column system developed by Parthasarathy et al., (2013). In the system, a 5 cm PEEK column is connected to a HPLC pump, a backpressure regulator and a sample auto-collector. The system has been shown to be capable of determining dissolution rates of minerals without mass transfer limitations (Parthasarathy et al., 2013). At moderate and slow rates of dissolution, as in the case of this study, the dissolution in the column is reaction-rate controlled (Parthasarathy et al., 2013). The column was filled with  $2.5\pm 0.07$  g of prepared arsenopyrite and connected to a backpressure regulator to maintain constant the desired pressure. Dissolved oxygen (D.O.) in the influent solutions was removed by purging with laboratory grade  $\text{N}_2$  for 15 hours prior to each experiment.  $\text{N}_2$  sparging was continued through the entire duration of each experiment. The D.O. in the system was measured using an Accumet XL 60 dissolved oxygen meter (Fisher Scientific). Deoxygenated influent solution was delivered at a constant flow-rate of 1.0 mL/min. The average pore volume of the system was  $0.45\pm 0.05$  mL. The entire system was cleaned prior to every experiment by passing 10%  $\text{HNO}_3$  (w/v) solution through the apparatus for 30 minutes followed by a rinse of deionized water for 30 minutes, to remove residual As and Fe from previous experiments. The experimental system was validated for its ability to maintain

temperature, pressure, and flow rate for the duration of experiments (see supporting information in Appendix D).

### **6.3.3 Reagents**

ACS grade NaCl, and CaCl<sub>2</sub> (Fisher scientific, USA) were used to prepare the synthetic brine solutions, while ACS grade HCl and ethanol (VWR, USA) were used in all cleaning experiments. All aqueous solutions were prepared using deionized water (18.2 MΩ-cm, Barnstead Nanopure purifying system). Laboratory grade nitrogen was used for deoxygenating the influent solutions, while laboratory grade CO<sub>2</sub> was used for experiments requiring CO<sub>2</sub> saturation.

### **6.3.4 Dissolution experiments**

Three sets of dissolution experiments as outlined below were conducted. A complete list of experiments can be found in Appendix D (Table D1).

#### Effect of brine composition

The effect of composition of Na-Ca-Cl brines on arsenic release rates from arsenopyrite was studied with brines of constant ionic strength of 1.54 M, but varying molar ratios of CaCl<sub>2</sub>/NaCl ( $R_{\text{CaCl}_2/\text{NaCl}}$ ). In addition to single electrolyte solutions of pure NaCl and CaCl<sub>2</sub>, binary mixtures with  $R_{\text{CaCl}_2/\text{NaCl}}$  of 0.11, 0.5, and 1 were used as influents in dissolution experiments (Table 6.2). Influent solutions were sparged with N<sub>2</sub> and dissolution experiments were conducted for 30 hours at ambient temperature and pressure. The effluent was sampled every 2 hours using an automated fraction collector (Dionex, USA).

**Table 6.2.** Composition of synthetic brines used in studying dissolution of arsenic from arsenopyrite.

<b>Brine</b>	<b>[NaCl] (M)</b>	<b>[CaCl<sub>2</sub>] (M)</b>	<b>R<sub>CaCl<sub>2</sub>/NaCl</sub></b>	<b>% CaCl<sub>2</sub> (by moles)</b>
1	1.506	0	0	0%
2	1.131	0.125	0.11	10%
3	0.602	0.301	0.5	33%
4	0.377	0.377	1	50%
5	0	0.502	NA	100%

#### Effect of CO<sub>2</sub> dissolution in brines

Experiments aimed at understanding the effect of CO<sub>2</sub> introduction in brines on the dissolution of arsenic from arsenopyrite were conducted with synthetic brines having the compositions described in Table 6.2. However, N<sub>2</sub> sparging was replaced by CO<sub>2</sub> sparging after 15 hours. pH of the influent was measured using an Accumet XL 60 pH meter. Effluent samples were collected every 2 hours for the first 15 hours, every 10 minutes for the next hour, and every 2 hours for the remaining 14 hours of experimentation so as to be able to observe short and long-term effects of CO<sub>2</sub> introduction.

#### Effect of GCS physical conditions

A dissolution experiment with synthetic brine of CaCl<sub>2</sub>-NaCl molar ratio  $R_{CaCl_2/NaCl} = 0.11$  (Table 6.2) was conducted at a temperature of 60°C and pressure of 100 bars to observe the effect of increased temperature and pressure. The pressure was adjusted using the backpressure regulator and was constantly monitored. CO<sub>2</sub> was pumped into the influent solution at 15 hours, to simulate CO<sub>2</sub> injection in a GCS system as explained earlier, and a similar sampling protocol was employed.

### 6.3.5 Analysis

Effluent samples were preserved in 5% HNO<sub>3</sub> (trace metal grade, VWR USA) before being analyzed for Fe and As using an Agilent 7700x Inductively couple plasma mass spectrometer (ICP-MS) equipped with a collision-reaction-cell. Matrix effects due to the high salinity of the brines was reduced by diluting the samples with 5% HNO<sub>3</sub> (20x) and using the High Matrix Interference (HMI) plasma mode. Polyatomic interferences were reduced by conducting the analysis in high energy Helium-collision mode and a four point calibration curve for each analyte was constructed before each set of samples, with  $r^2 > 0.99$ . A multi-element standard mixture from Agilent Technologies Inc. was used to prepare standard solutions. The detection limits were 0.15 ppb for Fe, and 0.25 ppb for As.

### 6.3.6 Data analysis

To enable direct comparison between experiments that may exhibit slight variations in experimental parameters such as mass of mineral packed in the column, residence time of the brine solution, and mass of liquid in pore spaces, the effluent concentrations were normalized to the surface area of the mineral by multiplying the effluent concentration with the ratio of mass of liquid in the column to mineral surface area (Eq. 6-1).

$$C_{normalized} \left( \frac{mol}{m^2 mineral} \right) = C \left( \frac{mol}{L} \right) \times \frac{1}{\rho_{solution}} \left( \frac{L}{g} \right) \times \frac{M}{A} \left( \frac{g solution}{m^2 mineral} \right) \quad (6-1)$$

where,  $C_{normalized}$  is the normalized effluent concentration;  $C$  is the measured effluent concentration;  $M$  is the mass of liquid in the pore volume;  $A$ , the specific surface area of the mineral, and  $\rho_{solution}$ , the density of influent solution.

Steady state was determined to be reached if the effluent concentration was within  $\pm 15\%$  of the average concentration over 10 hours of influent flow in the small-scale flow-through system. Typically, steady state concentrations were calculated after 15 hours of dissolution, to allow for preferential dissolution from surface irregularities. A large variation was observed in Fe effluent concentrations, which could indicate the presence of amorphous Fe phases in these natural samples of arsenopyrite. As the objective of this study was to determine arsenic release rates, Fe concentrations were averaged over the same time frame as As for each experiment.

Arsenopyrite dissolution concentrations are also affected by the dissolution mechanism. Asta et al., (2010) proposed a shrinking core model for arsenopyrite dissolution with dissolved  $O_2$ , while others (Yu et al., 2007; McKibben et al., 2008) have observed incongruent dissolution of arsenopyrite with As and Fe dissolving at a rate faster than S. Such mechanisms would lead to continuous decrease in effluent As concentration resulting in the lack of a clear steady state. To circumvent such mechanistic limitations and to compare between experiments, steady state concentrations were obtained by averaging the effluent As concentrations over the same time period in each experiment. However, in the case of  $CO_2$  injection experiments, a clear steady state was not reached which resulted in larger error bars. The calculated steady state concentrations were converted to reaction rates based on the method described in Parthasarathy et al., (2013).

## 6.4 Results and Discussion

### 6.4.1 Effect of brine composition

The effect of composition of Na-Ca-Cl brines at a constant ionic strength of 1.54 M, on the dissolution of arsenic from arsenopyrite is shown in Figure 6.1. Two single electrolyte brines (NaCl and CaCl<sub>2</sub>), and three binary electrolyte mixtures with  $R_{\text{CaCl}_2/\text{NaCl}} = 0.11, 0.5, \text{ and } 1$ , were used as influent solutions to study dissolution of arsenopyrite. Figure 1A depicts the surface-area normalized arsenic effluent concentration as a function of time. The steady state effluent concentrations derived from Figure 6.1A were used to calculate reaction rates and are represented as a function of % CaCl<sub>2</sub> (by moles) content in the brine solutions in Figure 6.1B. All error bars represent  $\pm 1\sigma$  standard deviation.

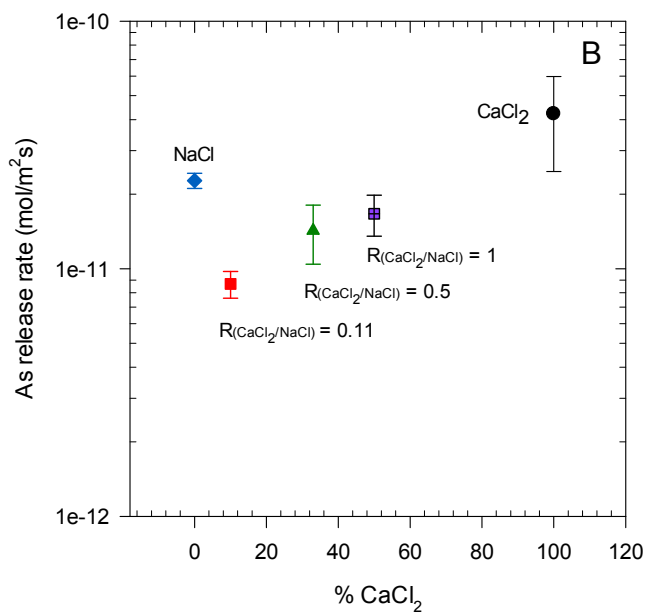
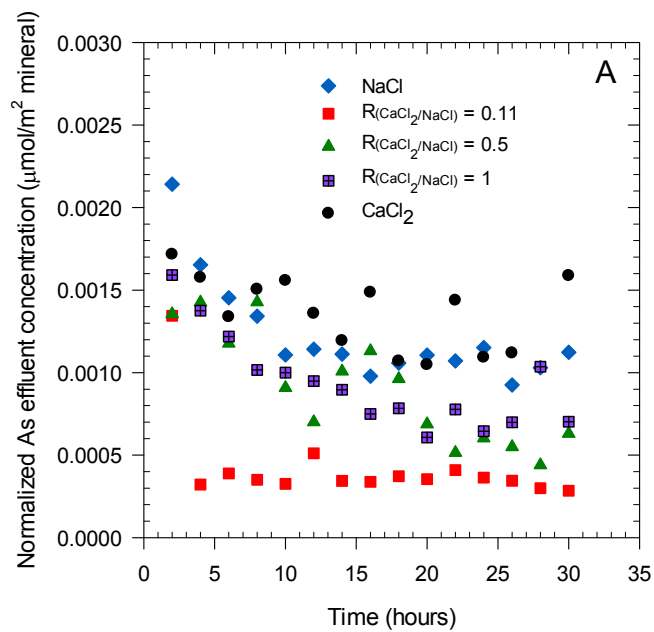


**Figure 6.1.** The effect of brine composition on the rate of arsenic release from arsenopyrite at  $T=25^\circ\text{C}$ ,  $P= 1$  bar,  $I=1.54\text{M}$ ; (A) As effluent concentrations normalized to mineral surface area as a function of time; (B) Rate of As release as a function of %  $\text{CaCl}_2$  (by moles) in the brine solutions.

The effluent arsenic release concentrations with different brines (Figure 6.1A) follow a similar pattern with high initial release that gradually reduces to reach a steady state after 15 hours. Similar trends have been observed in arsenopyrite dissolution experiments using mixed-flow reactor systems and have been attributed to initial preferential dissolution from cracks and sharp edges of the mineral particles (Walker et al., 2006). The steady state concentrations of As, calculated after 15 hours, vary between experiments (Figure 6.1A) and were converted to rates of As release by dividing the surface area normalized effluent As concentration by the residence time of the liquid in the column (Figure 6.1B).

At the same ionic strength, single-electrolyte brines i.e. NaCl and CaCl<sub>2</sub>, result in higher arsenic release rates than their binary mixtures (Figure 6.1B). Within binary brines, CaCl<sub>2</sub> content seems to have a discernible effect on the release rates of arsenic, with brines having higher % CaCl<sub>2</sub> resulting in higher dissolution rates of arsenic (Figure 6.1B). In general, arsenic release from arsenopyrite caused by brines containing CaCl<sub>2</sub> seems to be directly proportional to the CaCl<sub>2</sub> concentration (Figure 6.1B) suggesting that the effect of CaCl<sub>2</sub> is greater than the effect of NaCl.

These results can be interpreted based on the mechanism of sulfide mineral dissolution by alkali and alkaline earth metal chlorides proposed by Parthasarathy et al., (2014b), where the reaction of sulfide minerals with alkali metal chlorides is considered as an electrophile-nucleophile interaction between the positively charged cations in solution and negatively charged mineral surface. Parthasarathy et al., (2014b) proposed that the dissolution of a sulfide mineral by alkali and alkaline earth metal chlorides is affected by the activity of chlorides in solution as well as activity of the cations that act as reactants. An extension of this hypothesis can aid in

understanding the trends observed in this study, where the limited surface area of arsenopyrite, and high chloride concentrations in the brines, influence dissolution rates of As.

#### Surface area and saturation of arsenopyrite

One factor that would influence the interaction between the mineral surface and cations in solution is the surface area of arsenopyrite, and the extent to which its surface sites are saturated. A preliminary analysis of the total available surface area of arsenopyrite particles in the column reveals that the concentration of hydrated  $\text{Ca}^{2+}$  and  $\text{Na}^+$  ions required to completely occupy the surface is 2.16 mM and 2.9 mM respectively (see Supporting Information for details on this calculation). The brines used in this study have much larger concentrations of these species (Table 6.1). Thus, the surface of arsenopyrite will be completely saturated with either  $\text{Ca}^{2+}$  or  $\text{Na}^+$ , depending on brine composition, even if a fraction of the ions are dehydrated. With pure NaCl and  $\text{CaCl}_2$  brines, the surface is saturated with  $\text{Na}^+$  and  $\text{Ca}^{2+}$  respectively. In the case of binary mixtures, we propose that the larger charge density and higher electronegativity (Li and Xue, 2009), of  $\text{Ca}^{2+}$  as compared to  $\text{Na}^+$  favors  $\text{Ca}^{2+}$  attraction to the surface even when it is present in lower concentrations. Based on the surface coverage calculations, the concentrations of  $\text{Na}^+$  and  $\text{Ca}^{2+}$  at the surface of mineral when saturated are 2.9mM and 2.16mM, respectively, for experiments with only NaCl and only  $\text{CaCl}_2$ . This should result in higher dissolution when the arsenopyrite surface is saturated with  $\text{Na}^+$  (as is the case with a NaCl brine) as compared to an arsenopyrite surface saturated with  $\text{Ca}^{2+}$  (as with mixed brines and  $\text{CaCl}_2$ ), as arsenic dissolution from arsenopyrite is proportional to cation activity (Parthasarathy et al., 2014b). However, as seen from Figure 6.1B, the  $\text{CaCl}_2$  brine experiment results in higher steady state As

release rate than the NaCl experiment. One possible reason is the higher chloride ion activity in solution, as explained below.

#### Chloride activity in solution

Another factor that affects arsenopyrite dissolution in brines is the activity of chloride ions in solution. The activities of  $\text{Na}^+$ ,  $\text{Ca}^{2+}$ , and  $\text{Cl}^-$  were calculated for the brines in this study at constant ionic strength using the Pitzer equation (Pitzer, 1992). The results of this model (Figure 6.2A) depict a decrease in  $\text{Cl}^-$  activity with increasing  $\text{CaCl}_2$  content, even at the same ionic strength. A lower  $\text{Cl}^-$  activity could result in higher dissolution rates (Parthasarathy et al., 2014b), as observed in this study (Figure 6.2B). Considering that all brines containing  $\text{CaCl}_2$  in this study saturate the arsenopyrite surface with  $\text{Ca}^{2+}$ , the  $\text{Cl}^-$  content in these brines controls dissolution and hence, a dependence on %  $\text{CaCl}_2$  is observed (Figure 6.1B). With the pure NaCl brine, the effect of higher cation activity is offset by the higher chloride activity in solution, resulting in the pure  $\text{CaCl}_2$  brine experiment showing a marginally higher arsenic release rate than the NaCl brine experiment (Figure 6.1B). At higher chloride concentrations (compared to the pure  $\text{CaCl}_2$  experiment) as with the mixed brine systems, dissolution rates were lower than that caused by NaCl due to the combined effect of lower  $\text{Ca}^{2+}$  activity (when the mineral surface is saturated) and higher  $\text{Cl}^-$  activity in solution.

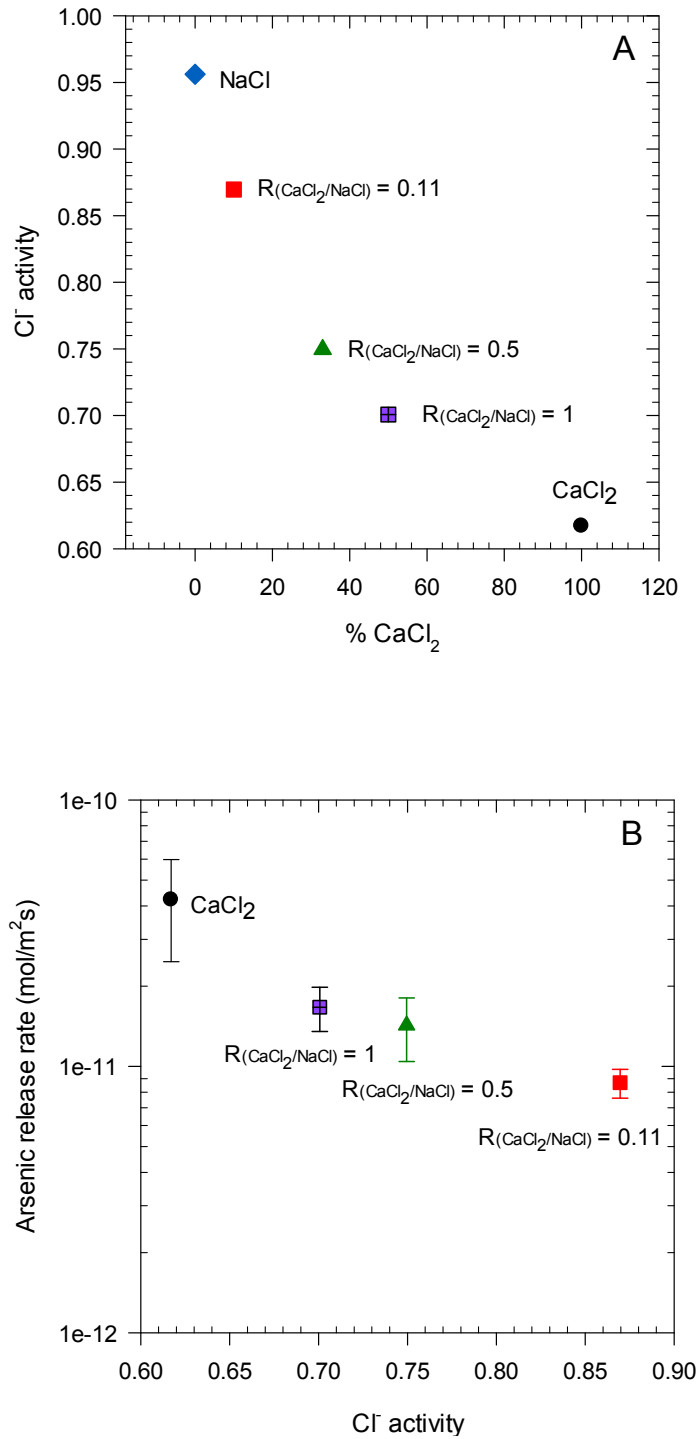


**Figure 6.2.** The effect of chloride activity on release rates of arsenic from arsenopyrite. (A) Chloride ion activity in brines as a function of % CaCl<sub>2</sub> content. (B) The effect of chloride ion activity on the rates of As release from arsenopyrite by CaCl<sub>2</sub> containing brines.

#### **6.4.2 Effect of CO<sub>2</sub> introduction**

The effect of CO<sub>2</sub> dissolution into the influent solution was determined by monitoring the concentration of arsenic in the effluent after CO<sub>2</sub> introduction (Figure 6.3). Brines of ionic strength 1.54 M, but with varying R<sub>CaCl<sub>2</sub>/NaCl</sub> (Table 6.2) were used as influents for dissolution experiments. When CO<sub>2</sub> was introduced in the influent, an immediate spike in As release observed in all experiments (Figure 6.3A). The released As concentrations decreased over time and steady state was achieved after 20 hours. Rates calculated from the steady state concentrations are shown in Figure 6.3C, which also depicts the rate of As release from experiments in the absence of CO<sub>2</sub> (from the previous set of experiments; as closed markers) to enable comparison between experiments with and without CO<sub>2</sub> dissolution in brines.

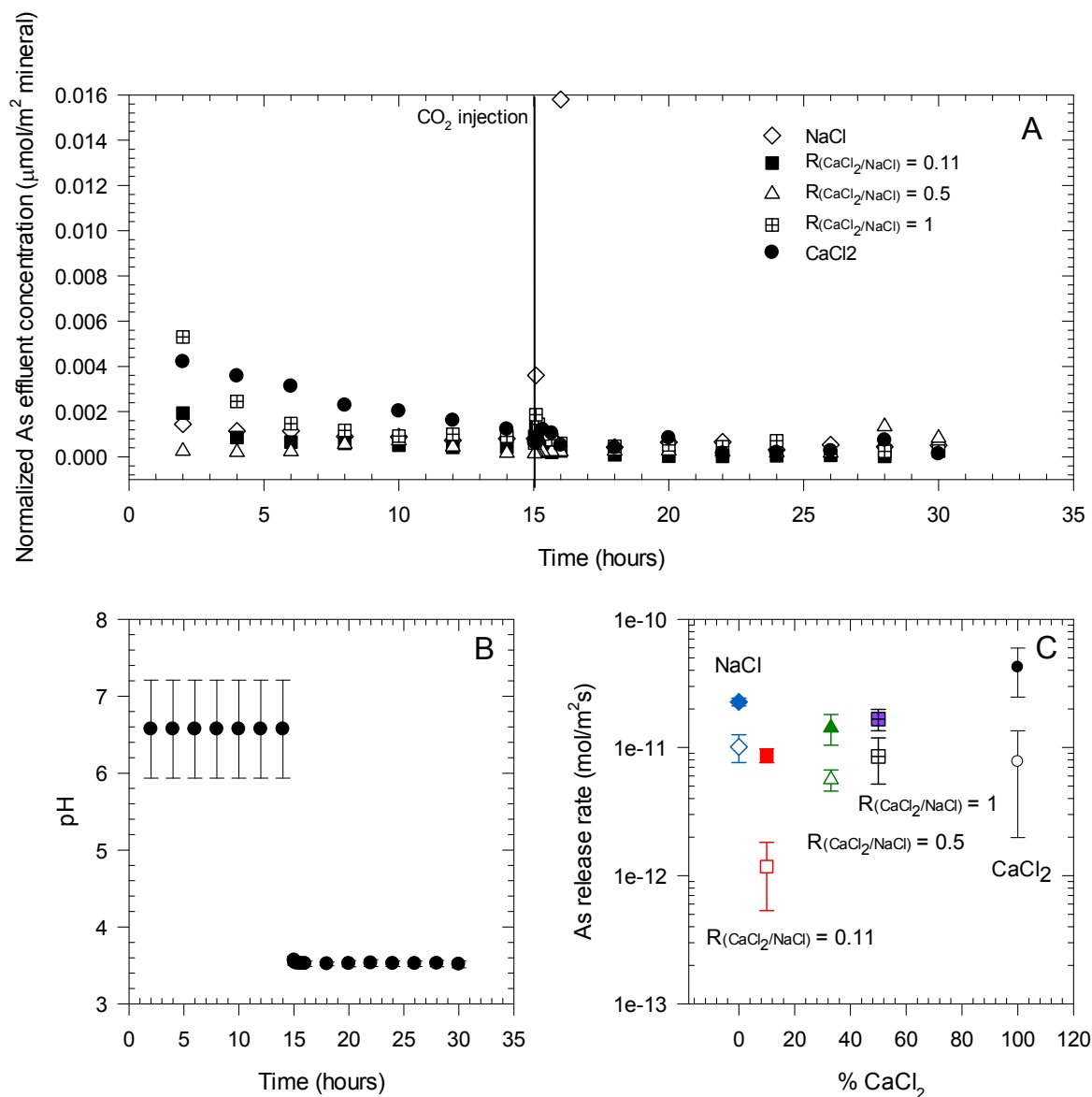


**Figure 6.3.** The effect of CO<sub>2</sub> dissolution in brines on the rate of arsenic release at T=25°C, 1 bar, I=1.54M. R represents molar ratio of CaCl<sub>2</sub> to NaCl ( $R_{\text{CaCl}_2/\text{NaCl}}$ ). (A) As effluent concentration normalized to mineral surface area as a function of time. CO<sub>2</sub> injection at 15h is depicted by a solid line. (B) Average brine pH as a function of time before and after CO<sub>2</sub> injection. (C) As release rate as a function of % CaCl<sub>2</sub> content in brines. Closed markers represent experiments without CO<sub>2</sub> (from Figure 6.1).

The dissolution rate trend with brines after CO<sub>2</sub> introduction was similar to the brine experiments without CO<sub>2</sub>. The release rates show a strong correlation to CaCl<sub>2</sub> concentration, with higher As dissolution rates observed with brines containing higher % CaCl<sub>2</sub> (Figure 6.3C). However, even though the pH of the influent solutions decreased to approximately 3.5 upon CO<sub>2</sub> dissolution (Figure 6.3B), the steady state As release rates post-CO<sub>2</sub> introduction were lower than those observed in experiments without CO<sub>2</sub> injection. This is in contrast to the dissolution of arsenopyrite by dissolved O<sub>2</sub> where arsenic release rates were shown to increase with a decrease in pH (McKibben et al., 2008). Figure 6.4 depicts the relationship between As release rates and chloride ion activity in solution, which is similar to experiments without CO<sub>2</sub> (Figure 6.2B). An increase in rates is seen with decreasing Cl<sup>-</sup> activities in brines containing CaCl<sub>2</sub>.

One approach to understanding these dissolution patterns is to consider the surface charge of the mineral. Bebie et al., (1998) showed that the p*H*<sub>i.e.p</sub> of arsenopyrite was lower than 2. Therefore, the net negative charge on the surface will be higher at higher pH. As a result, a decrease of pH reduces the interaction of the surface with the cations in solution, leading to a decrease in the rate of arsenic release. Additionally, the dissolution of CO<sub>2</sub> results in an increase of CO<sub>3</sub><sup>2-</sup> ions in solution, which could impede the cations in solution interacting with the surface of the mineral (Parthasarathy et al., 2014b).

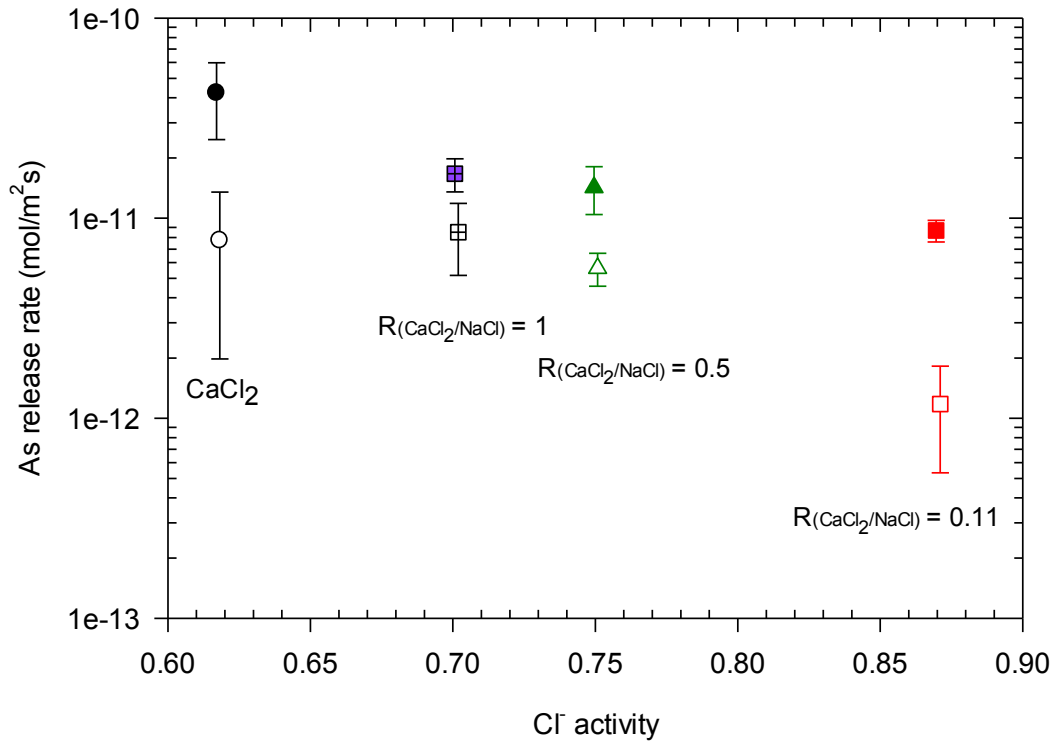


**Figure 6.4.** The effect of chloride ion activity on the dissolution of arsenic from arsenopyrite by brines containing CaCl<sub>2</sub> after CO<sub>2</sub> injection. Closed markers represent dissolution rates in the absence of CO<sub>2</sub>.

### 6.4.3 Effect GCS physical conditions

To evaluate arsenopyrite dissolution under geologic carbon storage conditions of high temperature and pressure, an experiment was conducted to measure the rate of arsenic release at 60°C and 100 bars (Figure 6.5). A Na-Ca-Cl brine with molar ratio ( $R_{CaCl_2/NaCl}$ ) of 0.11 was used to study dissolution, and CO<sub>2</sub> was introduced continuously into the brine influent solution at 15 hours to simulate CO<sub>2</sub> injection in the subsurface. The brine was sparged with CO<sub>2</sub> at ambient temperature and pressure and then subjected to GCS conditions inside the column. The

concentration of dissolved CO<sub>2</sub> corresponded to 3.5% of the maximum solubility at 60°C and 100 bars, as calculated using the CO<sub>2</sub> solubility model developed by Wang et al., (2013).

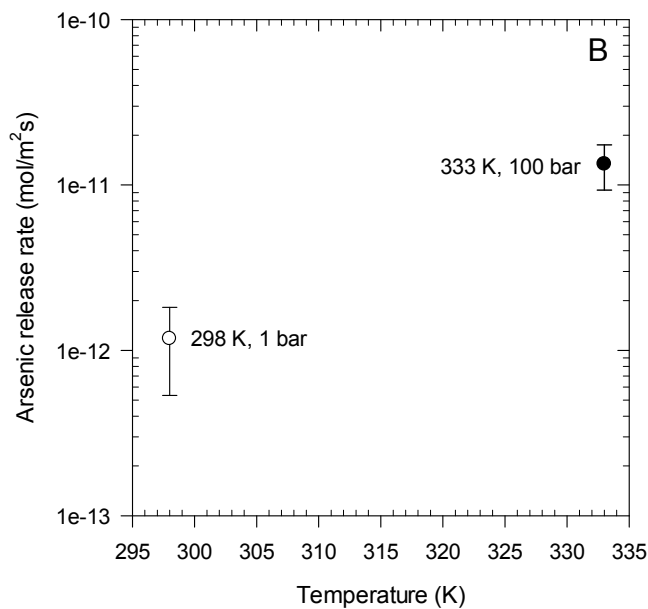
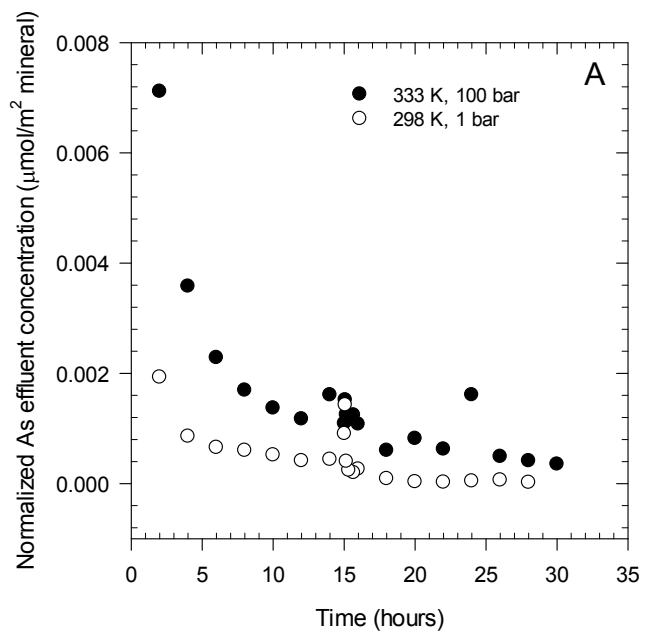


**Figure 6.5.** The effect of GCS physical conditions on arsenic release from arsenopyrite with Na-Ca-Cl brine of  $R_{CaCl_2/NaCl}=0.11$ . (A) As effluent concentration normalized to mineral surface area, at 298K, 1 bar and 333K and 100 bars. (B) The effect of temperature on arsenic release rate.

The steady state concentration of As was observed to be higher at higher temperature and pressure than at ambient conditions (Figure 6.5A). The rate of dissolution increased by 1 log unit with an increase in temperature and pressure to 60°C and 100 bars respectively (Figure 6.5B). Drjaca et al., (1998) calculated activation energies for some aqueous reactions, which suggested that an increase in pressure from 1- 100 bars will result in an increase in dissolution rate by at most 0.05 log units. Theoretically, the increase in reaction rates can be attributed to an increase in temperature. The increase of dissolution rate at higher temperatures is similar to that observed by others (Rimstidt et al., 1994; McKibben et al., 2008) while studying arsenopyrite dissolution with strong oxidants such as dissolved oxygen and  $\text{Fe}^{3+}$ .

The dissolution of arsenopyrite by Na-Ca-Cl brines was studied under anoxic conditions.

In general, the results of this study reveal that (a) Na-Ca-Cl brines are capable of causing release of arsenic from dissolution of arsenopyrite, even under anoxic conditions, (b) the dissolution rate of arsenic is dependent on brine composition, with  $\text{CaCl}_2$  content in Na-Ca-Cl brines having a strong influence on the rate of dissolution, (c)  $\text{CO}_2$  dissolution in brines resulted in a decrease in dissolution rate, even though the pH decreased to  $\sim 3.5$ , and (d) the rate of dissolution increased by 1 log unit with an increase in temperature and pressure from ambient conditions to 60°C and 100 bars while studying dissolution using a Na-Ca-Cl brine with  $R_{\text{CaCl}_2/\text{NaCl}} = 0.11$ .

#### **6.4.4 Limitations and implications of this study**

While this study focused on the effect of composition of Na-Ca-Cl brines, the effect of other brine constituents such as  $\text{Mg}^{2+}$ , and  $\text{SO}_4^{2-}$  on the rate of arsenic dissolution remains unexplored. Further, a more detailed study on the effect of temperature is required to determine activation

energies for different brine systems. This study focused on the effect of reduced pH due to CO<sub>2</sub> injection, but the effect of higher CO<sub>2</sub> concentrations at high temperature and pressure, and the effect of supercritical CO<sub>2</sub> merits further examination.

## 6.5 References

- Asta, M.P., Cama, J., Ayora, C., Acero, P., de Giudici, G. (2010) Arsenopyrite dissolution rates in O<sub>2</sub>-bearing solutions. *Chemical Geology*. 273.3. 272-285.
- Bachu, S. (2008) CO<sub>2</sub> storage in geological media: Role, means, status and barriers to deployment. *Prog. Energy Combust. Sci.* 8, 34, 254–273.
- Bebie, J., Schoonen, M., Fuhrmann, M., Strongin, D. (1998) Surface charge development on transition metal sulfides: an electro kinetic study. *Geochimica et Cosmochimica Acta*. 62. 633-642.
- Corkhill, C. L., Vaughan, D.J. Arsenopyrite oxidation—A review. (2009) *Applied Geochemistry*. 24.12, 2342-2361.
- Drljaca, A., Hubbard, C. D., van Eldik, R., Asano, T., Basilevsky, M. V., le Noble, W. J. (1998) Activation and reaction volumes in solution. 3. *Chemical Reviews* 98.6, 2167-2290.
- Karamalidis, A.K., Torres, S.G., Hakala, J.A., Shao, H., Cantrell, K.J., Carroll, S. (2012) Trace metal source terms in carbon sequestration environments. *Environmental Science & Technology* 47.1, 322-329.
- Li, KeYan, DongFeng Xue. (2009) New development of concept of electronegativity. *Chinese Science Bulletin* 54.2, 328-334.
- McKibben, M. A., Tallant, B.A., Del Angel, J.K. (2008) Kinetics of inorganic arsenopyrite oxidation in acidic aqueous solutions. *Applied Geochemistry* 23.2, 121-135.
- NETL (2003) *U.S. Brine wells Database*, DOE/NETL-2003/119. National Energy Technology Laboratory, U.S. Department of Energy. Morgantown, WV.
- NETL (2010) *Carbon Utilization and Storage Atlas of the United States and Canada, 3rd ed.* National Energy Technology Laboratory, U.S. Department of Energy. Morgantown, WV
- NACAP (2012) *The North American Carbon Storage Atlas, 1<sup>st</sup>*, ed. North American Carbon Atlas Partnership
- Oldenburg, C. M., Rinaldi, A. P. (2011) Buoyancy effects on upward brine displacement caused by CO<sub>2</sub> injection. *Transp. Porous Media*. 87, 525–540.
- Parthasarathy, H., Dzombak, D.A., Karamalidis, A.K. (2013) A small-scale flow-through column system to determine the rates of mineral dissolution at high temperature and pressure. *Chemical Geology* 354, 65-72.

- Parthasarathy, H., Baltrus J.P., Dzombak, D.A., Karamalidis, A.K. (2014) A method for preparation and cleaning of uniformly sized arsenopyrite particles. *Geochemical Transactions* 15.1, 1-7.
- Parthasarathy, H., Dzombak, D.A., Karamalidis, A.K. (2014b) Alkali And Alkaline Earth Metal Chloride Solutions As Reactants In Sulfide Mineral Dissolution. *Environmental Science and Technology Letters*. In review.
- Pitzer, K.S. Ion interaction approach: theory and data correlation. (1992) In *Activity coefficients in electrolyte solutions*, Pitzer, K.S. Eds. 2<sup>nd</sup>, ed. C.R.C. Press. pp.75–153.
- Rimstidt, J. D., Chermak, J.A., Gagen, P.M. (1994) Rates of reaction of galena, sphalerite, chalcopyrite, and arsenopyrite with Fe (III) in acidic solutions. *ACS symposium series*. Vol. 550. Washington, DC: American Chemical Society,[1974]-.
- Walker, F. P., Schreiber, M.E., Rimstidt, J.D. (2006) Kinetics of arsenopyrite oxidative dissolution by oxygen. *Geochimica et Cosmochimica Acta* 70.7, 1668-1676.
- Wang, Z.; Small, M.J., Karamalidis, A.K. (2013) Multimodel Predictive System for Carbon Dioxide Solubility in Saline Formation Waters. *Environmental Science & Technology* 47.3, 1407-1415.
- Yu, Y., Zhu, Y., Gao, Z., Gammons, C.H., Li, D. (2007) Rates of Arsenopyrite Oxidation by Oxygen and Fe (III) at pH 1.8-12.6 and 15-45°C. *Environmental Science & Technology* 41.18, 6460-6464.

## CHAPTER 7

### **DISSOLUTION OF ARSENIC AND IRON FROM THE LOWER TUSCALOOSA FORMATION OF THE CRANFIELD FIELD CO<sub>2</sub> SEQUESTRATION SITE**

The information presented in this chapter is a part of a manuscript under preparation. The co-authors of this manuscript are: Christina Lopano<sup>1</sup>, Mengling Stuckman<sup>1</sup>, David A. Dzombak and Athanasios K. Karamalidis

[Drs. Lopano and Stuckman conducted all the Micro-XANES and XRD analyses presented in this chapter.]

<sup>1</sup>U.S. Department of Energy, National Energy Technology Laboratory, Pittsburgh PA

## 7.1 Abstract

Cranfield oil field is a CO<sub>2</sub>-Enhanced Oil Recovery (EOR) site in southwestern Mississippi, concurrently used as a field study site for geologic CO<sub>2</sub> storage (GCS) as a part of the Southeastern Regional Carbon Storage Project (SECARB) sponsored by the U.S. Department of Energy. CO<sub>2</sub> is injected into the lower Tuscaloosa formation, a sedimentary sandstone deposit. Field studies and laboratory experiments on the reservoir rock and overlying shale seal rock were performed to assess the effects of short term CO<sub>2</sub> injection on mineral dissolution. This study focused on understanding the sources of arsenic and the dissolution of As and Fe from seal rock samples under conditions representative of GCS. Dissolution experiments were conducted on primary and secondary seal rocks using a small-scale plug flow column system with 105 g/L NaCl as the leach solution. Solid samples were analyzed before and after dissolution using Micro-X-ray Adsorption Near Edge Structure ( $\mu$ -XANES). Results indicate that As in the seal rock samples is commonly associated with sulfides and iron oxides. An increase in Fe dissolution upon CO<sub>2</sub> injection was observed while As dissolution did not change significantly.  $\mu$ -XANES analyses on post-reaction secondary seal rock samples revealed that As was oxidized and then mobilized into the leach solution or adsorbed onto iron oxides. Dissolution of the primary seal rock sample was hampered by the immediate precipitation/swelling of clays upon CO<sub>2</sub> injection, resulting in an increase in column pressure.

## 7.2 Introduction

Geologic carbon dioxide storage (GCS) is defined as the safe and permanent storage of CO<sub>2</sub> in subsurface reservoirs (NACAP, 2012). It involves the separation and capture of CO<sub>2</sub> from industrial emissions, followed by injection into deep (>800 m) geologic formations where it is stored as a super-critical fluid (NACAP, 2012). In the United States, five storage reservoir types are currently under investigation as potential sites for GCS: (i) oil and gas reservoirs, (ii) unmineable coal, (iii) saline sedimentary formations, (iv) organic rich shales, and (v) basalt formations (NACAP, 2012). Of these potential reservoirs, saline sedimentary formations have been estimated to possess large storage capacities, of the order of 2000-20,000 Gt per unit (NETL, 2010).

Although injected CO<sub>2</sub> is trapped by various physical and chemical mechanisms (NETL, 2010), zones of high permeability have been identified as potential leakage pathways for upward migration of CO<sub>2</sub>, formation water, and formation water saturated with CO<sub>2</sub> (Wilkin and Diguilio, 2010). Escaped fluids may interact with overlying aquifers, thereby altering the geochemistry of the water (Wilkin and Diguilio, 2010). Among the potential impacts of such leakage, one concern is the enhanced dissolution of hazardous metals such as As and Pb from reservoir and cap rock minerals and their subsequent transport to overlying aquifers (Karamalidis et al., 2012).

Field experiments at the Zero Emission Research and Technology Center (ZERT) in Bozeman, MT involving the injection of CO<sub>2</sub> into a test site showed mobilization of As and Pb, with an increase in the aqueous concentrations of these metals in shallow groundwater monitoring wells

(Kharaka et al., 2010). Rocking autoclave experiments by Karamalidis et al. (2012) involving rock-brine-CO<sub>2</sub> interaction experiments on rock samples from several potential GCS reservoir formations in the United States, Canada, and Algeria showed release of Pb, Cr, Fe, and Mn in concentrations that exceeded the U.S. Environment Protection Agency's Maximum Contaminant Levels for drinking water. The authors further observed that although CO<sub>2</sub> injection and the subsequent pH decrease caused an increase in release of trace metals, their actual impact on ground water quality would depend on reservoir and formation specific processes (Karamalidis et al., 2012).

The Cranfield oil field, Mississippi is a Southeast Regional Carbon Sequestration Partnership field test site (SECARB, 2010) sponsored by the U.S. Department of Energy (DOE). At the Cranfield site, ongoing CO<sub>2</sub>-EOR operations are being leveraged to collect continuous data for long-term GCS analysis (NETL, 2012). The reservoir is a salt-cored simple domal structure located approximately 20km from Natchez in southwestern Mississippi (Lu et al., 2012). The reservoir (CO<sub>2</sub> injection zone) is in the lower Tuscaloosa formation at depths of 3000m (Lu et al., 2012) and is composed of porous and permeable fluvial, deltaic, shoreline, and marine sandstones, separated by regionally extensive thick impermeable marine and non-marine mudrocks that isolate fluids (SECARB, 2010). The Tuscaloosa marine shale serves as the primary seal rock for the reservoir with the Selma group and Midway shales acting as secondary and tertiary seals respectively (Griffith et al., 2011). Field and laboratory experiments (Lu et al., 2012) with the reservoir rocks have suggested that the sandstone-rock formation water system is not very reactive in contact with CO<sub>2</sub> in the short term, although variations in pH resulted in corresponding changes in aqueous Fe concentrations. Further, laboratory dissolution experiments

with reservoir rock samples from the Lower Tuscaloosa formation reacted with synthetic brine solutions resulted in As release concentrations below method detection limits (Karamalidis et al., 2012). However, the sources and dissolution of As from the shale seal rocks of the Cranfield field CO<sub>2</sub> sequestration site have not been determined.

The objective of this study was to investigate the dissolution of Fe and As from shale seal rocks of the lower Tuscaloosa formation under conditions representative of GCS. The specific objectives were to (i) measure the dissolution of Fe and As from seal rocks in contact with 105 g/L NaCl in the presence of CO<sub>2</sub>, (ii) detect variations in Fe and As release in response to CO<sub>2</sub> injection between primary and secondary seal rocks, and (iii) determine the changes in solid phase speciation of As before and after dissolution to determine potential mechanisms for As release.

### **7.3 Materials and Methods**

#### **7.3.1 Sample preparation and characterization**

The shale seal rock samples required for this study were obtained from above the lower Tuscaloosa formation in the Cranfield oil field CO<sub>2</sub> sequestration site, Mississippi. The primary seal rock (Tuscaloosa marine shale) above the Lower Tuscaloosa is a fissile, fine-grained, dark gray shale with some limestone, claystone, siltstone, and mudstones while the secondary seal rocks (Selma group) contains chalk, chalky marl, and limestone members (Griffith et al., 2011). Three samples were collected from different depths: a primary seal rock sample from a depth of 10,193 ft., and secondary seal rocks from 7913.8 ft. and 7930.1 ft. The rock samples were crushed in a mortar and pestle and size sieved using nylon sieves to a size range of 150 – 250

$\mu\text{m}$ . The chemical composition of the samples was determined by acid digestion using HF with ICP analysis of the digest solutions. Crystalline phases were identified qualitatively by X-Ray diffraction (XRD). A.C.S grade NaCl and deionized water (18.2 M $\Omega$ ; Barnstead U.S.A) were used to prepare influent simulated brine solutions for dissolution experiments. Laboratory grade N<sub>2</sub> and laboratory grade CO<sub>2</sub> were used for influent deoxygenation and CO<sub>2</sub> injection respectively.

### **7.3.2 Dissolution Experiments**

#### Experimental Setup

Dissolution experiments were conducted in a small-scale flow-through column system developed by Parthasarathy et al., (2013). The system consisted of a 5cm long poly-ether-ether-ketone (PEEK) column filled with crushed and size sieved rock, connected to an influent reservoir using an HPLC pump. Influent solutions were supplied at a constant flow rate of 0.8 ml/min (interstitial velocity of 0.13 cm/s) to overcome mass transfer limitations (Parthasarathy et al., 2013). The pressure inside the column was maintained at 100 bars using an adjustable backpressure regulator and the temperature of the influent solution was controlled at 60°C using a bench top hot plate (Corning Inc., USA). The column was insulated with polyethylene pipe insulation (Armacell Inc, USA) to prevent loss of heat over the duration of the experiments. Samples were collected at regular intervals of time and analyzed for total Fe using an ICP-OES and total As using an ICP-MS. The detection limits were 3.1 ppb for Fe and 2.8 ppb for As. Prior to each experiment, the system was washed with 5% HNO<sub>3</sub> for 2 hours to ensure removal of Fe, As, and other metals from prior experiments.

### CO<sub>2</sub>-Brine Experiments

The effect of CO<sub>2</sub> on the dissolution of Fe and As from the three seal rock samples was investigated using an influent simulated brine solution of 105 g/L NaCl. The solution was deoxygenated for 15 hours prior to each experiment by sparging with N<sub>2</sub>, which was continued for the first 20 hours of the flow-through testing, to determine the dissolution of Fe and As prior to CO<sub>2</sub> injection with samples collected at 2 hour intervals. At 20 hours, N<sub>2</sub> was replaced with CO<sub>2</sub> as the sparging gas, and the effluent was sampled every 30 minutes for the first 2 hours and every 2 hours for the next 18 hours. The pH after CO<sub>2</sub> dissolution in the simulated brine was measured using an Accumet XL 60 pH meter (Fisher Scientific, U.S.A) and was found to be 3.6. The approximate dissolved CO<sub>2</sub> concentration was found to be 0.2M

### The effect of pH on mineral dissolution

To determine if the effect of CO<sub>2</sub> dissolution in the simulated brine on Fe and As release was purely due to a reduction in pH of the influent solution, dissolution of the seal rock sample from 7930.1 ft. was studied with 105 g/L NaCl at a pH of 3.6 (adjusted with 1N trace metal grade HCl). Similar to the other experiments, 105g/L NaCl deoxygenated with N<sub>2</sub> was used for the first 20 hours of the experiment and effluent was sampled every 2 hours. At 20 hours, the influent brine was replaced by deoxygenated low-pH brine solution (HCl; pH 3.6) and a similar sampling protocol was employed. The temperature and pressure were maintained at 60 °C and 100 bar respectively, for the entire duration of the experiments. Details of dissolution experiments conducted are shown in Table 7.1.

**Table 7.1.** List of experiments conducted to investigate Fe and As release from seal rock samples of the lower Tuscaloosa formation.

<b>Sample No</b>	<b>Seal Rock</b>	<b>Influent solution</b>	<b>CO<sub>2</sub></b>	<b>T, P</b>
1	7913.8 ft.	105 g/L NaCl	Yes	60 °C, 100 bars
2	7930.1 ft.	105 g/L NaCl	Yes	60 °C, 100 bars
3	10193 ft.	105 g/L NaCl	Yes	60 °C, 100 bars
4	7930.1 ft	105 g/L NaCl followed by 105 g/L NaCl at pH 3.6	No	60 °C, 100 bars

### **7.3.3 Micro-X-ray adsorption near edge structure ( $\mu$ -XANES) analysis**

To determine the effects of brine-CO<sub>2</sub> interaction on the solid samples, primary seal rock samples (10193 ft.) and secondary seal rock samples from 7913.8 ft. were analyzed using ( $\mu$ -XANES), before and after dissolution experiments. Details of the  $\mu$ -XANES method and data analysis can be found in the supporting information section (Appendix E).

## 7.4 Results and Discussion

### 7.4.1 Material characterization

The elemental compositions determined by HF acid digestion of the seal rock samples are shown in Figure 7.1. Al, Ca, Fe, K, Na, and Si are the major elemental components of the three samples.

The average Fe and As concentrations are 50,000  $\mu\text{g/g}$  and 1000  $\mu\text{g/g}$  respectively.

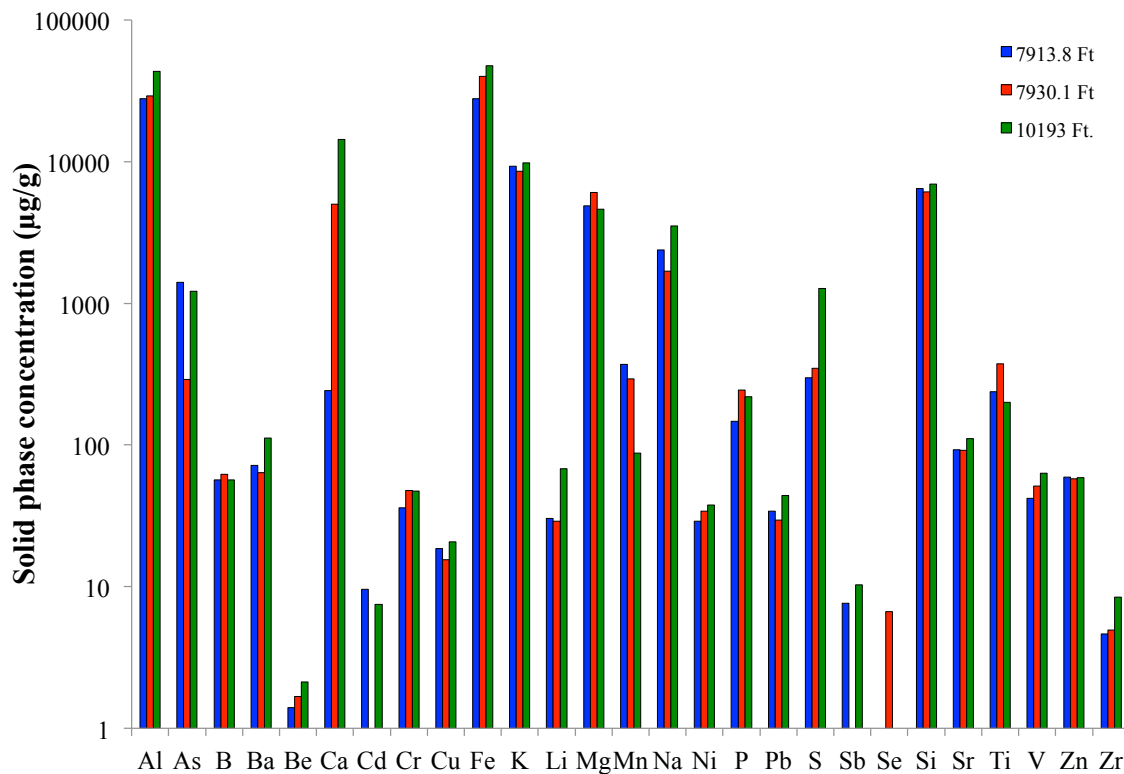


**Figure 7.1.** Elemental compositions of primary and secondary seal rocks.

The results of qualitative XRD analyses of the samples are shown in Table 7.2. The major phases in the three seal rocks were determined to be quartz, and illite/mica, while minor phases of kaolinite and albite were also detected. Trace quantities of pyrite and calcite were observed.

Similar results have been reported with semi-quantitative XRD on these seal rock samples (Griffith et al., 2011)

**Table 7.2.** Qualitative XRD results for Mudstone Starting Materials Where Major ~ > 25%; Minor ~ 5-25%, and Trace ~ <5%; ND = not detected. (Source: Lopano, C. and Stuckman, M)

Seal rock	Quartz	Pyrite	Illite/Mica	Kaolinite	Calcite	Albite
7913 ft.	Major	Trace	Major	Minor	Trace	Minor
7930 ft.	Major	Trace	Major	Minor	Trace	Minor
10193 ft.	Major	Trace	Major	Minor	Trace	ND

#### 7.4.2 Dissolution Experiments

##### CO<sub>2</sub>- Brine experiments

Effluent concentrations of As and Fe from the dissolution experiments with 105 g/L NaCl simulated brine solution were monitored as a function of time (Figure 7.2). The solid line at time= 20 hours corresponds to CO<sub>2</sub> injection.

As seen in Figure 7.2, the injection of CO<sub>2</sub> in the influent solution resulted in an immediate increase in the release of Fe and As in all three samples. The release of Fe gradually decreased with time, and at the completion of experiments at 40 hours was higher than the concentrations prior to CO<sub>2</sub> injection. There was no significant increase in the steady state arsenic concentration released from the 7930.1 ft. sample, but a new arsenic steady state concentration was achieved for the 7913.8 ft. sample, which was marginally higher than the pre-CO<sub>2</sub> injection steady state concentration. Experiments conducted with primary seal rock samples could not be completed as

CO<sub>2</sub> injection caused clogging of the system and high-pressure buildup. XRD analyses on post reaction sample from 10193 ft. revealed potential swelling or precipitation of clay (Figure 7.3), which could have led to column clogging.

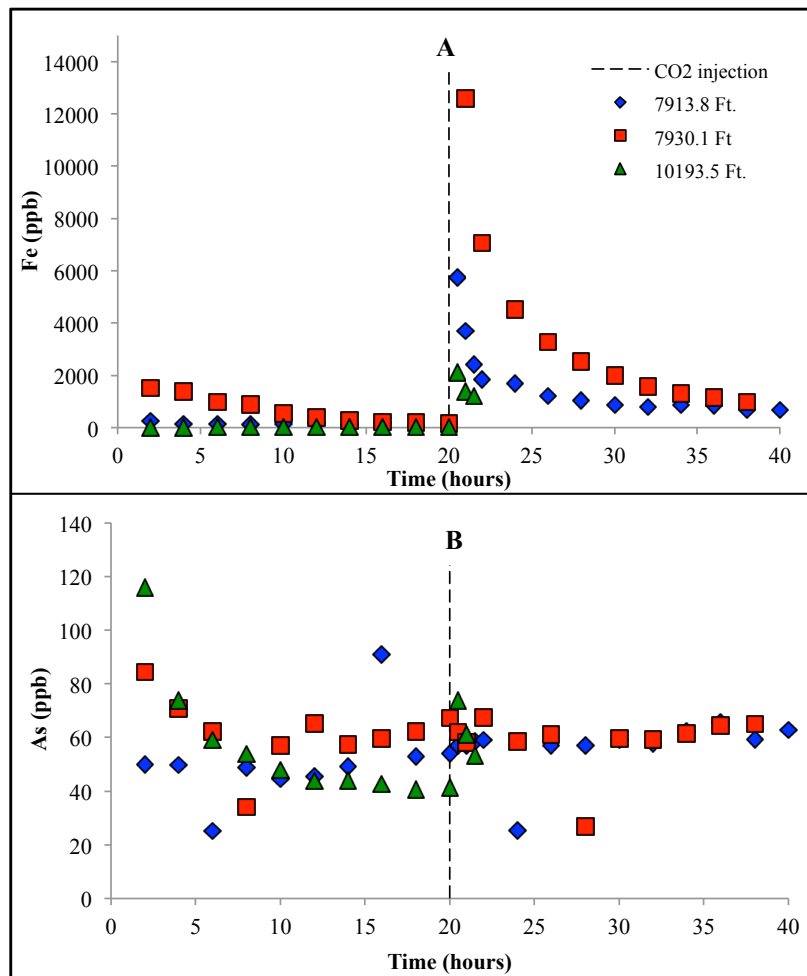


**Figure 7.2.** Effluent concentration of (A) Fe, and (B) As, as a function of time in experiments with seal rock samples and 105 g/L NaCl influent solution. CO<sub>2</sub> injection in influent solution at 20 hours; T =60 °C; P= 100 bars.

In general, the effluent concentration of As was two orders of magnitude lower than that of Fe, which is consistent with the relative abundance of Fe compared to As in the samples (Figure

7.1). However, effluent concentrations and trends of Fe and As are inconsistent with the solid-phase elemental concentration data (for instance, even though 10193 ft. had the highest Fe content, it exhibited lowest Fe release concentrations), suggesting that the mobility of metals from these samples involves multiple processes including adsorption and/or precipitation (Cheng et al., 2009). Effluent As concentrations of both secondary seal rock samples reached similar steady states due to a similarity in starting material, but dissolution experiments with the primary seal rock could not be completed due to column clogging.

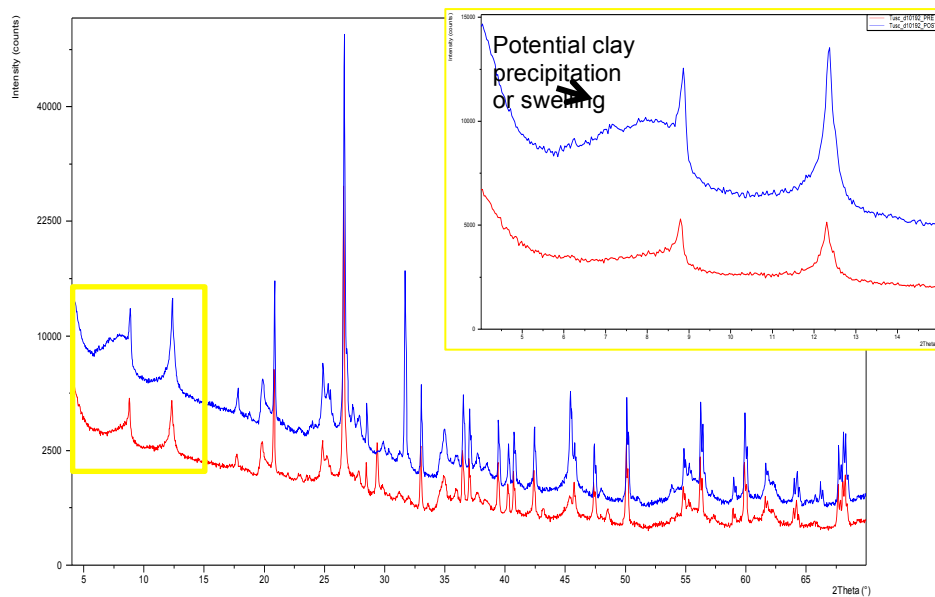


**Figure 7.3.** XRD patterns for sample from 10,193 ft. – Pre (red) and Post (blue) reaction. Inset: Enlarged image of a section of the spectra (yellow box), revealing potential clay precipitation or swelling. (Source: Lopano, C. and Stuckman, M.)

## The effect of pH on mineral dissolution

Effluent As and Fe concentrations released from a secondary seal rock (7930.1 ft.) when subjected to dissolution experiments involving CO<sub>2</sub> injection in the influent solution, and influent pH change, are presented in Figure 7.4.

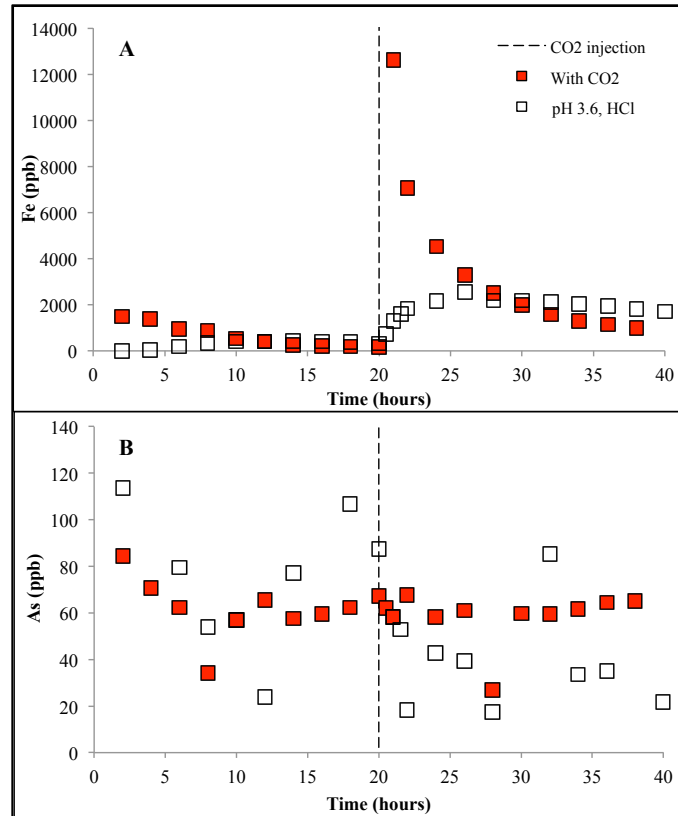


**Figure 7.4.** Effects of CO<sub>2</sub> injection (closed markers) and pH adjustment (open markers) in the influent solution on the effluent concentrations of (A) Fe, and (B) As, as a function of time.

CO<sub>2</sub> injection at 20 hours; T =60 °C; P= 100 bars. Influent = 105 g/L NaCl.

The dissolution of Fe, as depicted in Figure 7.4A, suggests that a decrease in pH has a similar effect to CO<sub>2</sub> injection since very similar release concentrations were observed. However, the

dissolution kinetics after 20 hours for the two experiments differs significantly. While CO<sub>2</sub> injection in the influent solution caused a rapid increase in Fe concentrations that gradually decreased over time, the low-pH influent experiment showed a gradual increase in release concentrations that reached similar steady state over time. This suggests that although the effluent concentrations are similar, the mechanisms involved could be different and that the effect of CO<sub>2</sub> on iron release is more than just a decrease in pH.

The As release concentrations observed with the low pH experiment appear to have a lower steady state as compared to those in the CO<sub>2</sub> injection experiments (Figure 7.4B). However, a large variability in As concentrations was observed even prior to 20 hours, which could be due to the heterogeneity of the rock samples and the presence of As rich pieces of the samples. Further the As concentration in a number of effluent samples was below detection limit resulting in gaps in Figure 7.4B. In general, the lower steady state concentration after 20 hours could mean either (i) rapid mobilization of As from the samples, which flushed out of the reactor in the first few minutes, or (ii) enhanced adsorption/immobilization in the reactor.

#### **7.4.3 Micro-XANES analysis and linear combination fitting (LCF)**

Primary (10193 ft.) and secondary (79301.1 ft.) seal rock samples were analyzed before and after dissolution using  $\mu$ -XANES to determine changes in As speciation and binding environment due to dissolution. Figure 7.5 depicts the As  $\mu$ -XANES spectra of reference materials (Figure 7.5A) and all the samples (Figure 7.5B). Details of edge position and white line comparison can be found in the supporting information section (Appendix E). Details of the samples and their sample ID in the synchrotron-based experiments are presented in Table 7.3.

**Table 7.3.** Sample IDs for  $\mu$ -XANES analysis (Source: Lopano, C., and Stuckman, M.)

SEAL ROCK SAMPLE	SAMPLE ID	
	PRE-REACTION	POST-REACTION
Primary – 10193 ft.	LT10193	LT10193post
Secondary- 7913.8 ft.	MT7913	MT7913post

The As reference spectra (Figure 7.5A) library was provided courtesy of Dr. Kirk Scheckel from USEPA (Beak & Wilkin, 2009; Smith et al., 2005) and include (1) references of As<sup>V</sup> sorbed on iron oxides, abbreviated as As<sup>V</sup>-FeOxide group: As<sup>V</sup> sorbed on goethite (As<sup>V</sup>\_Goethite), As<sup>V</sup> sorbed on ferrihydrite (As<sup>V</sup>\_Ferrihydrite), scorodite; (2) references of As<sup>III</sup> sorbed on iron oxides, abbreviated as As<sup>III</sup>-FeOxide group: As<sup>III</sup> sorbed on magnetite (As<sup>III</sup>\_Magnetite), As<sup>III</sup> sorbed on Siderite (As<sup>III</sup>\_Siderite), As<sup>III</sup> sorbed on ferrihydrite (As<sup>III</sup>\_Ferrihydrite), (3) references of As<sup>III</sup> sorbed on iron sulfides, abbreviated as As<sup>III</sup>-Sulfide group: As<sup>III</sup> sorbed on pyrite (As<sup>III</sup>\_Pyrite), As<sup>III</sup> sorbed on mackinawite (As<sup>III</sup>\_Mackinawite); and (4) references of arsenite directly bonded with sulfur, as As<sup>III</sup> in sulfide group: Arsenopyrite [FeAsS<sub>2</sub>], Realgar [As<sub>4</sub>S<sub>4</sub>], amorphous Arsenite sulfides (AsS\_Poor), orpiment [As<sub>2</sub>S<sub>3</sub>], and amorphous orpiment (Am Orpiment).

Two distinctive white-line peaks at approximately 11868eV and 11875eV exist in most micro-XANES samples (Figure 7.5B). For the secondary seal rock from 7913 ft. prior to dissolution experiments, the As  $\mu$ -XANES Spectra (black lines in Figure 7.5B) indicate the dominance of As<sup>III</sup> in sulfide species, while the spectra from the post-reaction sample (green lines in Figure 7.5B) suggest a dominance of As<sup>V</sup>-FeOxide species. Most of the As  $\mu$ -XANES Spectra from the primary seal rock at 10193 ft. pre-reaction (red lines in Figure 7.5B) and post-reaction (blue lines

in Figure 7.5B) samples had multiple major peaks, indicating co-existence of As<sup>III</sup> in sulfide, As<sup>III</sup>-sulfide and As<sup>III</sup>/As<sup>V</sup>-FeOxide species.

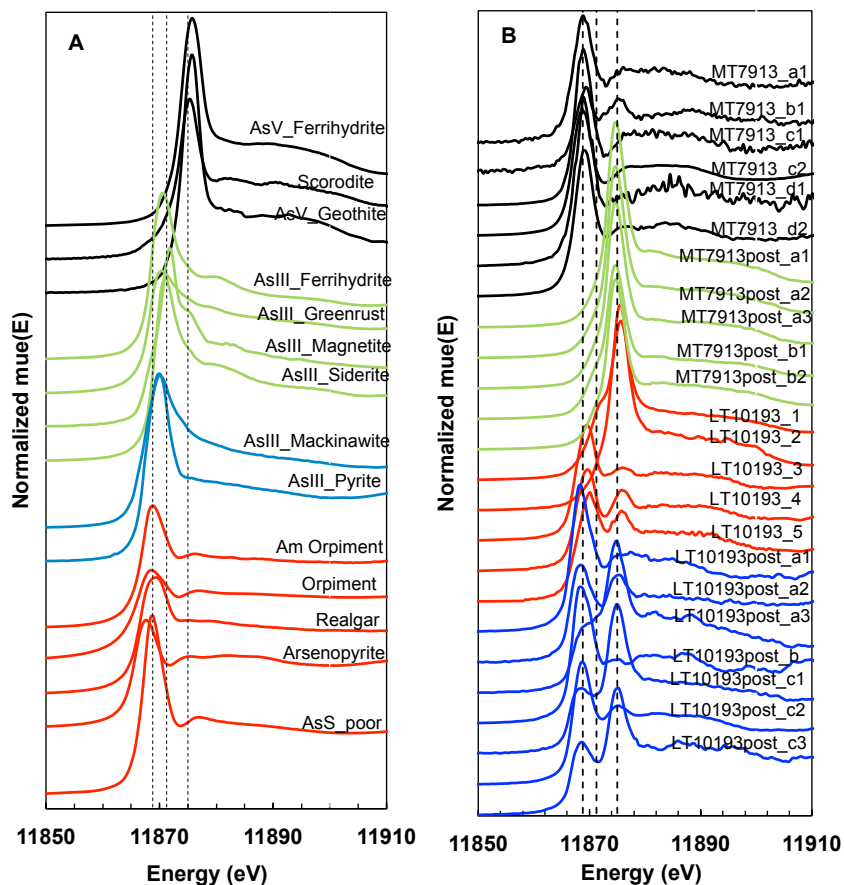


**Figure 7.5.** XANES spectra for (A) 14 As references and (B) all measured micro-spots in different samples. Dash vertical lines from right to left display energies at 11868.8eV, 11871.26eV, 11875eV, representing white line peaks for As<sup>V</sup>-FeOxide group, As<sup>III</sup>-FeOxide group and As<sup>III</sup> in Sulfide group, respectively. (Source: Lopano, C. and Stuckman, M.)

In an attempt to quantify more accurately the XANES spectra, an LCF of reference spectra was performed. Details of the analysis can be found in Appendix E. Results of the least squares fitting are presented in Table 7.4.

LCF results demonstrated that 77-100% of As species in the hotspots of the secondary seal rock from 7930.1 ft. prior to dissolution, exist as As in sulfide species and the rest as As<sup>V</sup> in scorodite (0-21%). LCF results from the same sample post reaction, demonstrated the dominance of As<sup>V</sup>-Feoxide group (76-100%), indicating As on the rock in these sampled hot spots was oxidized during the dissolution experiment. LCF results for the primary seal rock (10193 ft.) before and after reaction, revealed more hotspot-dependent mineral compositions than those from the secondary seal rock samples. Arsenic mineral phases in the pre-reaction primary seal rock sample included 16-88% As<sup>V</sup>-FeOxide; 0-35% as As<sup>III</sup>-FeOxide; 0-39% as As<sup>III</sup>-sulfide; and 0-84% As<sup>III</sup> in sulfide speciation group as Am Orpiment and AsS\_poor (Table 7.4). Arsenic mineral phases in the sample after dissolution experiments, contained 0-65% As<sup>V</sup>-FeOxide speciation group and 35-100% As<sup>III</sup> in sulfide speciation group as 0-41% arsenopyrite and 21-66% AsS\_poor.

The results of the  $\mu$ -XANES analyses reveal the inherent heterogeneity of these natural samples and the multiple As binding environments that exist within them. While As in the secondary seal rock samples are oxidized from As<sup>III</sup> to As<sup>V</sup> during the dissolution process (potentially by released Fe in the brine phase), and are either released into the effluent or adsorbed onto Fe-Oxides in the sample, the dissolution from primary seal rock samples is much more complex owing to the presence of As<sup>V</sup>-Fe oxides in the sample prior to dissolution. This is further compounded by the swelling/precipitation of clay, which resulted in the truncation dissolution experiments.

**Table 7.4.** Relative abundance of As reference groups from LCF analyses of  $\mu$ -XANES spectra of all seal rock samples.  $E_0$  shift of all

phases were restrained to  $\pm 0.5$  eV. R factor is defined as  $\frac{\sum [(data - fit)^2]}{\sum (data^2)}$ . (Source: C.Lopano and M.Stuckman)

Sample I.D. <sup>†</sup>	White-line peak	Edge position	AsV-FeOxide	AsIII-FeOxide	AsIII-Sulfide	AsIII in Sulfide	R <sup>‡</sup>
MT7913_a1	11868.9	11867.3	13			87	0.0095
MT7913_b1	11869.5	11867.3	23			77	0.0160
MT7913_c1	11869.0	11867.5	9			91	0.0248
MT7913_c2	11868.8	11867.1	8			92	0.0192
MT7913_d1	11869.0	11868.2				100	0.2671
MT7913_d2	11869.1	11867.6	8			92	0.0108
MT7913post_a1	11875.0	11873.6	100				0.0022
MT7913post_a2	11874.9	11873.7	94		6		0.0011
MT7913post_a3	11875.0	11873.7	93		7		0.0014
MT7913post_b1	11874.9	11873.7	76	24			0.0017
MT7913post_b2	11874.9	11873.7	95	5			0.0019
LT10193_1	11875.7	11874.5	65	35			0.0005
LT10193_2	11875.6	11874.6	88	12			0.0016
LT10193_3	11869.5	11868.3	16			84	0.0141
LT10193_4	11869.6	11867.6	28			72	0.0165
LT10193_5	11870.1	11868.0	28	13	39	20	0.0103
LT10193post_a1	11868.6	11867.2	4			96	0.0183
LT10193post_a2	11868.7	11866.8	27			73	0.0076
LT10193post_a3	11875.2	11867.4	65			35	0.0060
LT10193post_b	11868.6	11867.4				100	0.0131
LT10193post_c1	11868.8	11866.8	53			47	0.0026
LT10193post_c2	11869.0	11867.3	15			85	0.0108
LT10193post_c3	11868.9	11867.0	52			48	0.0081

<sup>†</sup>Sample ID: Secondary seal rocks before reaction (MT7913), after reaction (MT7913post); Primary seal rock before reaction (LT10193), after reaction (LT10193post). a1, a2, a3 etc. indicate hotspots on each sample. <sup>‡</sup>R-factor is a measure of mean square sum of misfit at each data point.

## 7.5 Summary

The dissolution of As and Fe from primary and secondary seal rocks of the Lower Tuscaloosa formation of the Cranfield oil field CO<sub>2</sub> storage test site was investigated by conducting a series of dissolution experiments using a columnar flow-through apparatus and crushed rock samples. Sample characterization results revealed that major As bearing phases in the rock samples were As<sup>III</sup> in sulfides, As<sup>III</sup> sorbed on iron sulfides, As<sup>V</sup> sorbed on Fe oxides, and As<sup>III</sup> sorbed on Fe oxides. Reaction of seal rocks with 105 g/L NaCl brine solution resulted in a steady state release of As in the range of 70 to 80 ppb. The introduction of CO<sub>2</sub> in the influent solution caused a rapid increase in Fe and As concentrations in these experiments. While the steady state Fe concentrations were higher after CO<sub>2</sub> introduction in the influent solution, no discernible difference was detected in As effluent concentrations compared to the case without CO<sub>2</sub>.  $\mu$ -XANES analyses of the pre- and post-dissolution secondary seal rock samples revealed the oxidation of As from As<sup>III</sup> to As<sup>V</sup> on the rock surfaces, with apparent subsequent dissolution and sorption on seal rock surfaces. Primary seal rock experiments did not reach completion due to a pressure buildup in the column, possibly due to swelling/precipitation of clays in the crushed samples. In general, the mobility of As in these samples is complex and governed by (i) oxidation and subsequent dissolution, which results in an increase in mobility, and (ii) adsorption onto sulfides, Fe-oxides, and clays that leads to a decrease in As mobilization.

While this study investigated patterns in dissolution and in solid-phase speciation, no attempt was made to quantify rates of dissolution owing to the multiple processes involved in the mobilization of As. These processes need to be investigated individually, under ideal conditions to enable quantification of the overall kinetics of As release.

## 7.6 References

- Beak, D. G., Wilkin, R. T. (2009). Performance of a zerovalent iron reactive barrier for the treatment of arsenic in groundwater: Part 2. Geochemical modeling and solid phase studies. *Journal of Contaminant Hydrology*, 106(1-2), 15-28.
- Cheng, H., Hu, Y., Luo J., Xu, B. and Zhao, J. (2009). Geochemical processes controlling fate and transport of arsenic in acid mine drainage (AMD) and natural systems. *Journal of Hazardous Materials*, 165(1-3), 13-26.
- Drahota, P., Rohovec, J., Filippi, M., Mihaljevic, M., Rychlovsky, P., Cervený, V., Pertold, Z. (2009). Mineralogical and geochemical controls of arsenic speciation and mobility under different redox conditions in soil, sediment and water at the Mokrsko-West gold deposit, Czech Republic. *Science of The Total Environment*, 407(10), 3372-3384.
- Griffith, C. A., Dzombak, D. A., & Lowry, G. V. (2011). Physical and chemical characteristics of potential seal strata in regions considered for demonstrating geological saline CO<sub>2</sub> sequestration. *Environmental Earth Sciences*, 64(4), 925-948.
- Horneman, A., Van Geen, A., Kent, D. V., Mathe, P. E., Zheng, Y., Dhar, R. K., O'Connell, S., Hoque, M.A., Aziz, Z., Shamsudduha, M., Seddique, A.A., Ahmed, K. M. (2004). Decoupling of As and Fe release to Bangladesh groundwater under reducing conditions. Part 1: Evidence from sediment profiles. *Geochimica Et Cosmochimica Acta*, 68(17), 3459-3473.
- Karamalidis, A.K., Torres, S.G., Hakala, J.A., Shao, H., Cantrell, K.J, Carroll, S. (2012) Trace metal source terms in carbon sequestration environments. *Environmental science & technology*, 47.1, 322-329.
- Kharaka, Y. K., Thordsen, J. J., Kakouros, E., Ambats, G., Herkelrath, W. N., Beers, S. R., Birkholzer, J.T., Apps, J.A., Spycher, N.F., Zheng, L., Trautz, R.C., Rauch, H.W., Gullickson, K. S. (2010). Changes in the chemistry of shallow groundwater related to the 2008 injection of CO<sub>2</sub> at the ZERT field site, Bozeman, Montana. *Environmental Earth Sciences*, 60(2), 273-284.
- Lu, J., Kharaka, Y. K., Thordsen, J. J., Horita, J., Karamalidis, A., Griffith, C., Hakala, J.A, Ambats, G., Cole, D.R., Phelps, T.J., Manning, M.A., Cook, P.J., Hovorka, S. D. (2012). CO<sub>2</sub>-rock-brine interactions in Lower Tuscaloosa Formation at Cranfield CO<sub>2</sub> sequestration site, Mississippi, USA. *Chemical Geology*, 291, 269-277.
- NETL (2012). *Carbon Utilization and Storage Atlas, Fourth Ed.* National Energy Technology Laboratory, U.S. Department of Energy. Morgantown WV.
- Neil, C. W., Yang, Y. J., Jun, Y. S. (2012). Arsenic mobilization and attenuation by mineral-water interactions: implications for managed aquifer recharge. *Journal of Environmental Monitoring*, 14(7), 1772-1788.

NACAP (2012). *North American Carbon Storage Atlas, First Ed.* North American Carbon Atlas Partnership.

Parthasarathy, H., Dzombak, D.A., Karamalidis, A.K. (2013) A small-scale flow-through column system to determine the rates of mineral dissolution at high temperature and pressure. *Chemical Geology*, 354, 65-72.

SECARB (2010) *Phase II- Gulf Coast Stacked Storage Project Report*. <[www.secarbon.org](http://www.secarbon.org)> , Southeast Regional Carbon Sequestration Partnership. (Nov. 13, 2014).

Wang, Z., Small, M.J., Karamalidis, A.K. (2013) Multimodel Predictive System for Carbon Dioxide Solubility in Saline Formation Waters. *Environmental science & technology*, 47.3, 1407-1415.

Wilkin, R. T., DiGiulio, D.C. (2010) Geochemical impacts to groundwater from geologic carbon sequestration: controls on pH and inorganic carbon concentrations from reaction path and kinetic modeling. *Environmental science & technology*, 44.12, 4821-4827.

## **CHAPTER 8**

### **SUMMARY, CONCLUSIONS, AND RECOMMENDATIONS FOR FUTURE WORK**

## **8.1 Summary and Conclusions**

The overall motivation of this dissertation was to understand the mobilization of As from subsurface sedimentary formations under conditions representative of GCS. Rates of As release from rocks and different mineral species under these conditions will enable the prediction the risks associated with GCS on groundwater quality.

The specific objectives were- (1) to determine the sources of As in sedimentary geologic formations, (2) to design, construct, and validate a small scale system for conducting dissolution experiments at high pressure, temperature, and salinity, (3) to investigate the dissolution of As from arsenopyrite by brines, under anoxic conditions, and (4) to study the dissolution of As from natural rock samples, under conditions representative of GCS. These objectives were divided into six specific tasks. Summary and key findings of each task presented below.

### **Objective 1 (Task1)**

A literature review of most commonly reported sources of arsenic in high and low permeability sedimentary formations was conducted (Chapter 2). Results revealed that the major sources of arsenic in both low and high permeability are arsenopyrite, arsenian pyrite, and sorbed As on iron oxides. Arsenopyrite was found to be the most common pure phase mineral source of As. Typically, As concentrations were reported in the range of 0-50 mg/kg, although concentrations exceeding 500 mg/kg have been reported in some cases.

## **Objective 2 (Task 2)**

A small-scale plug flow column system to determine the dissolution of minerals at high pressure, temperature, and salinity was developed (Chapter 3). The system consists of a 5cm Poly-ether-ether-ketone column and is capable of withstanding pressures up to 300 bars, and temperatures up to 100°C and can be used with both liquids (e.g. brines) and mixtures of liquids with gases (e.g. brines with CO<sub>2</sub>). Further, since plug-flow systems have higher solid-liquid ratios than other reactor systems, this system can determine very small dissolution rates. The capacity of the system to measure dissolution rates without mass transfer limitations was investigated by studying arsenopyrite dissolution with 10<sup>-4</sup> M Fe<sup>3+</sup>, under anoxic conditions. The maximum rate of dissolution that can be studied with this setup was found to be 5×10<sup>-05</sup> mol/m<sup>2</sup>s, for a maximum flow rate of 10 mL/min (interstitial velocity of 1.7 cm/s). Currently, rocking autoclave batch systems are used for measuring dissolution rates of minerals and rock samples under GCS conditions. The plug-flow system developed in this study is capable of measuring dissolution rates similar to those measured using rocking-autoclave systems with the added advantages of being easier to setup, maintain, and operate. Further, data analysis and calculating dissolution rates is simpler.

## **Objective 3 (Tasks 3, 4, and 5)**

Following the development of the experimental setup, arsenopyrite dissolution under GCS conditions was investigated.

To enable the accurate determination of arsenopyrite dissolution rates, a method for preparation of uniformly sized arsenopyrite particles free of surface oxides was developed (Chapter 4).

Arsenopyrite particles in the size fraction of 150-250  $\mu\text{m}$  were obtained by sonication of suspensions of crushed particles in 50% v/v ethanol and verified by particle size distribution and SEM analysis. Four methods of cleaning the surface were investigated and the method involving 12N HCl and 50% ethanol was found to be the most effective. XPS analysis revealed the method succeeded in removing all oxide species of S and As on the surface to below detection by XPS, while only 12% of surface Fe remained oxidized.

Once a reproducible method for arsenopyrite preparation was developed, experiments on the dissolution of arsenopyrite, pyrite, and galena by 10mM NaCl, CaCl<sub>2</sub>, and MgCl<sub>2</sub> were conducted to identify the effects of alkali and alkaline metal chlorides on sulfide mineral dissolution (Chapter 5). Results showed that NaCl, MgCl<sub>2</sub>, and CaCl<sub>2</sub> can no longer be considered inert with respect to reactivity, at least for sulfide minerals. The rate of dissolution of sulfide minerals under anoxic conditions is controlled by the relative activities of the reactive cation(s) and the inhibitory anion(s) in solution. The rates of dissolution are low relative to dissolution under oxic conditions but are measurable and, in the case of arsenopyrite, yield As to solution. Further, the propensity to react with a cation was found to be dependent on the nucleophilicity of the anion species in the mineral surface.

Subsequently, the effect of high salinity Na-Ca-Cl brines on arsenopyrite dissolution was investigated under anoxic conditions (Chapter 6). The results of this study revealed that Na-Ca-Cl brines are capable of causing dissolution of arsenic from arsenopyrite, even under anoxic conditions. The dissolution rate of arsenic from arsenopyrite under anoxic conditions was found to be in the range of  $10^{-10}$  to  $10^{-11}$  mol/m<sup>2</sup>s and was dependent on brine composition, with CaCl<sub>2</sub>

content in Na-Ca-Cl brines controlling the rate of dissolution. CO<sub>2</sub> dissolution in brines resulted in a decrease in dissolution rate, even though a reduction in pH was observed. Further, experiments at GCS physical conditions revealed that the rate of dissolution increased 10 fold with an increase in temperature and pressure from ambient conditions to 60 °C and 100 bars.

#### **Objective 4 (Task 6)**

Finally, the dissolution into brine of arsenic from natural seal rock samples of the Cranfield field CO<sub>2</sub> sequestration site was investigated.  $\mu$ -XANES analysis on the rock samples revealed that major As bearing phases in these rocks are As (III) in sulfides, As(III) sorbed on iron sulfides, As(V) sorbed on Fe oxides, and As(III) sorbed on Fe oxides. Dissolution experiments with rock samples and 105g/L NaCl brine revealed a steady state As release of 70-80 ppb, even under anoxic conditions. While the steady state Fe concentrations were higher after CO<sub>2</sub> introduction, a significant difference was not detected in As effluent concentrations. Although primary seal rock experiments did not reach completion due to potential swelling/precipitation of clays,  $\mu$ -XANES analysis on secondary seal rock samples revealed that As (III) on the minerals were potentially oxidized to As (V) during the dissolution experiments and are subsequently removed in the effluent or sorbed on to Fe oxides.

The major contributions of this dissertation are:

- (i) The development of a robust small-scale plug-flow through system for rapid determination of mineral dissolution rates avoiding mass transfer limitations.
- (ii) The development of a method for arsenopyrite preparation and sulfide mineral surface cleaning protocol that enables accurate determination of dissolution rates.

- (iii) Demonstration that alkali and alkaline metal chloride electrolytes cause dissolution of sulfide minerals under anoxic conditions and proposal of a hypothesis that explains the dissolution process.
- (iv) Determination of As release rates in Na-Ca-Cl brines contacted with arsenopyrite under GCS conditions
- (v) Analysis of sources of As in selected primary and secondary seal rocks of GCS sites and potential mechanisms for As mobilization under GCS environments.

## **8.2 Recommendations for Future Work**

The conclusions of this study can serve as the basis for future research on mineral dissolution as well as on the fate and transport of As under a variety of environments. Three distinct areas for future research have been identified.

### **8.2.1 The reactivity of alkaline salt solutions in mineral dissolution**

The results of this study indicate that alkali and alkaline metal chloride electrolytes can induce metal sulfide mineral dissolution under anoxic conditions, but the mechanisms involved merit further investigation. The experiments conducted in this thesis were confined to three sulfide minerals and the effect of chloride salts on their dissolution. The results obtained suggest that the reactivity of alkali chloride salt solutions on sulfide minerals is dependent on the anions in the mineral, and the cations and anions in solution. Other minerals that contain nucleophilic anions (such as carbides and cyanides) could be of potential interest in GCS environments. While chlorides are of interest with regard to GCS, the effects of other alkali halides (fluorides, iodides, etc.) merit examination. The variation in polarizability and nucleophilicity of halides will

determine the extent to which they inhibit mineral dissolution caused by cations in solution. Within the halide group, basicity decreases but nucleophilicity increases moving down the periodic table.  $F^-$  is therefore expected to have a higher inhibitory effect on  $H^+$  while  $I^-$  ion would inhibit other cations to a larger extent. Verification of these trends will enable a generalization of the hypothesis presented in this thesis.

### **8.2.2 Arsenopyrite dissolution- rates, rate laws, and mechanism**

Chapters 5 and 6 discuss the reactivity of chloride salt solutions (specifically  $NaCl$ ,  $CaCl_2$  and  $MgCl_2$ ) with regard to arsenopyrite dissolution. Further, the effect of binary electrolyte mixtures on arsenic release from arsenopyrite was determined. However, complete rate laws for arsenopyrite dissolution with different electrolytes were not developed. A database of rate laws will be of help to assess risks of As dissolution under specific conditions. In addition, the exact mechanism of dissolution including a step-by-step process by which alkali metal chlorides cause dissolution needs to be established. Of particular interest is the fate of Fe and S in the mineral. Fe and S are redox active and may participate in the dissolution process. Speciation analysis of these elements in the mineral and in solution may lead to a better understanding of the exact mechanism involved in the release of arsenic.

### **8.2.3 The biogeochemistry of As in the subsurface**

A major portion of this thesis was focused on As dissolution from a pure phase mineral. However, as detailed in Chapter 7 multiple sources of As exist in sedimentary rocks. The fate of mobilized As in groundwater is determined by dissolution of these minerals/mineral phases as well as by other processes such as sorption and precipitation. Further, the effect of microbial

activity on the fate of As has been documented in many environments (Casiot et al., 2003; Ehrlich, 1964; Islam et al., 2004 ). An overall understanding of these processes and their relative rates is another possible area of research that can build on this dissertation. Rates of arsenic mobilization and immobilization obtained from these individual processes can complement the data obtained in this dissertation. A suite of such rate information can be utilized in models to predict more accurately the overall fate and mobility of As and its potential impact on groundwater.

### 8.3 References

Casiot, C., Morin, G., Juillot, F., Bruneel, O., Personné, J. C., Leblanc, M., Duquesne, K., Bonnefoy, V., Elbaz-Poulichet, F. (2003). Bacterial immobilization and oxidation of arsenic in acid mine drainage (Carnoulès creek, France). *Water research*, 37(12), 2929-2936.

Ehrlich, H. L. (1964) Bacterial oxidation of arsenopyrite and enargite. *Economic Geology* 59(7), 1306-1312.

Islam, F. S., Gault, A. G., Boothman, C., Polya, D. A., Charnock, J. M., Chatterjee, D., & Lloyd, J. R. (2004). Role of metal-reducing bacteria in arsenic release from Bengal delta sediments. *Nature*, 430(6995), 68-71.

**APPENDIX A**

**Supporting Information for Chapter 2**

**Table A1: Arsenic in High Permeable Sedimentary Formation**

Location	Aquifer Material	Conc. Of Arsenic	Parent Mineral	Chemical Name & Formula	Comment	Reference
Northern New South Wales, Australia	Unconsolidated, Holocene sand deposits of the Stuarts Point region	at 10-11m, [As]= 52-85 µg/L, at 25m [As]= 337 µg/L (No solid phase analysis)	Arsenopyrite	Iron arsenic sulfide (FeAsS)	Reductive dissolution of Fe, Mn and Al oxyhydroxides and arsenical pyrite oxidation, though not forming dominant correlations, are still evident and influence As chemistry at this site.	Smith, et al., 1986
Northwestern Chaco-Pampean Plain, Argentina	Upper loessic sediments alternate with the Salt' River flood plain deposits, while in depth, basal Quaternary sediments consist of highly permeable fluvial-borne gravel and conglomerates that alternate with layers of silt and clay.	Highest conc. more than 1000 µg/L Solid phase: 4-10 mg/Kg	volcanic glass in loess, rich in As		The highest concentrations of As were found in the shallow aquifer, made of As-rich loess, while the lowest As concentrations were found in the deep confined aquifer, consisting of alternating layers of alluvial coarse sands/gravels and clays.	Garcia et al., 2007
			Biotite	phylllosilicate mineral K(Mg,Fe) <sub>2</sub> AlSi <sub>3</sub> O <sub>10</sub> (F,OH) <sub>2</sub>		
			Magnetite	Fe <sub>3</sub> O <sub>4</sub>		
Loess aquifer of La Pampa, Argentina	Sediment comprise of predominantly unconsolidated silts and fine sands and a significant components of rhyolitic volcanic ash.	high concentrations of As (up to 5300 µg/L) Solid Phase: 18 mg/Kg	Ilmenite	crystalline iron titanium oxide (FeTiO <sub>3</sub> )	Fe and Mn minerals are the dominant source and sink of Arsenic.	Smedley et al., 2005
			Biotite	phylllosilicate mineral K(Mg,Fe) <sub>2</sub> AlSi <sub>3</sub> O <sub>10</sub> (F,OH) <sub>2</sub>		
			Fe oxyhydroxide	anhydrous (FeO(OH)) or hydrated (FeO(OH)·nH <sub>2</sub> O)		
Ron Phibun District, Nakhon Si Thammarat Province, southern Thailand	A shallow aquifer, with a depth of < 10m, consists of unconsolidated alluvial gravel, sand, and clay. A deeper carbonate-hosted aquifer is developed in solution cavities, bedding planes, and fault zones at depths of > 15 m.	>100 µg/L Solid Phase: 5000 mg/Kg	Mn oxyhydroxide		Analyses of the silty alluvium have highlighted As probably carried by disseminated arsenopyrite. Following sulfide dissolution, the mobility of As in this material may be high (with resultant contamination of shallow groundwater) due to the low Fe content of the soil.	Williams et al, 1996
			Arsenopyrite	Iron arsenic sulfide (FeAsS)		

Ron Phibun, Nakhon Si Thammarat Province, Thailand	Quaternary alluvium	~2200 mg/Kg (max)	Arsenopyrite	Iron arsenic sulfide (FeAss)	The As mineralogy of mine-waste samples was found to be dominated by arsenopyrite, with scorodite as the principal secondary phase.	Williams et al., 1998
			Scorodite	(FeAsO <sub>4</sub> ·2H <sub>2</sub> O)		
			Arsenolite	(As <sub>2</sub> O <sub>3</sub> )		
	Saflitorite (<1%)			((Co,Fe,Ni)As <sub>2</sub> )		
Aquifers of Cambodia and the Ceu Long Delta of Vietnam	Four Zone: 1. Recent thin shallow to surface sediments. 2. Holocene, incised river silts and coastal sand dunes up to 20 m thick. 3. Upper to mid Pleistocene, freshwater to saline, 10–30 m thick, widely used. 4. Lower Pleistocene, freshwater to saline, underlies about 90% of the delta.	10-600 µg/L 10-30 µg/L (most common) Solid Phase: 8- 16 mg/Kg	Arsenopyrite	Iron arsenic sulfide (FeAss)	Arsenic, associated with iron and organic-rich flood-plain sediments subject to very large flood-related fluctuations in water level, resulting in transient arsenopyrite dissolution under oxidizing conditions.	Stanger et al., 2005
Mekong Delta, Cambodia & Southern Vietnam	Strongly reducing aquifer with high concentrations of iron, manganese, and (in some areas) ammonium.	1-1610 µg/L (avg 217 µg/L) in Cambodia 1-845 µg/L (avg 39 µg/L) in Southern Vietnam Solid Phase: 2-33 mg/Kg	Sediment bound As, from erosion and weathering, results in enrichment of arsenic onto ferric oxyhydroxides followed by fluvial transport and sedimentation	anhydrous (FeO(OH)) or hydrated (FeO(OH)•nH <sub>2</sub> O)	The groundwater arsenic pollution seems to be of natural origin and caused by reductive dissolution of arsenic bearing iron phases buried in aquifers.	Berg et al., 2007
Red River alluvial tract in the city of Hanoi, Vietnam	Due to naturally occurring organic matter in the sediments, the groundwaters are anoxic and rich in iron	1-3050 µg/L (avg 159 µg/L), Highly affected area (avg 430 µg/L) Solid Phase: 6-33 mg/Kg (peak)	Associated with Fe oxyhydroxide	anhydrous (FeO(OH)) or hydrated (FeO(OH)•nH <sub>2</sub> O)		Berg et al., 2001

Upper Triassic Keuper Sandstone, Northern Bavaria, Germany	Different zone: soil, sand and gravel, sandstone, Mudstone, limestone	Data from 500 well, 160 well cone is 10-150 µg/L, Deep seated source of groundwater As: up to 550 µg/L <2-10 mg/Kg (solid phase)	As associated with Sandstone, mudstone, limestone, gravel		Four selected well cores show that arsenic has accumulated in the rocks, this is the source of arsenic in the groundwater of certain facies of the middle unit of the Keuper Sandstone.	Heinrichs and Udluft, 2008
Hetao Basin of Inner Mongolia, china	Shallow alluvial-lacustrine aquifers, which are mainly composed of black (or dark grey) fine sands in a reducing environment	0.6- 572 µg/L. Solid phase: 7.3-73.3 mg/kg (average of 18.9 mg/kg).				
Canal Fulton, Ohio	Sandstone and Gravel deposit	0 – 96 µg/L Solid Phase: 335 mg/Kg	Fe oxyhydroxide	anhydrous (FeO(OH)) or hydrated (FeO(OH)•nH <sub>2</sub> O		Matishoff et al., 1982
Kalix River estuary, northern Sweden	Silty sediment	160 – 170 mg/Kg	Fe oxyhydroxide Fe(III) oxides	anhydrous (FeO(OH)) or hydrated (FeO(OH)•nH <sub>2</sub> O		Widerlund and Ingrid, 1995
Zimapan valley, Mexico	Carbonate rock	1.097 mg/Kg	Arsenopyrite	iron arsenic sulfide (FeAsS)	Arsenopyrite oxidation and scorodite dissolution appear to be the geochemical processes	Armentia et al., 2001
			scorodite	FeAsO <sub>4</sub> ·2H <sub>2</sub> O		
			tennantite	copper arsenic sulfosal mineral Cu <sub>12</sub> As <sub>4</sub> S <sub>13</sub>		

North of Barasat, near Kolkata (Calcutta), in southern West	Anoxic ground water in alluvial aquifers	200- 2000 µg/L Solid Phase: 10-30 mg/Kg	Fe oxyhydroxide	anhydrous (FeO(OH)) or hydrated (FeO(OH)•nH <sub>2</sub> O	by reductive dissolution of FeOOH and release of the sorbed As driven by natural organic matter	McArthur et al., 2004
			Mn oxyhydroxide	MnO <sub>x</sub>		
Ganges- Brahmaputra- Meghna Delta Plain	Alluvial aquifer	2.5- 846 µg/L Solid Phase: 0.5-17.7 mg/Kg	Fe oxyhydroxide	anhydrous (FeO(OH)) or hydrated (FeO(OH)•nH <sub>2</sub> O	by reductive dissolution of FeOOH and release of the sorbed As driven by natural organic matter	Ahmed et al., 2004
			Fe oxyhydroxide	anhydrous (FeO(OH)) or hydrated (FeO(OH)•nH <sub>2</sub> O		
Ganges- Brahmaputra- Meghna Delta Plain	Alluvial aquifer	No solid phase analysis	Fe oxyhydroxide	anhydrous (FeO(OH)) or hydrated (FeO(OH)•nH <sub>2</sub> O	Reduction of FeOOH, and release of sorbed As driven by microbial degradation, no pyrite oxidation, pyrite in Bangladesh aquifers is a sink for, not a source of, arsenic.	McArthur et al., 2007
			hydrated-iron-oxide (HFO), Fe(III)	HFO		
Bengal delta & Middle Ganga Flood plains	Alluvial aquifer	No solid phase analysis	hydrated-iron-oxide (HFO), Fe(III) and Mn(IV) oxides	K(Mg,Fe) <sub>3</sub> AlSi <sub>3</sub> O <sub>10</sub> (OH) <sub>2</sub>	Reductive dissolution of HFO released sorbed As to groundwater and enriched it in Fe. Pyrite in volcanic and shear zone rocks, although locally As-bearing is a minor source of As in groundwater	Acharyya and Shah, 2007
			biotite in granite			
Bengal Basin, Ganga Flood plain	Alluvial aquifer	100- 3000 mg/Kg	hydrated-iron-oxide (HFO), Fe(III) and Mn(IV) oxides	K(Mg,Fe) <sub>3</sub> AlSi <sub>3</sub> O <sub>10</sub> (OH) <sub>2</sub>	Reductive dissolution of Fe(III)-oxyhydroxides and release of its adsorbed As is considered to be the principal mechanism responsible for mobilisation of As	Acharyya et al., 2005
			chlorite in granite			
Matiab Upatza, Southern Bangladesh	Alluvial aquifer	No solid phase analysis	Fe oxyhydroxide	anhydrous (FeO(OH)) or hydrated (FeO(OH)•nH <sub>2</sub> O	Reductive dissolution of Fe(III)-oxyhydroxides and release of its adsorbed As is considered to be the principal mechanism responsible for mobilisation of As	Brömssen et al., 2008
			hydrated-iron-oxide (HFO), Fe(III) and Mn(IV) oxides			
Bengal Basin	Alluvial aquifer	No solid phase analysis	Arsenian Pyrites: Fe(III) and Mn(IV) oxides	FeAsS		Acharyya et al., 2000
Mumshigong,	Alluvial aquifer	640 µg/L Solid Phase: 15-40	Arsenian Pyrites: Arsenopyrite	FeAsS		Polizzotto et al., 2006

Dhaka, Bangal Basin		mg/Kg	Realgar	Arsenic Sulfide, $As_4S_4$		
			Orpiment	Monoclinic Arsenic Sulfide, $As_2S_3$		
Bengal Basin	Alluvial Aquifer	517 ppm Solid Phase: 10-30 mg/Kg	Framboidal Pyrites		Reduction of the Fe is driven by microbial metabolism of sedimentary organic matter.	Nickson et al., 2000
			Fe bearing minerals: Biotite	$K(Mg,Fe)_3AlSi_3O_{10}(F,OH)$		
Meghna riverbank	Alluvial sediments	Surface sediment As conc= $16 \pm 7$ mg/kg. Subsurface sediment As conc from 100 to 23,000 mg/kg	Hornblende	$Ca_2(Mg,Fe,Al)_3(Al,Si)_8O_{22}(OH)_2$	A significant portion of dissolved As sorbs to iron-bearing minerals. Recycling of this sediment-bound As to the Ganges-Brahmaputra-Meghna Delta aquifer provides a potential source of As to further contaminate groundwater.	Datta et al., 2009
			Goethite	$FeO(OH)$		
			Magnetite	$Fe_3O_4$		
			Vivianite	$Fe_3(PO_4)_2 \cdot 8(H_2O)$		
			Arsenian Pyrites: Arsenopyrite	$FeAsS$		
			Realgar	Arsenic Sulfide, $As_4S_4$		
Southeast Michigan	Marshall Sandstone	0.8 to 72.1 mg/Kg	Orpiment	Monoclinic Arsenic Sulfide, $As_2S_3$	The carbonation of arsenic sulfide minerals, including orpiment ( $As_2S_3$ ) and realgar ( $As_4S_4$ ), is an important process in leaching arsenic into groundwater under anaerobic conditions. The arsenocarbonate complexes formed, believed to be $As(CO_3)_2^-$ , $As(CO_3)(OH)_2^-$ , and $AsCO_3^+$ , are stable in groundwater. The reaction of ferrous ion with the thioarsenic from carbonation process can result in the formation of arsenopyrite which is a common mineral in arsenic-rich aquifers.	Kim et al., 2000
			Thioarsenic (sulfarsenites, Sulfosalt with arsenic )	Sulfide mineral with general formula: $A_mB_nS_p$ , where A=metal like Fe, B=semi-metal like As, S=Sulfur		
English East Midlands	Red-bed Sherwood Sandstone	13 $\mu$ g/L (max) Solid Phase: 2 – 10 mg/Kg	Fe oxyhydroxide	anhydrous ( $FeO(OH)$ ) or hydrated ( $FeO(OH) \cdot nH_2O$ )	As concentration is higher in the aerobic section than the anaerobic section, but deepest most saline groundwater has high pH and low Eh, that favor As desorption from iron oxide surface.	Smedley and Edmunds, 2002

Southeastern Michigan	Marshall Sandstone bedrock aquifer, which contains 0 to 8.5% wt arsenic-rich pyrite.	well waters range from 1 to 1310 µg/L, with most common levels being 5-50 µg/L. (No Solid phase analysis)	Arsenopyrite	FeAsS	Pyrite oxidation is not the sole mechanism of arsenic release in these waters, but it may be the primary mechanism of release. Strong correlation with bicarbonate is observed.	Sloznick et al., 2003
Genesee and Huron county, Southeastern Michigan	Marshall Sandstone bedrock and unconsolidated aquifer	Bed rock: 161 µg/L (max) Unconsolidated well: 46 µg/L (max) (No Solid Phase Analysis)	Arsenian pyrite and arsenic-rich iron oxy-hydroxides are found in unconsolidated deposits and arsenian pyrite is found in Marshall Sandstone bedrock	Fe(AsS) <sub>2</sub> , Fe oxyhydroxide	Arsenic contamination is more prevalent in bedrock wells that are cased in proximity to the bedrock unconsolidated interface, because of differences in organic matter content between these geological strata.	Melker et al., 2009
Parts of Brown, Outagamie, and Winnebago Counties, Wisconsin	Platteville/Galena Dolomites overlie the Saint Peter Sandstone. Beneath the sandstone are the Prairie du Chien Dolomites and the Cambrian Sandstone	Upper portion of St. Peter Sandstone exhibits higher As conc. 450 µg/L (34.7 to 43.9 m) than those found in the base of that (43.9 to 62.2 m), that is 50 µg/L. (No Solid Phase Analysis)	Arsenic bearing pyrites  Marcasite	FeS <sub>2</sub>  FeS <sub>2</sub>	Three wells in this study had an unusually low pH, which appears to be caused by the presence and oxidation of pyrite.	Burkel and Stoll, 1999
Eastern Wisconsin	Confined Sandstone aquifer; static water level intersect an As bearing sulfide cement horizon (SCH) in the aquifer.	Up to 12,000 µg/L, Solid Phase: 15-674 mg/Kg	Arsenic bearing sulfide, marcasite  As bearing Fe oxyhydroxide	FeS <sub>2</sub>  anhydrous (FeO(OH)) or hydrated (FeO(OH)•nH <sub>2</sub> O)	Arsenic occurs in pyrite and marcasite as well as in iron oxyhydroxides but not as a separate arsenopyrite phase.	Schreiber et al., 2000
Washington, United States	Surficial silt deposit	4.4-84 mg/Kg	Fe oxyhydroxide  Mn oxyhydroxide	anhydrous (FeO(OH)) or hydrated (FeO(OH)•nH <sub>2</sub> O)  MnO <sub>x</sub>		Thornburg and Sahai, 2004

Northeastern Wisconsin	Confined sandstone aquifer	161 - 510 mg/Kg	Arsenic bearing sulfide, marcasite	FeS <sub>2</sub>		Golkowitz et al., 2004
			As bearing Fe oxyhydroxide			
Southern Choushuni River, Central Taiwan	Alluvial fan	20-130 mg/Kg	Fe oxyhydroxide	anhydrous (FeO(OH)) or hydrated (FeO(OH)•nH <sub>2</sub> O)	Fe oxyhydroxides and sulfides were likely to be the major sinks of As	Anawar et al., 2010
			Arsenopyrite (Framboidal)			
			Authigenic Pyrite (also)			
Eastern Australia	Unconsolidated sediment overlying bedrock	1.4-14.0 mg/Kg	Antimony bearing mineral, Stibnite (common association with Arsenopyrite and arsenian pyrite)	Sb <sub>2</sub> S <sub>3</sub>	Derived from erosion of arsenic rich (Sb <sub>2</sub> S <sub>3</sub> ) mineralization	O'Shea et al., 2007
			Fe oxyhydroxide			
southeastern Arkansas	alluvial	40-70 mg/Kg	Mn oxyhydroxide	MnO <sub>x</sub>		Sharif et al., 2008
Mahomet and Glasford Aquifers, Central Illinois	Sand and gravel deposit upto 20 m thick	No solid phase analysis	Sulfide Mineral		Sulfate reduction and sorption of arsenic to sulfide minerals.	Holm et al., 2005
			Fe oxyhydroxide	hydrrous (FeO(OH))	Reductive dissolution of (hydr)oxide minerals	Root et al., 2005
Lake Geneva, Wisconsin	Glacial deposit 150 m thick	< 2mg/Kg to 4 mg/Kg	Mn oxyhydroxide	MnO <sub>x</sub>		Bacteria mediated reductive dissolution of As bearing hydrous Ferric oxides.
			Fe oxyhydroxide	hydrrous (FeO(OH))		
			Mn oxyhydroxide	MnO <sub>x</sub>		
			As bearing Pyrite	FeCO <sub>3</sub>		
Kansas city and Alabama	Alluvial	10-20 mg/Kg	As poor Siderite	FeCO <sub>3</sub>		Saunders et al., 2005
			Rhodochrosite	MnCO <sub>3</sub>		

**Table A2: Arsenic in Low Permeable Sedimentary Formation**

<b>Location</b>	<b>Rock</b>	<b>Parent Mineral</b>	<b>Chemical Name and Formula</b>	<b>Concentration mg/kg</b>	<b>Reference</b>
<b>SOUTH KOREA</b>					
Chu-Bu	Black Shale	Arsenopyrite	Iron arsenic sulfide (FeAss)	0.5-6.2	Lee 1998
Chung-Loo	Black Shale	Arsenopyrite	Iron arsenic sulfide (FeAss)	0.5-8.4	Lee 1998
Duk-Pyung	Black Shale	Arsenopyrite	Iron arsenic sulfide (FeAss)	5.0-110.0	Lee 1998
<b>U.S.A</b>					
Erie, PA	Cascade Creek Shale	Arsenopyrite	Iron arsenic sulfide (FeAss)	5.5; 9.9	Murnock 2002
North central USA	Claystone	Pyrite	FeS <sub>2</sub>	3-10	Tourtelot 1964
Erie, PA	Mill Creek Shale	Arsenopyrite	Iron arsenic sulfide (FeAss)	8.8	Murnock 2002
Rodeo Creek formation, Nevada	Mudstone(limy)	Arsenopyrite	Iron arsenic sulfide (FeAss)	23;84	Turkenian and Wedepohl 1961

Green River Formation	Oil Shale	Skutterudite Safflorite	CoFeNiAs <sub>3</sub> CoFeAs <sub>2</sub>	48.0 ± 0.7	Jagannath et al., 1986
East Texas	Pepper Shale	Clay minerals, pyrite		6.0-8.0	Abraham 1998
East Texas	Sandstone Paluxy(>90% Quartz)	Quartz		<1	Abraham 1998
North central USA	Shale Non marine	Pyrite		3-12	Tourtrelot 1964
North Central USA	Shale and claystone (offshore marine)	Pyrite Clay minerals		3-490	Tourtrelot 1964
Illinois river basin	Shale Balck Shale	Organic rich - carbonate bed rock		5-55 12-21	Warner 2001
New Albany	Shale	N/A		4-45	Frost et al., 1985
Weches formation, TX	Shale	Accessory pyrite, pyrite, Amorphous FeOH3and		100	Ledger and Judy 2003

			goethite			
Eastern Wisconsin	Shale	Pyrite, Marcasite, Ironoxyhydroxides		<10-500		Gotkowitz et al., 2001
Georgia	Shale	N/A		30		Zhabin et al., 1990
<b>IRAN</b>						
Zarshuran	Black Shale	Orpiment, Realgar, Au-As pyrite	Arsenic Sulfide, As <sub>4</sub> S <sub>4</sub>	200-82000		Mehrabi et al., 1999
<b>ANTARCTICA</b>						
Pensacola Mountains, Antarctica	Sandstone	N/A		80		Altschuler 1980
<b>CANADA</b>						
Wolfville Formation	Shale	Arseniferous Pyrite Tennantite Proustite	And various other sulphide minerals	2-27		Boyle and Jonasson 1973
Walton area, Nova Scotia	Shale	Arseniferous Pyrite Tennantite Proustite		<1-32		Boyle and Jonasson 1973

		And various other sulphide minerals			
Cobalt Area, Ontario	Shale	Arseniferous Pyrite Tennantite Proustite		3	Boyle and Jonasson 1973
Walton area, Nova Scotia	Shale	And various other sulphide minerals Arseniferous Pyrite Tennantite Proustite		1-45	Boyle and Jonasson 1973
Northern Labrador	Shale	And various other sulphide minerals Arseniferous Pyrite Tennantite Proustite		3-500	Boyle and Jonasson 1973
<b>MEXICO</b>					
Trancas and Soyatol formation	Shale and claystone	Arsenopyrite	Iron arsenic sulfide (FeAsS)	10-360	Armienta et al., 2001

Tamailpas formation	Shale and Claystone	Arsenopyrite	Iron arsenic sulfide (FeAsS)	15-125	Armentia et al., 2001
<b>INDIA</b>					
Kanker Basin	Shale and Clay	Iron Hydroxide		12	Pandey et al. 2006
<b>SPAIN</b>					
	Siltstone( marly)			89 ± 94	
Cantabrian Mountains	Siltstone	Arsenic bearing pyrite and arsenopyrite	Iron arsenic sulfide (FeAsS)	142 ± 236	Crespo et al., 2000

## References

- Abraham, J., (1998) Spatial distribution of major and trace elements in shallow reservoir sediments: an example from lake Waco, Texas. *Environmental Geology*, 36 (3-4), 349-363.
- Acharyya, S.K. and Shah B.A., (2007) Groundwater arsenic contamination affecting different geologic domains in India - a review: influence of geological setting, fluvial geomorphology and Quaternary stratigraphy. *Journal of Environmental Science and Health part A toxic hazardous substances & Environmental Engineering*, 42(12), 1795-1805.
- Acharyya, S.K., Shah, B.A., Ashyia, I.D. and Pandey, Y., (2005) Arsenic contamination in groundwater from parts of Ambagarh-Chowki block, Chhattisgarh, India: source and release mechanism. *Environmental Geology*, 49(1), 148-158.
- Acharyya, S.K., Lahiri, S., Raymahashay, B.C. and Bhowmik, A., (2000) Arsenic toxicity of groundwater in parts of the Bengal basin in India and Bangladesh: the role of Quaternary stratigraphy and Holocene sea-level fluctuation. *Environmental Geology*, 39(10), 1127-1137.
- Ahmed, K.M., Bhattacharya, P., Hasan, M.A., Akhter, S.H., Alam, S.M.M., Bhuyian, Badrul Imam, M.B., Khan, A.A., and Sracek, O., (2004) Arsenic enrichment in groundwater of the alluvial aquifers in Bangladesh: an overview. *Applied Geochemistry*, 19, 181-200.
- Altschuler, Z.S., (1980) The geochemistry of trace elements in Marine Phosphorites , Part I : Characteristic Abundances and Enrichment , SEPM special publication 29, SEPM, 19-30.
- Anawar, H.M., Akai, J., Komaki, K., Terao, H., Yoshioka, T., Ishizuka, T., Safiullah, S. and Kato, K., (2010) Primary sink and source of geogenic arsenic in sedimentary aquifers in the southern Choushui River alluvial fan, Taiwan. *Journal of Geochemical Exploration*, 25(5), 684-695.
- Armienta, M.A., Villasenor, G., Rodriguez, R., Ongley, L.K. and Mango, H., (2001) The role of arsenic-bearing rocks in groundwater pollution at Zimapan Valley, Mexico. *Geology*, 40(4-5), 571-581.
- Berg, M., Tran, H.C., Nguyen, T.C., Pham, H.V., Schertenleib, R., and Giger, W., (2001) Arsenic contamination of groundwater and drinking water in Vietnam: A human health threat. *Environmental Science and Technology*, 35(13), 2621-2626.
- Berg, M., Stengel, C., Tran, P.T.K., Viet, P.H., Sampson, M.L., Leng, M., Samreth, S., and Fredricks, D., (2007) Magnitude of arsenic pollution in the Mekong and Red River Deltas — Cambodia and Vietnam. *Science of the Total Environment*, 372, 413–425.
- Boyle, R.W., Jonasson, I.R., (1973) Geochemistry of arsenic and its use as indicator in element in geochemical prospecting. *Journal of Geochemical Exploration*, 2(3), 43-57.

- Brömssen, M.V., Larsson S.H., Bhattacharya, P., Hasan, M.A., Ahmed, K.M., Jakariya, M., Shikder, M.A., Sracek, O., Biven, A., Dousova, B., Patriarca, C., Thunvik, R. and Gunnar Jacks, (2008) Geochemical characterisation of shallow aquifer sediments of Matlab Upazila,
- Burkel, R.S. and Stoll, R.C., (1999) Naturally Occurring Arsenic in Sandstone Aquifer Water Wells of Northeastern Wisconsin. *GWMR*, 114-121.
- Crespo, J.L., Moro, M.C. and Fadon, (2000) The salamon gold deposit (Leon, Spain). *Journal of Geochemical Exploration*, 71(2), 191-208.
- Datta, S., Mailloux, B., Jung, H.B., Hoque, M.A., Stute, M., Ahmed, K.M. and Zheng, Y., (2009) Redox trapping of arsenic during groundwater discharge in sediments from the Meghna riverbank in Bangladesh. *Proceedings of the National Academy of Sciences*, Volume 106(40), 16930-16935.
- Frost, J.K., Zierath, D.L. and Shimp, N.F., (1985) Chemical Composition and Geochemistry of the new Albany Shale group (Devonian- Mississipi) in Illinois, Illinois state Geological Survey, Champaign, IL.
- Garcia, M.G., Sracek, O., Fernandez, D.S., and Hidalgo, M., (2007) Factors affecting arsenic concentration in groundwaters from Northwestern Chaco-Pampean Plain, Argentina. *Environmental Geology*, 52(7), 1261-1275.
- Gotkowitz, M.B., Schreiber, M.E. and Simo, J.A., (2004) Effects of water use on arsenic release to well water in a confined aquifer. *Ground Water*, 42(4), 568-575.
- Gotkowitz, M.B., Simo, J.A. and Schreiber, M.E., (2001) Geologic and geochemical control on arsenic release to groundwater in eastern Wisconsin, Abstracts with programs. *The Geological Society of America*, 33(6), 54.
- Heinrichs, G. and Udluft, P., (1999) Natural arsenic in Triassic rocks: A source of drinking-water contamination in Bavaria, Germany. *Hydrogeology Journal*, 7, 468-476.
- Holm T.R., Kelly, W.R., Wilson, S.D., Roadcap, G.S., Talbott, J.L. and Scott, J.S., (2005) Arsenic Distribution and Speciation in the Mahomet and Glasford Aquifers, Illinois. In: P.A. O'Day, D. Vlassopoulos, X. Meng & L.G. Benning, ed. *Advances in Arsenic Research*. Washington, DC: ACS Symposium Series 915. Ch.11.
- Guo, H., Yang, S., Tang, X., Li, Y. and Shen, Z., (2008) Groundwater geochemistry and its implications for arsenic mobilization in shallow aquifers of the Hetao Basin, Inner Mongolia. *Science of the Environment*, 393, 131-144.
- Jaganathan, J., Mohan, M.S. and Zingaro, R.A., (1986) Identification of arsenic bearing minerals in a sample of Green River Oil Shal. *Fuel*, 65(2) 266-69.

Kim, M.J., Nriagu, J. and Haack, S., (2000) Carbonate ions and arsenic dissolution by groundwater, *Environmental Science & Technology*, 34(15), 3094-3100.

Ledger, E.B. and Judy, K., (2003) Elevated arsenic concentration in Weches Formation, Nacogdoches County, Texas, Transaction of the gulf coast association of geological societies, LIII, 453-61.

Lee, J-S. Enrichment of potentially toxic elements in areas underlain by black shales and slates in Korea. *Environmental Geochemistry and Health*, (20), 135-147.

Matishoff, G., Khourey, C.J., Hall, J.F., Varnes, A.W. and Strain, W.H., (1982) The nature and source of Arsenic in Northeastern Ohio Groundwater. *Ground Water*, 20(4).

McArthur, J.M., Banerjee, D.M., Hudson-Edwards, K.A., Mishra, R., Purohit, R., Ravenscroft, P., Cronin, A., Howarth, R.J., Chatterjee, A., Talukder, T., Lowry, D., Houghton, S. and Chadha, D.K., (2004) Natural organic matter in sedimentary basins and its relation to arsenic in anoxic ground water: the example of West Bengal and its worldwide implications. *Applied Geochemistry*, 19(8), 1255-1293.

McArthur, J.M., Ravenscroft, P., Safiulla, S. and Thirlwall, M.F., (2001) Arsenic in groundwater: Testing pollution mechanisms for sedimentary aquifers in Bangladesh. *Water Resources*, 37(1), 109-117.

Mehrabi, Yardley and Cann, (1999) Sediment hosted gold mineralization at Zarshuran, NW IRAN, *Mineralium Deposita*, 34, 673-696.

Meliker, J.R., Slotnick, M.J., Avruskin, G.A., Haack, S.K. and Nriagu, J.O., (2009) Influence of groundwater recharge and well characteristics on dissolved arsenic concentrations in southeastern Michigan groundwater. *Environmental Geochemistry & Health*, 31(1), 147-157.

Murnock, J.M., (2002) Vertical and seasonal distributions and relationships of Arsenic in presques Isle Sediments, Master of science thesis, Gannon University, Erie, Pennsylvania. 4(6), 461-68.

Nickson, R.T., McArthur, J.M., Ravenscroft, P., Burgess, W.G. and Ahmed, K.M., (2000) Mechanism of arsenic release to groundwater, Bangladesh and West Bengal. *Applied Geochemistry*, 15(4), 403-413.

O'Shea, B., Jankowski, J. and Sammut, J., (2007) The source of naturally occurring arsenic in a coastal sand aquifer of eastern Australia. *Science of the Total Environment*, 379, 155-166.

Pandey, P.K., Sharma, R., Roy, (2006) Arsenic estimation in the Kanker district of central east India: geology and health effects. *Environmental Geochemistry and Health*, 28(5), 409-20.

Peterson, M.L. and Carpenter, R., (1986) Arsenic distribution in porewaters and sediments of Puget Sound, Lake Washington and the Washington coast and Saanich Intel, B.C. *Geochimica et Cosmochimica Acta*, 50, 353-369

Polizzotto, M.L., Harvey, C.F., Li, G.C., Badruzzaman, B., Ali, A., Newville, M., Sutton, S. and Fendorf, S., (2006) Solid phases and desorption processes of arsenic within Bangladesh sediments. *Chemical Geology*, 228(1-3), 97-111.

Root, T.L., Bahr, J.M. and Gotkowitz, M.B., (2005) Controls on Arsenic Concentrations in Groundwater near Lake Geneva, Wisconsin. In: P.A. O'Day, D. Vlassopoulos, X. Meng & L.G. Benning, ed. *Advances in Arsenic Research*. Washington, DC: ACS Symposium Series 915. Ch.12.

Saunders, J.A., Mohammad, S., Korte, N.E., Lee, M.-K., Fayek, M., Castle, D. and Barnett, M.O., (2005) Groundwater Geochemistry, Microbiology, and Mineralogy in two arsenic bearing Holocene alluvial aquifers from the United States. In: P.A. O'Day, D. Vlassopoulos, Schreiber, M.E., Simo, J.A. and Freiberg, P.G., (2000) Stratigraphic and geochemical controls on naturally occurring arsenic in groundwater, eastern Wisconsin, USA. *Hydrological Journal*, 8(2), 161-176.

Sharif, M.U., Davis, R.K., Steele, K.F., Hays, P.D., Kresse, T.M. and Fazio, J.A., (2008) Distribution and variability of redox zones controlling spatial variability of arsenic in the Mississippi River Valley alluvial aquifer, southeastern Arkansas, *Journal of Contaminant Hydrology*, 99(1-4), 49-67.

Slotnick, M.J., Meliker, J. and Nriagu, J., (2003) Natural sources of arsenic in Southeastern Michigan groundwater. *Journal De Physique Iv*, 107(2), 1247-1250.

Smedley, P.L., Kinniburgh, D.G., Macdonald, D.M.J., Nicolli, H.B., Barros, A.J., Tullio, J.O., Pearce, J.M., and Alonso, M.S., (2005) Arsenic associations in sediments from the loess aquifer of La Pampa, Argentina, *Applied Geochemistry*, 20(5), 989-1016.

Smedley, P.L. and Edmunds, W.I., (2002) Redox Patterns and Trace- Element Behavior in the East Midland Triassic Sandstone Aquifer, U.K. *Ground Water*, 40(1), 44-58.

Smith, J.V.S., Jankowski, J., and Sammut, J., (1986) Vertical distribution of As(III) and As(V) in a coastal sandy aquifer: factors controlling the concentration and speciation of arsenic in the Stuarts Point groundwater system, northern New South Wales, Australia. *Applied Geochemistry*, ISSN 0883-2927.

Stanger, G., VanTruong, T., Le Thi My Ngoc, K.S., Luyen, T.V., and Thanh, T.T., (2005) Arsenic in groundwaters of the Lower Mekong. *Environmental Geochemistry and Health*, 27, 341-357.

- Thornburg, K., & Sahai, N. (2004). Arsenic occurrence, mobility, and retardation in sandstone and dolomite formations of the Fox River Valley, Eastern Wisconsin. *Environmental science & technology*, 38(19), 5087-5094.
- Tourtelot, H.A., (1964) Minor element composition and organic carbon content of marine and non marine shales of late cretaceous age in the western interior of united states. *Geochimica et Cosmochimica Acta*, 28, 1579-1604.
- Turekian, K.K. and Wedepohl, K.H., (1961) Distribution of the elements in some major units of the earth's crust. *Geological Society of America Bulletin*, 72, 175-92.
- Warner, K.L., Arsenic in glacial drift aquifers and the implication for drinking water- lower Illinois River Basin, *Ground Water*, 39 (3), 433-442.
- Widerlund, A. and Ingri, J., (1995) Early diagenesis of arsenic in sediments of the Kalix River estuary, northern Sweden. *Chemical Geology*, 125, 185-196.
- Williams, M., Fordyce, F., Pajitprapapon, A., and Charoenchaisri, P., (1996) Arsenic contamination in surface drainage and groundwater in part of the southeast Asian tin belt, Nakhon Si Thammarat Province, southern Thailand. *Environmental Geology*, 27(1), 16-33.
- Williams, T.M., Rawlins, B.G., Smith, B., and Breward, N., (1998) In-Vitro Determination of Arsenic Bioavailability in Contaminated Soil and Mineral Beneficiation Waste from Ron Phibun, Southern Thailand: A Basis for Improved Human Risk Assessment. *Environmental Geochemistry and Health*, 20, 16-177.
- X. Meng & L.G. Benning, ed. *Advances in Arsenic Research*. Washington, DC: ACS Symposium Series 915. Ch.14.
- Zhabin, A.G., Samsonova, N.S. and Chuchua, I.B., (1990) Ore- bearing metasomatically altered limestones of the black shale association. *International Geology Review*, 32(11), 1145-55.

**APPENDIX B**

**Supporting Information for Chapter 3**

## **B1. Reactor systems to measure mineral dissolution**

The majority of experiments measuring dissolution rate of minerals use three basic types of reactor systems: batch reactors, mixed-flow reactors and plug flow reactor systems (Levenspeil, 1972; Hill, 1977; Rimstidt and Dove, 1986). Each of these three systems has its advantages but experiments to measure dissolution rates are typically conducted in mixed flow reactor systems owing to simplicity in data analysis and interpretation. Mixed flow systems, however, are expensive to construct and tedious to operate. Table B1 summarizes the properties of typical reactor systems used for studying dissolution at high pressure, temperature and salinity.

**Table B1.** Summary of reactor properties for studying dissolution at high temperature, pressure and salinity

	<b>Batch</b>	<b>Mixed Flow</b>	<b>Plug Flow</b>
<b>Material of Construction</b>	Titanium/Gold	Titanium/Gold	PEEK
<b>Cost</b>	Expensive	Expensive	Inexpensive
<b>Data Analysis</b>	Moderate	Simple	Complex
<b>Mass transfer limitations</b>	Yes	No	No
<b>Setup difficulty</b>	Moderate	Difficult	Easy
<b>Data collection</b>			Easy
<b>Experimental time to reach the same outcome (e.g. dissolution rates of FeAsS)</b>	Weeks to months	Weeks to months	Days

Since plug flow systems are inexpensive to construct and the least labor intensive they are ideal for multiple, long-term dissolution experiments. Plug flow systems, suffer from mass transfer complications, and complexities in data analysis. If these problems are addressed, plug flow systems would be ideal for long term dissolution and rate determination studies.

## B2. A Model to predict dispersivity

While the dimensions, porosity, and solid/liquid ratio in the column were measured, dispersion coefficients were modeled. The models showed that dispersive effects lasted for only around 20 pore volumes, for a range of flow rates even for high values of dispersivity (Figure B1). Assuming that the influent was non reactive, the effluent concentration was plotted with respect to pore volumes passed. Typical values of axial dispersion coefficient ( $\alpha_L$ ) range from 0.1-1 cm. The figure shows that even for values of  $\alpha_L$  of 10 cm, the effect of dispersion is overcome after 50 pore volumes. Thus, the need for including dispersivity in our models was obviated. We have added this information to the manuscript.

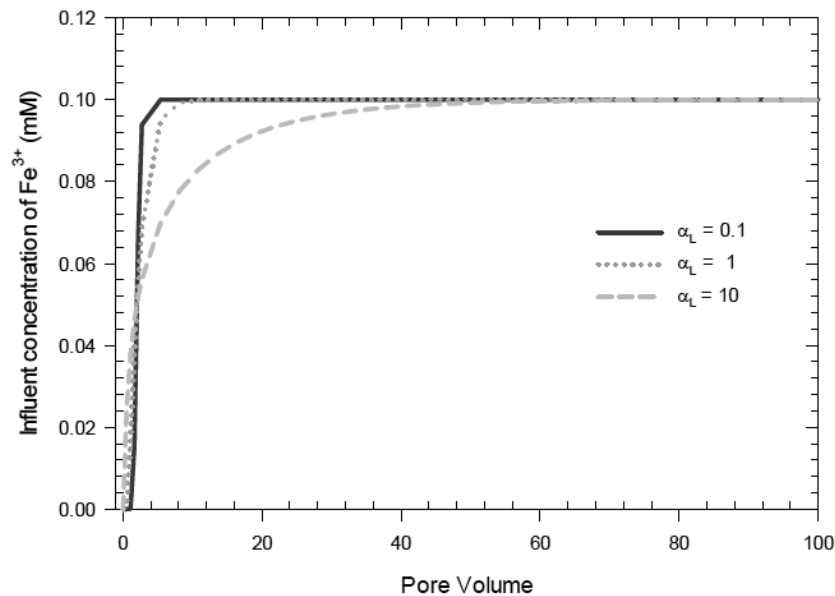


**Figure B1.** Modeled effluent tracer concentration with respect to pore volume

### **B3. References**

Levenspiel, O. (1972). *Chemical Reaction Engineering*, 2<sup>nd</sup> ed., John Wiley and Sons, New York, 578.

Rimstidt, J.D., Dove, P.M. (1986). Mineral/solution reaction rates in a mixed flow reactor: Wollastonite hydrolysis. *Geochimica et Cosmochimica Acta* 450, 2509-2516.

## **APPENDIX C**

### **Supporting Information for Chapter 5**

## **C1. Materials and Methods:**

### C1.1 Mineral preparation and characterization

Arsenopyrite, galena, and pyrite were obtained from Wards Sci. Inc. (Rochester, NY) and were crushed in a porcelain mortar and pestle and size fractionated using nylon sieves to a range of 150- 250  $\mu\text{m}$ . The mortar and pestle as well as sieves were soaked overnight in 10% (w/V)  $\text{HNO}_3$  prior to use. The crushed minerals were then prepared as follows, based on the method for arsenopyrite developed by Parthasarathy et al., (2014).

A. Pyrite and arsenopyrite were prepared by the following steps -

1. Sonicated in 50% (w/v) ethanol for 5 minutes. Supernatant drained. Repeated three times.
2. Rinsed with 12N HCl for 3 minutes.
3. Rinsed with DI water for 1 minute
4. Dried in  $\text{N}_2$  atmosphere

B. Galena was prepared by the following steps-

1. Sonicated in 50% (w/v) ethanol for 5 minutes. Supernatant drained. Repeated three times.
2. Rinsed with 1 N HCl for 3 minutes.

3. Rinsed with DI water for 1 minute.
4. Dried in N<sub>2</sub> atmosphere

XRD analysis confirmed the primary mineral phases were arsenopyrite, pyrite, and galena (Figure C1). The X-ray diffraction spectra were collected for the samples on beamline 11-3 at the Stanford Synchrotron Radiation Lightsource (SSRL). Incident X-rays (0.9744 Å, 12,724 eV) were focused using a bent cube root I-beam Si (311) monochromator. A MAR345 area detector positioned 148.7 mm downstream of the sample was used to collect diffraction scans with a dwell time of 10s. Calibrations were performed using a LaB<sub>6</sub> standard fit using WxDiff software obtained from Stefan Mannsfeld from SSRL. The collected images were converted into degrees 2θ space using Area Diffraction Machine (open source) software. The background was not subtracted to prevent the removal of the minor peaks that may indicate crystalline phases. The data was matched to a database of existing XRD patterns using the X'Pert Highscore Plus software and a database obtained from the Crystallography Open Database website. The XRD spectra of samples and standards are shown in Figure C1 (A-C).

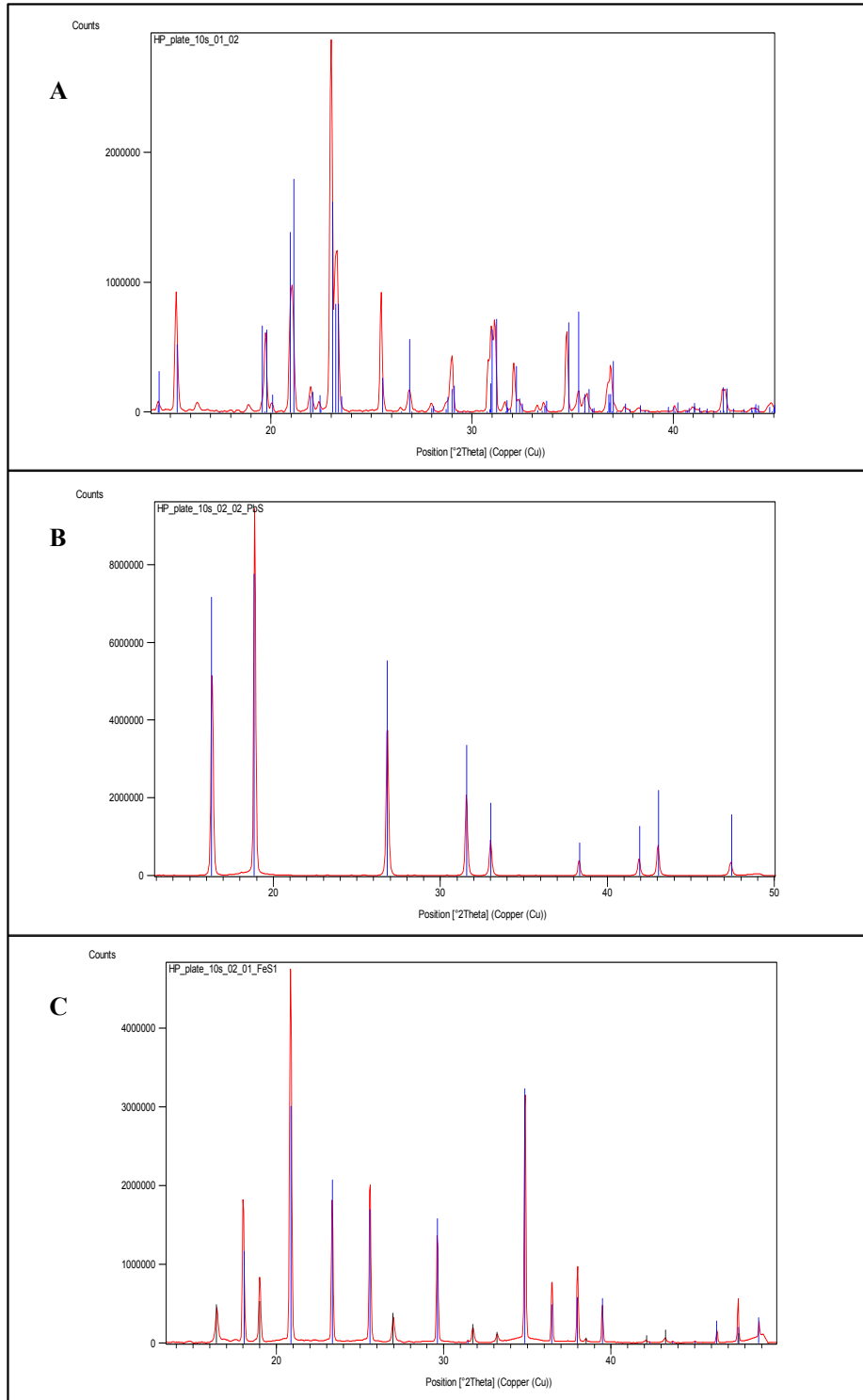


**Figure C1.** XRD Spectra for (A) Arsenopyrite, (B) Galena, and (C) Pyrite are shown in red with the standard reference peaks in blue.

The surface stoichiometry of each mineral was measured using a Philips XL30 FEG scanning microscope (SEM) equipped with an SE Everhart Thornley detector and an Oxford INCA EDS with full quantitative composition analysis. The operating conditions were, accelerating voltage 10 kV, spot size 3, and a working distance of 10 mm. The SEM-EDS had a detection limit of 1% by weight. The results of these analyses for all three minerals are shown in Table C1.

**Table C1.** Solid phase characterization of mineral samples for dissolution experiments

<b>Mineral</b>	<b>SEM-EDS Stoichiometry</b>
Arsenopyrite (FeAsS)	$\text{Fe}_{1.03\pm 0.05}\text{As}_{1.01\pm 0.05}\text{S}_{0.87\pm 0.05}$
Galena (PbS)	$\text{Pb}_{0.97\pm 0.01}\text{S}_{1.14\pm 0.08}$
Pyrite (FeS <sub>2</sub> )	$\text{Fe}_{1.03\pm 0.03}\text{S}_{1.94\pm 0.06}$

### C1.2 Reagents

Ultra high pure NaCl (99.9999%, metal basis), CaCl<sub>2</sub> (99.99%, metal basis), and MgCl<sub>2</sub> (99.99%, metal basis) purchased from Alfa Aesar, USA, were used to make influent solutions for dissolution experiments. 1M ultra pure HCl (Fisher Scientific Inc.) was used to adjust the pH. All solutions were made with deionized water (18.2 MΩ; Barnstead, USA).

### C1.3 Experimental Setup and Dissolution experiments

Dissolution experiments were conducted in a small-scale flow through column system developed by Parthasarathy et al., 2013<sup>10</sup>, consisting of a 5 cm PEEK column and a HPLC pump. The column was filled with prepared mineral (150-250  $\mu\text{m}$ ) and influent solution was pumped at a constant flow rate of 1ml/min. Effluent samples were collected at 2-hour intervals and analyzed for dissolution products. All dissolution experiments were conducted at ambient temperature (25 °C) and pressure (1 atm.). Influent solutions for each experiment were prepared using reagents stated above and the pH was adjusted to  $2.55\pm 0.05$  by adding  $6\pm 0.4$  ml of 1N HCl to 2L of reactant solution. The pH was measured using an accumet XL 60 (Fisher scientific) pH meter and an Orion<sup>TM</sup> 8165BNWP ROSS<sup>TM</sup> Sure-Flow<sup>TM</sup> pH electrode (Thermo Scientific for pH measurements of high-TDS solutions. The entire system was placed in a 280L glove bag (Sigma Aldrich USA), which was filled with nitrogen. Dissolved oxygen in the influent solutions was removed by sparging laboratory grade N<sub>2</sub> for 18 hours prior to each experiment. The N<sub>2</sub> bubbling was continued throughout the duration of the experiments. The oxygen concentration inside the glove bag and the dissolved oxygen in the influent solution were measured using an Accumet XL 60 DO meter (Fisher scientific). The detection limits were 0.1% saturation (atmospheric oxygen) and 0.01mg/L (dissolved oxygen).

A list of experiments that were conducted for each individual mineral is shown in Table C2.

**Table C2.** List of experiments for each mineral at equal electrolyte concentrations

<b>S.N</b>	<b>Electrolyte</b>	<b>Concentration (M)</b>	<b>[HCl] (M)</b>	<b>Ionic Strength (M)</b>	<b>Anion Activity</b>	<b>Cation Activity</b>
1	HCl	-	0.003	0.0030	0.0028	0.0028
2	NaCl	0.01	0.003	0.0130	0.0115	0.0089
3	CaCl <sub>2</sub>	0.01	0.003	0.0330	0.0192	0.0053
4	MgCl <sub>2</sub>	0.01	0.003	0.0330	0.0192	0.0056

Experiments with 10mM NaCl, 10mM CaCl<sub>2</sub>, and 10mM MgCl<sub>2</sub> (Table C2, S.N 2-4) at pH 2.55 were conducted to determine the influence of equal concentrations of different electrolytes on the dissolution of each mineral. A blank experiment with D.I Water (pH 2.55 HCl) was conducted to account for the effect of reduced pH. Experiments were conducted at low pH to prevent precipitation inside the column, which could lead to mass transfer limitations.

The experiments outlined in Table C2 have varying ionic strengths, which could have a significant effect on the activity of species in solution. An additional experiment with 5.6mM NaCl was therefore conducted for arsenopyrite to determine the effect of individual cations at the same activity on arsenopyrite dissolution. Activity coefficients were calculated using the Extended Debye Huckel equation and used to estimate the cation and anion activity in solution.

This allows direct comparison of different electrolytes without complications arising from ionic strength. These experiments are shown in Table C3.

**Table C3.** Equal cation activity experiments for arsenopyrite dissolution

S.N	Electrolyte	Concentration (M)	[HCl] (M)	Ionic Strength	Anion Activity	Cation Activity
1	NaCl	0.0056	0.003	0.0085	0.0076	<u>0.0051</u>
2	CaCl <sub>2</sub>	0.01	0.003	0.0330	0.0192	<u>0.0053</u>
3	MgCl <sub>2</sub>	0.01	0.003	0.0330	0.0192	<u>0.0056</u>

#### C1.4 Analysis

##### *Iron, lead and arsenic*

Samples collected were preserved with 5% HNO<sub>3</sub> (trace metal grade). Samples were diluted (5x) with 5% HNO<sub>3</sub> and analyzed for iron and arsenic (arsenopyrite), iron (pyrite), and lead (galena) using an Agilent 7700x ICP-MS equipped with a collision-reaction-chamber. Polyatomic interference for Fe and As were reduced by conducting the analysis in Helium-collision mode. A four point calibration curve for each analytes was constructed before each set of samples with  $r^2 > 0.99$ . A multi-element standard mixture from Agilent Technologies Inc. was used to prepare standard solutions and a midrange standard was used to check the calibration after every 10

samples. The detection limits were 0.15 ppb for Fe, 0.04 ppb for As, and 0.003 ppb for Pb.

### *Sulfur*

All samples were exposed to air for a minimum of 24h upon collection, and sulfur was converted to sulfate. For sulfate determination an ion-suppressed chromatography was employed. The high-pressure liquid chromatography (HPLC) system consisted of an anion suppressor (AERS 500, Dionex), an anion separation column (AS-14A, Dionex) and a conductivity detector (ED40 Electrochemical detector, Dionex). The eluent was 0.8mM NaHCO<sub>3</sub>/10mM Na<sub>2</sub>CO<sub>3</sub> at a flow rate of 1.2 mL/min at 35 °C. The same temperature (35 °C) was used for the detector. The injection volume was 100 µL. A four-point calibration was used and calibration curves were developed with  $r^2 > 0.99$  for SO<sub>4</sub><sup>2-</sup>. The sulfate concentration was determined according to USEPA<sup>1</sup> and Standard Methods<sup>3</sup>. The calibration curve for sulfate was constructed each time that fresh eluent was used or otherwise every 20 injections. A midrange standard was used every 10 injections to verify good quality of IC performance. Standard solutions were prepared daily with dilutions of a stock standard sulfate solution, dilution of its respective salts was used. The method detection limit (MDL) depended upon the matrix that was used. The MDLs are shown in the table below (Table C4).

**Table C4.** Method detection limits for sulfate using ion chromatography

<b>Matrix</b>	<b>MDL (ppb)</b>
HCl	1
NaCl	1
CaCl <sub>2</sub>	20
MgCl <sub>2</sub>	10

## C2. Dissolution Results

### C2.1 Arsenopyrite dissolution

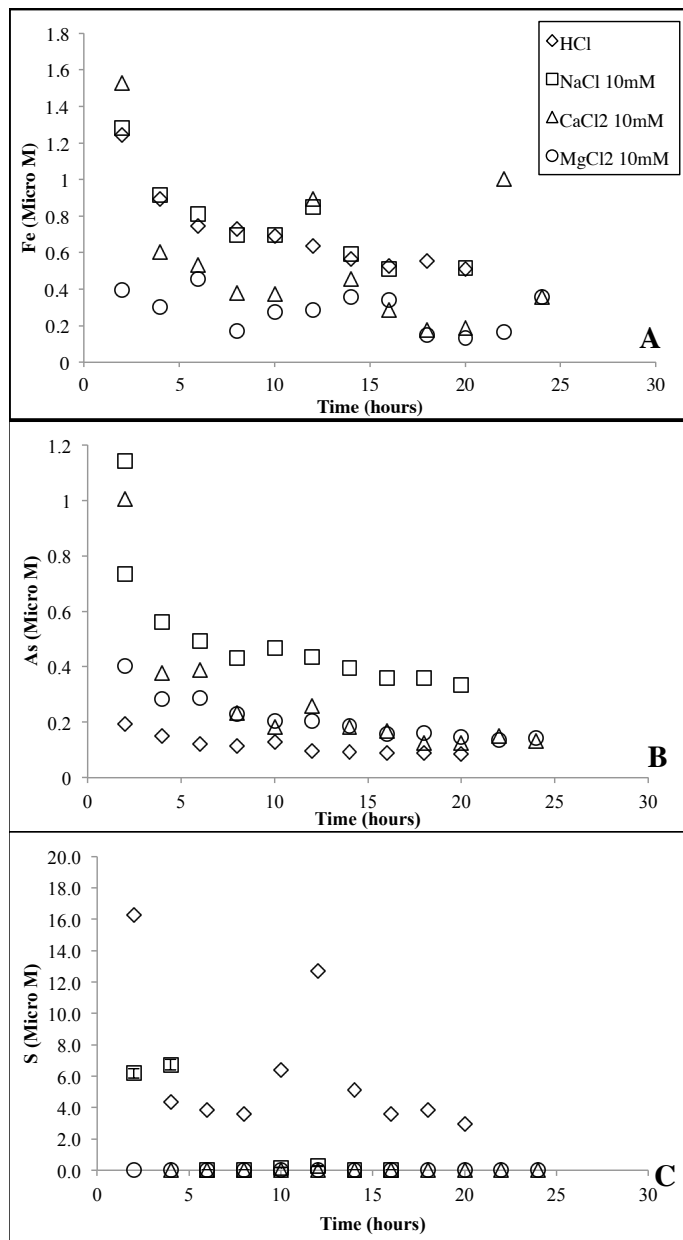


**Figure C2.** Dissolution of arsenopyrite with 10mM NaCl, CaCl<sub>2</sub>, and MgCl<sub>2</sub> at T= 25°C, P= 1 bar, pH = 2.55: **(A)** Concentration of Fe (μM) vs. time; **(B)** Concentration of As (μM) vs. time; **(C)** Concentration of S (μM) vs. time

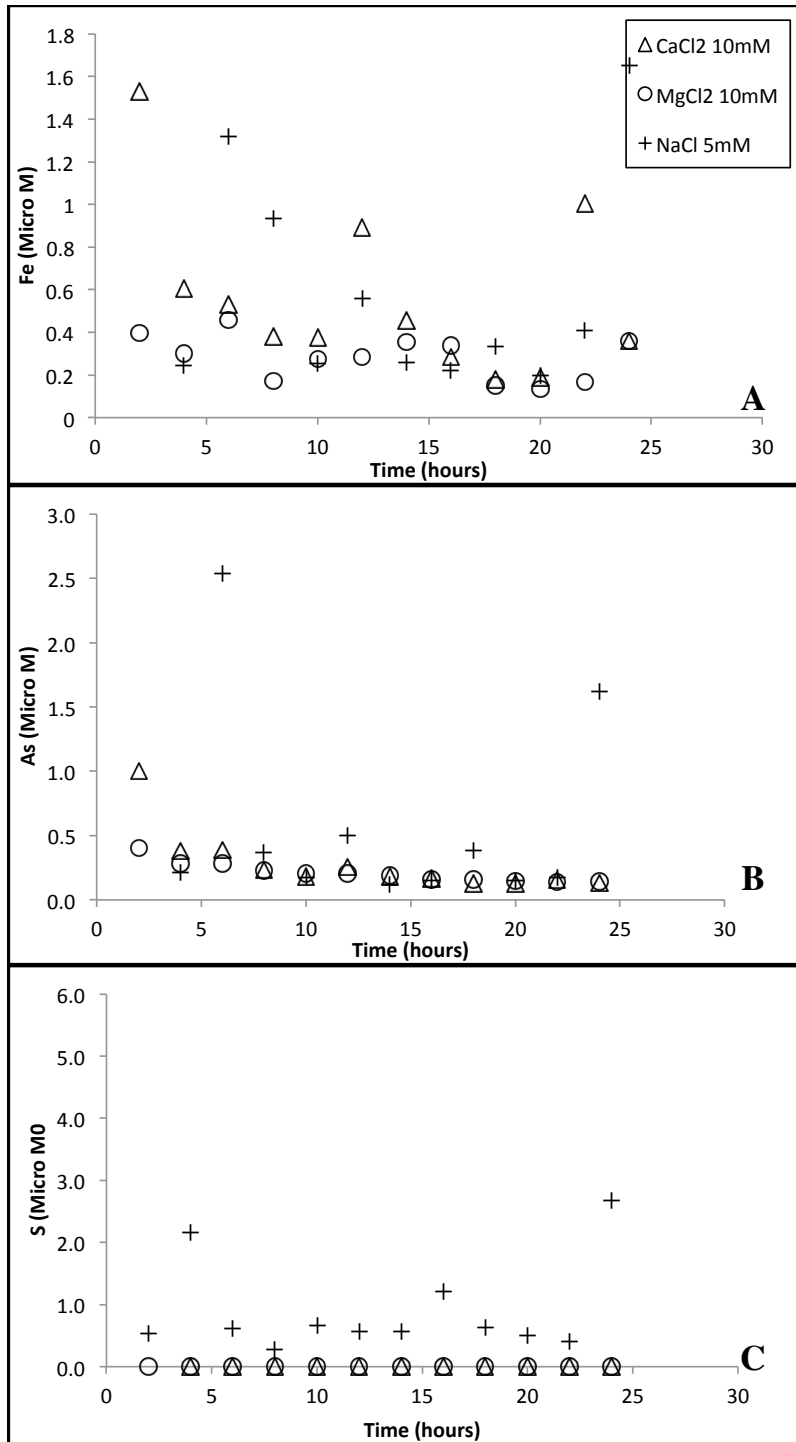


**Figure C3.** Dissolution of arsenopyrite at equal cation activity.  $\{Na^+\} = \{Ca^{2+}\} = \{Mg^{2+}\} = 0.0051$  at  $T = 25^\circ C$ ,  $P = 1$  bar,  $pH = 2.55$ : **(A)** Concentration of Fe ( $\mu M$ ) vs. time; **(B)** Concentration of As ( $\mu M$ ) vs. time; **(C)** Concentration of S ( $\mu M$ ) vs. time

## C2.2 Galena dissolution

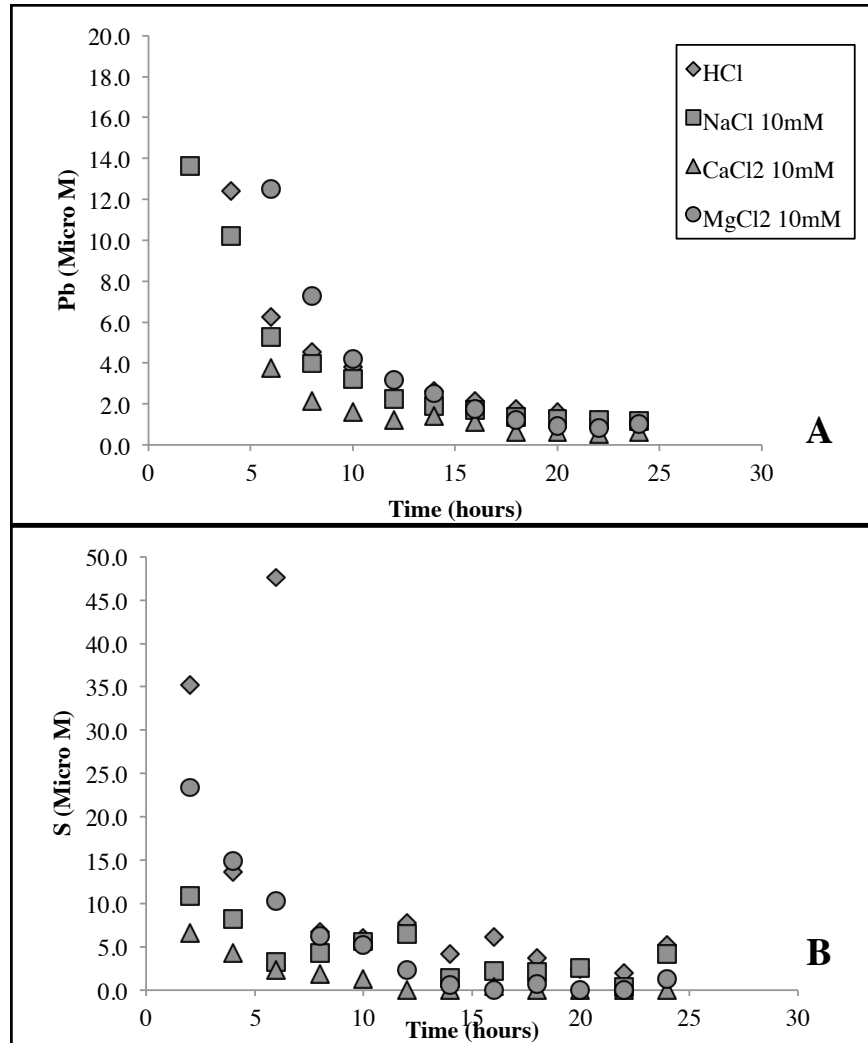


**Figure C4.** Dissolution of galena with 10mM NaCl, CaCl<sub>2</sub>, and MgCl<sub>2</sub> at T= 25°C, P= 1 bar, pH = 2.55: (A) Concentration of Pb (µM) vs. time; (B) Concentration of S (µM) vs. time

### C2.3 Pyrite dissolution

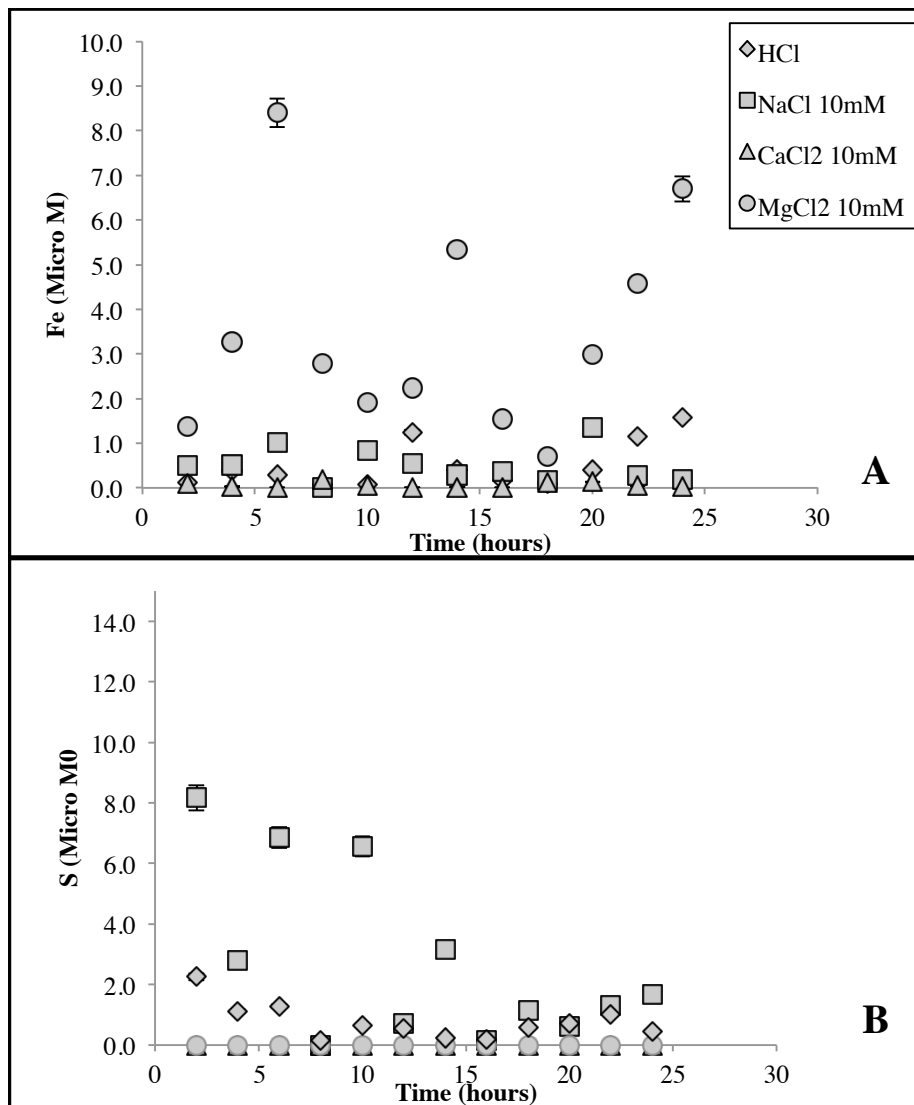


**Figure C5.** Dissolution of pyrite with 10mM NaCl, CaCl<sub>2</sub>, and MgCl<sub>2</sub> at T= 25°C, P= 1 bar, pH = 2.55: **(A)** Concentration of Fe (µM) vs. time; **(B)** Concentration of S (µM) vs. time

### **C3. References**

APHA, AWWA and WEF, in: L.S. Clesceri, A.E. Greenberg, A.D. Eaton (Eds.), Standard Methods for the Examination of Water and Wastewater, 20th ed., APHA, AWWA and WEF, 1998.

Parthasarathy, H.; Baltrus, J.P.; Dzombak, D.A.; Karamalidis, A.K. (2014) A method for preparation and cleaning of uniformly sized arsenopyrite particles. *Geochemical Transactions*, 15.1, 1-7.

USEPA, Determination of Inorganic Anion by Ion Chromatography method 9056, is published in "Test Methods for Evaluating Solid Waste, Physical/Chemical Methods", EPA Publication SW-846, July 1992.

**APPENDIX D**

**Supporting Information for Chapter 6**

## **D1. Methods:**

### D1.1 Mineral characterization

XRD-

XRD analysis confirmed the primary mineral phases were arsenopyrite, pyrite, and galena (Figure D1). The X-ray diffraction spectra were collected for the samples on beamline 11-3 at the Stanford Synchrotron Radiation Lightsource (SSRL). Incident X-rays (0.9744 Å, 12,724 eV) were focused using a bent cube root I-beam Si (311) monochromator. A MAR345 area detector positioned 148.7 mm downstream of the sample was used to collect diffraction scans with a dwell time of 10s. Calibrations was performed using a LaB<sub>6</sub> standard fit using WxDiff software obtained from Stefan Mannsfeld from SSRL. The collected images were converted into degrees 2θ space using Area Diffraction Machine (open source) software. The background was not subtracted to prevent the removal of the minor peaks that may indicate crystalline phases. The data was matched to a database of existing XRD patterns using the X'Pert Highscore Plus software and a database obtained from the Crystallography Open Database website. The XRD spectra of samples and standards are shown in Figure D1.

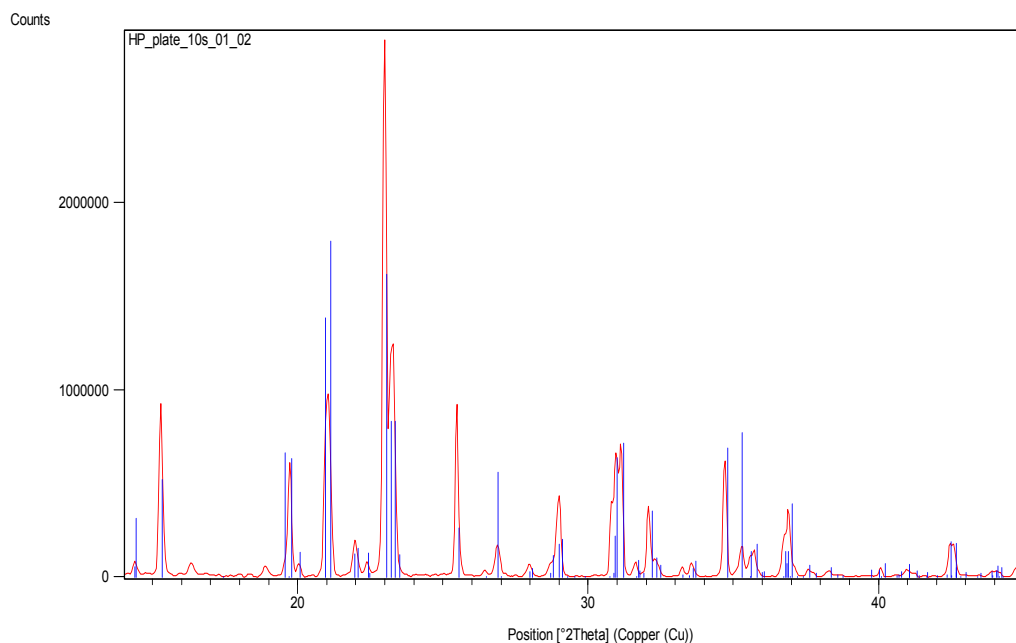


**Figure D1.** XRD Spectra for Arsenopyrite sample is shown in red with the standard reference peaks in blue.

#### D1.2 SEM

The surface stoichiometry of each mineral was measured using a Philips XL30 FEG scanning microscope (SEM) equipped with an SE Everhart Thornley detector and an Oxford INCA EDS with full quantitative composition analysis. The operating conditions were, accelerating voltage 10 kV, spot size 3, and a working distance of 10 mm. The SEM-EDS had a detection limit of 1% by weight. The results of these analyses for all three minerals are shown in Table D1.

**Table D1.** Solid phase characterization of arsenopyrite samples for dissolution experiments

<b>Mineral</b>	<b>SEM-EDS Stoichiometry</b>
Arsenopyrite (FeAsS)	$\text{Fe}_{1.03\pm 0.05}\text{As}_{1.01\pm 0.05}\text{S}_{0.87\pm 0.05}$

## D2. Dissolution Experiments

**Table D2.** Complete list of experiments conducted to investigate the effect of brines on arsenic dissolution from arsenopyrite

No.	$R_{CaCl_2/NaCl}$	CO <sub>2</sub>	[NaCl] M	[CaCl <sub>2</sub> ] M	pH	T,P (°C, bars)	[CO <sub>2</sub> ] aq. <sup>-1</sup> M	Ionic Strength <sup>2+</sup> (M)	{Na <sup>+</sup> } <sup>3+</sup>	{Ca <sup>2+</sup> } <sup>3+</sup>	{Cl <sup>-</sup> } <sup>3+</sup>
1	0	No	1.506	0	6.5	25,1	NA	1.56	1.24	0.00	0.96
2	0.11	No	1.131	0.125	6.5	25,1	NA	1.55	0.93	0.04	0.87
3	0.5	No	0.602	0.301	6.5	25,1	NA	1.53	0.49	0.09	0.75
4	1	No	0.377	0.377	6.5	25,1	NA	1.53	0.31	0.11	0.70
5	CaCl <sub>2</sub>	No	0	0.502	6.5	25,1	NA	1.53	0.00	0.14	0.62
6	0	Yes	1.506	0	3.5	25,1	0.025	1.56	1.24	0.00	0.96
7	0.11	Yes	1.131	0.125	3.5	25,1	0.0262	1.55	0.93	0.04	0.87
8	0.5	Yes	0.602	0.301	3.5	25,1	0.028	1.54	0.50	0.09	0.75
9	1	Yes	0.377	0.377	3.5	25,1	0.0288	1.54	0.31	0.11	0.70
10	CaCl <sub>2</sub>	Yes	0	0.502	3.5	25,1	0.0302	1.54	0.00	0.15	0.62
11	0.11	Yes	1.131	0.125	3.5	60, 100	0.0262	1.55	0.93	0.04	0.87

<sup>†</sup> Calculated using PHREEQC (Version 3), which utilizes a Pitzer ion-specific-interaction model for activity calculation

### D3. Results

#### D3.1 Validation Experiments

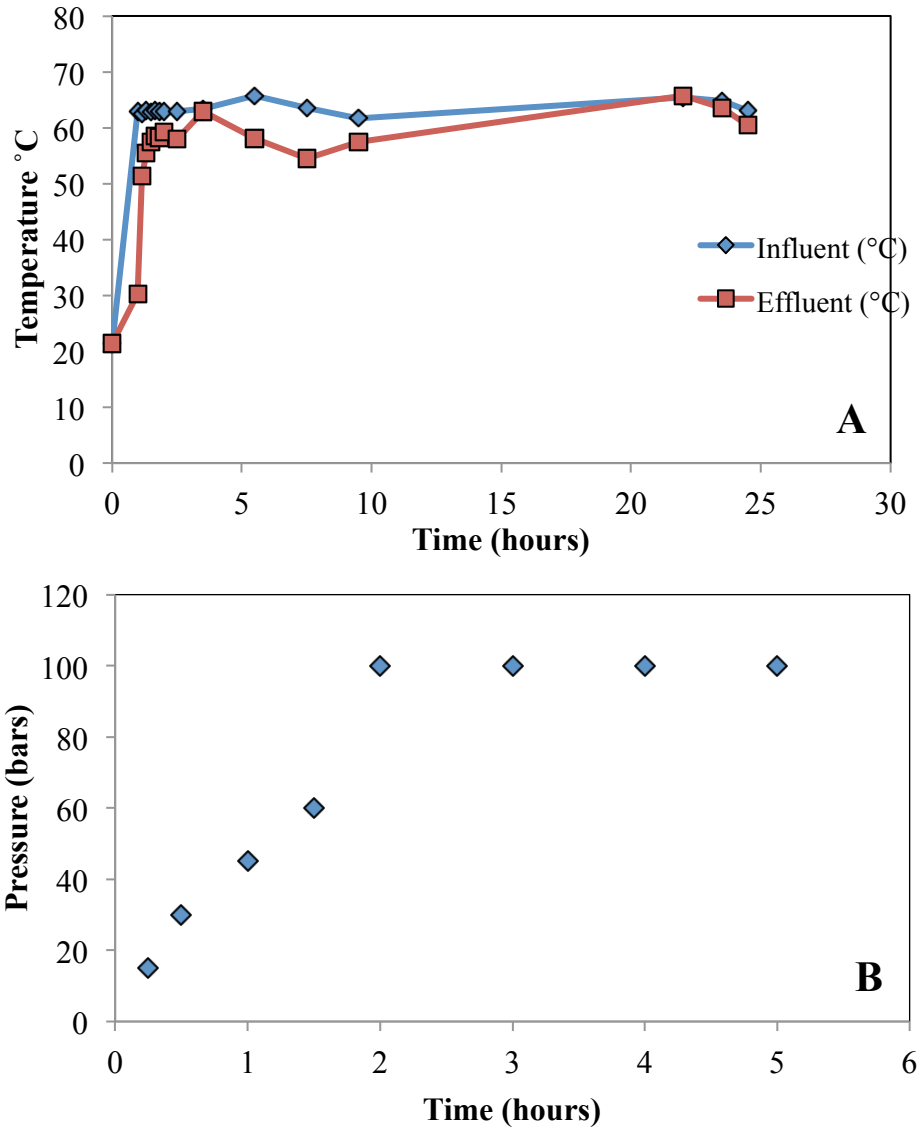


**Figure D2.** System validation (A) Influent and Effluent Temperature over time (B) Pressure stability over time

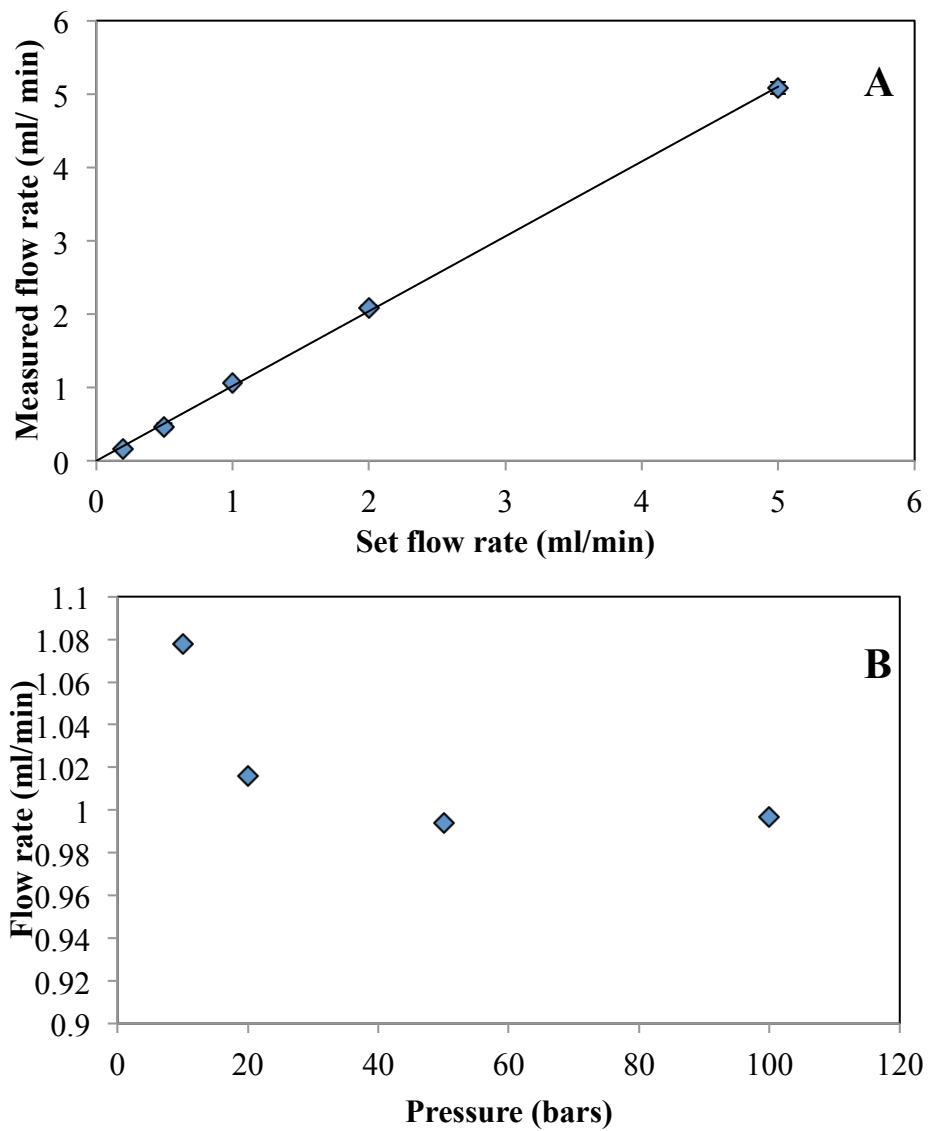


**Figure D3.** Flowrate stability over time. (A) Set flowrate vs measured flowrate; (B) Flowrate vs pressure.

### D3.2 Model for surface saturation concentrations

A simplistic model was used to calculate the concentration of ions that would saturate the surface of the mineral. The total surface area of the mineral was calculated by using the B.E.T surface area and mass of mineral packed in the column. Column specific parameters are provided in table D3.

The hydrated ion radii of  $\text{Ca}^{2+}$  and  $\text{Na}^{+}$  were used to calculate the ionic surface area of each ion. The number of ions of  $\text{Ca}^{2+}$  and  $\text{Na}^{+}$  required to saturate the surface were calculated, which was then converted to minimum pore volume concentration of each ion required to saturate the surface. Specific ion calculations are provided in Table D4.

**Table D3.** Column Characteristics

Specific Surface area	0.125	$\text{m}^2/\text{g}$
Mass of mineral	2.5	g
Total Surface Area	0.3125	$\text{m}^2$
Pore Volume	0.45	ml

**Table D4.** Ion Specific Calculations for surface saturation assuming hydrated ions

Parameter	Ca <sup>2+</sup>	Na <sup>+</sup>
Diameter of ion <sup>†</sup> (Hydrated shell) (m)	8.24E-10	7.16E-10
Area covered/ion (m <sup>2</sup> )	5.33E-19	4.02E-19
No. of ions required to saturate the surface	5.86E+17	7.77E+17
Mass of ions (moles)	9.73E-07	1.29E-06
Minimum pore volume concentration of ions required (M)	2.16E-03	2.87E-03

<sup>†</sup> From Volkov et al., 1997

The minimum concentration of either Ca<sup>2+</sup> or Na<sup>+</sup> available in the synthetic brine solutions (from Table D2) is 125mM and 327mM respectively. Under such high concentrations the surface will be saturated by either one of these cations, even if the actual reactive surface area available is 50 times greater than that used in this calculation.

Even if we assume that all the ions (Ca<sup>2+</sup>, Na<sup>+</sup>) are dehydrated when they interact with the surface, calculations reveal that the concentrations are in excess required to saturate the surface. The results are tabulated in Table D5.

**Table D5.** Ion Specific Calculations for surface saturation assuming dehydrated ions

<b>Parameter</b>	<b>Ca<sup>2+</sup></b>	<b>Na<sup>+</sup></b>
Diameter of ion <sup>4</sup> (Bare diameter) (m)	2.00E-10	2.34E-10
Area covered/ion (m <sup>2</sup> )	3.14E-20	4.30E-20
No. of ions required to saturate the surface	1.04E+19	7.56E+18
Mass of ions (moles)	1.72E-05	1.26E-05
Minimum pore volume concentration of ions required (M)	3.82E-02	2.79E-02

As shown in the table the pore concentration of ions corresponding to saturation of the arsenopyrite surface are 38.2mM and 27.9 mM for Ca<sup>2+</sup> and Na<sup>+</sup> respectively. Note that the concentration is higher for Ca<sup>2+</sup> than Na<sup>+</sup> when assuming dehydrated ions, due to the smaller bare ion radius of Ca<sup>2+</sup>.

#### D4. References

Parkhurst, D.L., and Appelo, C.A.J., 2013, Description of input and examples for PHREEQC version 3—A computer program for speciation, batch-reaction, one-dimensional transport, and inverse geochemical calculations: U.S. Geological Survey Techniques and Methods, book 6, chap. A43, 497 p., available only at <http://pubs.usgs.gov/tm/06/a43/>.

Pitzer, K.S. (editor) (1991). Activity coefficients in electrolyte solutions (2nd ed.). C.R.C. Press. ISBN 0-8493-5415-3. Chapter 3. \*Pitzer, K.S. Ion interaction approach: theory and data correlation, pp. 75–153.

Volkov, A. G., S. Paula, and D. W. Deamer. "Two mechanisms of permeation of small neutral molecules and hydrated ions across phospholipid bilayers." *Bioelectrochemistry and Bioenergetics* 42.2 (1997): 153-160.

Wang, Zan, Mitchell J. Small, and Athanasios K. Karamalidis. "Multimodel Predictive System for Carbon Dioxide Solubility in Saline Formation Waters." *Environmental Science & Technology* 47.3 (2013): 1407-1415

## APPENDIX E

### **Supporting Information for Chapter 7<sup>†</sup>**

<sup>†</sup>Dr. Christina Lopano and Dr. Mengling Stuckman, National Energy Technology Laboratory, Pittsburgh, PA performed all  $\mu$ -XANES experiments and data analysis presented in this appendix.

### **E.1 Micro-x-ray adsorption near edge structure ( $\mu$ -XANES): Method**

$\mu$ -XANES was collected at beamline 20-ID-B in March 2011, and January and August 2014 and at beamline 13-ID-E in October 2011, at the Advanced Photon Source (APS) at Argonne National Laboratory, Argonne, IL. The electron storage ring operated at 7 GeV with a top-up fill status. The redox-sensitive thin-sectioned pre-reaction samples (LT10193 and MT7913) and their post-reaction samples (LT10193post and MT7913post), were prepared by Spectrum Petrographics, Inc.

Briefly, samples were dried and cured in EPOTEK301-2FL resin under anoxic conditions, sectioned to 30  $\mu\text{m}$  thickness and mounted on quartz slides. The thin sections were mounted 45° towards the incident beam. A double crystal Si (220) monochromator was used for energy selection.  $\mu$ -XANES spectra were collected with 4  $\mu\text{m}$  spot size microprobe at room temperature in fluorescence mode. For each pre-reaction sample, regions of the map area of particular interest for As hotspots were identified from a coarse elemental map of each thin section at 11900 eV (2500  $\mu\text{m}$   $\times$  2500  $\mu\text{m}$  with 25  $\mu\text{m}$  step size) at an integration time of 0.4 sec per pixel. The single-element detector allowed simultaneous detection of fluorescence signals for multiple elements (e.g., S, Si, P, Cl, Ca, Mn, Fe, Cu, Zn and As) at 11900eV. These As K-edge mappings were collected at a finer scale (e.g., 500  $\mu\text{m}$   $\times$  500  $\mu\text{m}$ ) with small step size of 4~7.5  $\mu\text{m}$  at an integration time of 0.1 sec.

For each post-reaction sample, multiple fine maps (500  $\mu\text{m}$   $\times$  500  $\mu\text{m}$  or 600  $\mu\text{m}$   $\times$  600  $\mu\text{m}$ ) were collected directly with 5 $\mu\text{m}$  step size at an integration time of 0.15 sec per pixel. Elemental maps for arsenic, Fe and Zn were collected at energy of 12500eV with 8 layers of Al foil in front of the

detector to attenuate high background caused by fluorescence from lighter elements, while elemental maps for light elements S, Si, P, Cl, Ca, Mn and Fe were collected at 7110eV without Al foil.

Prior to As  $\mu$ -XANES measurements, 4 or 8 layers of Al foil were placed in front of the single element detector to attenuate interference from Fe fluorescence signal. Arsenic “hotspots” in the elemental maps were analyzed with  $\mu$ -XANES using 4  $\mu$ m spot size to determine the As speciation. The sample spectra were collected from 150 eV pre-edge to 8k post-edge around the As K-edge of 11867 eV with an Au foil reference. Three to 6 scans were collected per sample depending on data quality.

## **E2. Data Analysis**

### $\mu$ -XANES Analyses and As Reference Spectra

Raw XANES data were processed using Athena software package (Ravel & Newville, 2005) based on IFEFFIT (Newville, 2001). Each scan was energy-aligned to the same edge position ( $E_0$ ) of its Au reference spectrum. Scans from the same sample were merged, calibrated against Au foil with an edge position of 11919.7eV, normalized and background subtracted. The energy at zero-crossing of the second-derivatives of the processed XANES was assigned to be the edge position ( $E_0$ ) of each spectrum. The edge positions and the white-line positions of all arsenic reference spectra are listed in Table E1. The As reference spectra library was provided courtesy of Dr. Kirk Scheckel from USEPA (Beak & Wilkin, 2009; Smith et al., 2005) or from previous APS trips. Both the edge-positions and the white-line positions are indicative of arsenic species (Rochette et al., 2000; Wilkin & Ford, 2006) and help determine the local bonding environment

surrounding the As atom. The As references include (1) references of As<sup>V</sup> sorbed on iron oxides, abbreviated as As<sup>V</sup>-Fe Oxide group: As<sup>V</sup> sorbed on goethite (As<sup>V</sup>\_Goethite), As<sup>V</sup> sorbed on ferrihydrite (As<sup>V</sup>\_Ferrihydrite), scorodite; (2) references of As<sup>III</sup> sorbed on iron oxides, abbreviated as As<sup>III</sup>-FeOxide group: As<sup>III</sup> sorbed on magnetite (As<sup>III</sup>\_Magnetite), As<sup>III</sup> sorbed on Siderite (As<sup>III</sup>\_Siderite), As<sup>III</sup> sorbed on ferrihydrite (As<sup>III</sup>\_Ferrihydrite), (3) references of As<sup>III</sup> sorbed on iron sulfides, abbreviated as As<sup>III</sup>-Sulfide group: As<sup>III</sup> sorbed on pyrite (As<sup>III</sup>\_Pyrite), As<sup>III</sup> sorbed on mackinawite (As<sup>III</sup>\_Mackinawite); and (4) references of arsenite directly bond with sulfur, as As<sup>III</sup> in Sulfide group: Arsenopyrite [FeAsS], Realgar [As<sub>4</sub>S<sub>4</sub>], amorphous Arsenite Sulfides (AsS\_Poor), orpiment [As<sub>2</sub>S<sub>3</sub>], and amorphous orpiment (Am Orpiment).

**Table E1.** Absorption edge positions and white-line peaks of reference spectra used in XANES data analysis. Edge position is defined as the maximum in the first-derivative of the energy vs. absorption function. White line position is defined as the maximum in the energy vs. absorption function.

Sample name	White-line peak	Edge position	Edge in Refs	Refs
<b>As<sup>V</sup>-FeOxide Group</b>				
As <sup>V</sup> _Goethite	11875.9	11874.3	11873.8- 11874.5eV	(Beak & Wilkin, 2009; Smith et al., 2005; Wilkin & Ford, 2006)
Scorodite	11875.5	11874.0		
As <sup>V</sup> _Ferrihydrite	11875.8	11874.0		
<b>As<sup>III</sup>-FeOxide Group</b>				
As <sup>III</sup> _Greenrust	11870.6	11868.4	11868.5- 11870.1eV	(Beak & Wilkin, 2009; Kachenko, Grafe, Singh, & Heald, 2010; Lowers et al., 2007; Smith et al., 2005; Wilkin & Ford, 2006)
As <sup>III</sup> _Magnetite	11872.0	11870.8		
As <sup>III</sup> _Siderite	11871.1	11869.4		
As <sup>III</sup> _Ferrihydrite	11870.7	11868.7		
<b>As<sup>III</sup>-Sulfide Group</b>				
As <sup>III</sup> _Pyrite	11870.1	11867.4	11867.6- 11868.0	(Beak & Wilkin, 2009; Lowers et al., 2007; Wilkin & Ford, 2006)
As <sup>III</sup> _Mackinawite	11870.1	11867.6		
<b>As<sup>III</sup> in Sulfide Group</b>				
Arsenopyrite	11867.7	11865.8	11865.8	(Polizzotto et al., 2006)
			11866.2	(Wilkin & Ford, 2006)
Realgar	11869.6	11866.9	11866.7	(Wilkin & Ford, 2006)
AsS_poor	11868.8	11867.4	11867.4	(Wilkin & Ford, 2006)
Orpiment	11868.6	11866.7	11866.7	(Beak & Wilkin, 2009; Polizzotto et al., 2006)
Am Orpiment	11868.9	11867.3		

#### Linear Combination Fit of $\mu$ -XANES Spectra using “Cycle Fit” Method

Linear combination fit (LCF) analysis was conducted using normalized XANES as well as 1<sup>st</sup> derivative XANES over the fitting range from 20 eV pre-edge to 35 eV post-edge using “cycle

fit” method (Mayhew et al., 2011). In detail, all 15 As reference spectra were loaded into LCF fitting program in Athena. The cycle fit was first conducted for 2-component combination fit using any 2 As references in the As reference library. The  $R^2$  values for each of the 2-component fits were reported and the As references with the best quality of fit smallest  $R^2$  value were included for the next series of 3-component fits. The cycle fit was repeated for 3-component fits using the selected As references with each of the remaining As references in the library. This process was repeated until there was no more fitting improvement that decreased the  $R^2$  value by 10% or greater. The sum of the components was not constrained to unity (mean sum = 0.99), negative fractions were not allowed, and  $E_0$  was not allowed to shift during cycle fitting. In the last manual fit,  $E_0$  for all reference compounds were allowed to shift up to 0.5 eV to compensate for inherent discrepancies caused by data collection of samples and As references on different beam lines. Both LCF for normalized XANES and derivative XANES were similar (within 15% error), suggesting sufficient reliability in LCF results independent on fitting spectra type.

### **E.3 Results**

#### *E.2.1 $\mu$ -XANES Edge position and white line comparison*

Both the As reference XANES (Figure E1A) and sample  $\mu$ -XANES spectra (Figure E1B) showed distinctive edge positions and white line positions (Table E1) corresponding to different As oxidation states and the local bonding environments surrounding the As atom species (Beak & Wilkin, 2009; Rochette et al., 2000; Wilkin & Ford, 2006). In general, the edge positions and white-line peaks shift to higher energy with increasing As oxidation state. The edge positions and white-line peaks from different As speciation groups are distinctive: the white-line peak energies ( $\sim 11875$  eV) for As<sup>V</sup>-FeOxide group are 3-4 eV higher than those for As<sup>III</sup>-Oxide group

(~11871eV), 5-6eV higher than those for As<sup>III</sup>-Sulfide group (~11870eV), and 6-7eV higher than those for As<sup>III</sup> in Sulfide group (~11868eV). These edge positions are consistent with reported values in the literature (within 0.4eV error) (See Table 1) (Beak & Wilkin, 2009; Kachenko, Grafe, Singh, & Heald, 2010; Lowers et al., 2007; Polizzotto et al., 2006; Smith et al., 2005; Wilkin & Ford, 2006). In sulfate reducing environments, arsenic is effectively reduced by sulfur resulting in lower edge energies (2-3eV) in As XANES for As in Sulfide group compared to those for As<sup>III</sup>-FeOxide group (Lowers et al., 2007; Wilkin & Ford, 2006). Edge positions for As<sup>III</sup> in Sulfide group (11865.8-11867.4eV) are slightly lower than those for As<sup>III</sup>-Sulfide group (11867.5eV), suggesting direct As-S bonds induces more As reduction than As sorption onto sulfides (Beak & Wilkin, 2009; Wilkin & Ford, 2006). Notice that As oxidation state in arsenopyrite [FeAsS] is -1 (Jones & Nesbitt, 2002; Simon et al., 1999), as As substitutes S in the [FeS<sub>2</sub>] mineral structure to form [FeAsS] (Bostick & Fendorf, 2003). As a result, the arsenopyrite XANES has the lowest edge position energy (11865.8eV) and white-line peak (11867.7eV) in As reference library. Note as well that the arsenic oxidation state in realgar [As<sub>4</sub>S<sub>4</sub>] would appear to be +2(O'Day, et al., 2004). Therefore, the realgar XANES has the highest white-line peak (11869.6eV) in As<sup>III</sup> in Sulfide Group.

### *E.2.2 Linear Combination Fitting of $\mu$ -XANES spectra*

LCF of reference spectra allowing up to 0.5eV energy shift in order to compensate for inherent discrepancies caused by data collection of samples and As references on different beam lines was performed. LCF analyses allowing energy shifts up to 0.5eV may not be reliable to differentiate two phases within an arsenic speciation group (e.g., the edge and white-line positions for Am Orpiment and AsS<sub>poor</sub> are 0.1eV away). The estimation of As in sulfide phase is not precise

and additional x-ray technologies (e.g., S XANES, Fe XANES, As EXAFS) can improve the evaluation of As mineral phases.

LCF results demonstrated that 77-100% of As species in the hotspots of the secondary seal rock from 7930.1 Ft. prior to dissolution, exist as As in sulfide species and the rest as As<sup>V</sup> in scorodite (0-21%). LCF results from the same sample post reaction, demonstrated the dominance of As<sup>V</sup>-Feoxide group (76-100%), indicating As was oxidized during the dissolution experiment. Major mineral phases included As<sup>V</sup>\_Ferrihydrite (32% max), scorodite (29% max), As<sup>V</sup>\_Goethite (54-67%), As<sup>III</sup>\_GR (20% max), As<sup>III</sup>\_Siderite (5% max), and As<sup>III</sup> sorbed on pyrite (6.4% max). LCF results suggest that As-bearing iron minerals transformed from crystalline pyrite or scorodite to more amorphous secondary phases, such as green rust, siderite and ferrihydrite. The LCF results were consistent with XRD results showing a decrease in pyrite after dissolution, as well as with effluent Fe concentration of 6000 ppb after 1 hr. of CO<sub>2</sub> injection. Arsenic was likely oxidized by dissolved Fe<sup>3+</sup> ions (Neil et al., 2012), resulting in either mobilization into the effluent or re-adsorption onto these secondary minerals (Horneman et al., 2004) detected by  $\mu$ -XANES Spectra

LCF results for the primary seal rock (10193 ft.) before and after reaction, revealed more hotspot-dependent mineral compositions than those from the secondary seal rock samples. Arsenic mineral phases in the pre-reaction primary seal rock sample included 16-88% As<sup>V</sup>-FeOxide speciation group (e.g., As<sup>V</sup>\_Ferrihydrite, scorodite and As<sup>V</sup>\_Goethite), 0-35% As<sup>III</sup>-FeOxide speciation group (e.g., As<sup>III</sup>\_Siderite, As<sup>III</sup>\_Magnetite, and As<sup>III</sup>\_GR), 0-39% As<sup>III</sup>-sulfide speciation group as As<sup>III</sup>\_pyrite and 0-84% As<sup>III</sup> in sulfide speciation group as Am

Orpiment and AsS\_poor (Table 7.4). The complex mineral compositions for these samples implies the samples experienced heterogeneous micro-reducing environments (e.g., iron and/or sulfate reduction), controlling different As (im)mobilization behavior (Drahota et al., 2009). Arsenic mineral phases in the sample after dissolution experiments, contained 0-65% As<sup>V</sup>-FeOxide speciation group and 35-100% As<sup>III</sup> in sulfide speciation group as 0-41% arsenopyrite and 21-66% AsS\_poor. Hotspots that contained high As<sup>V</sup> were LT10193post\_a3 (65% As<sup>V</sup>, LT10193post\_c1 (53% As<sup>V</sup>) and c3 (52% As<sup>V</sup>). These high As<sup>V</sup> hotspots suggest potential As oxidation in these micro-environments, compared to the other spots (0-27% As<sup>V</sup> in the sample. As<sup>V</sup> was not detected uniformly as a major mineral phase, probably due to incomplete As oxidation from dissolved iron as a result of column clogging.

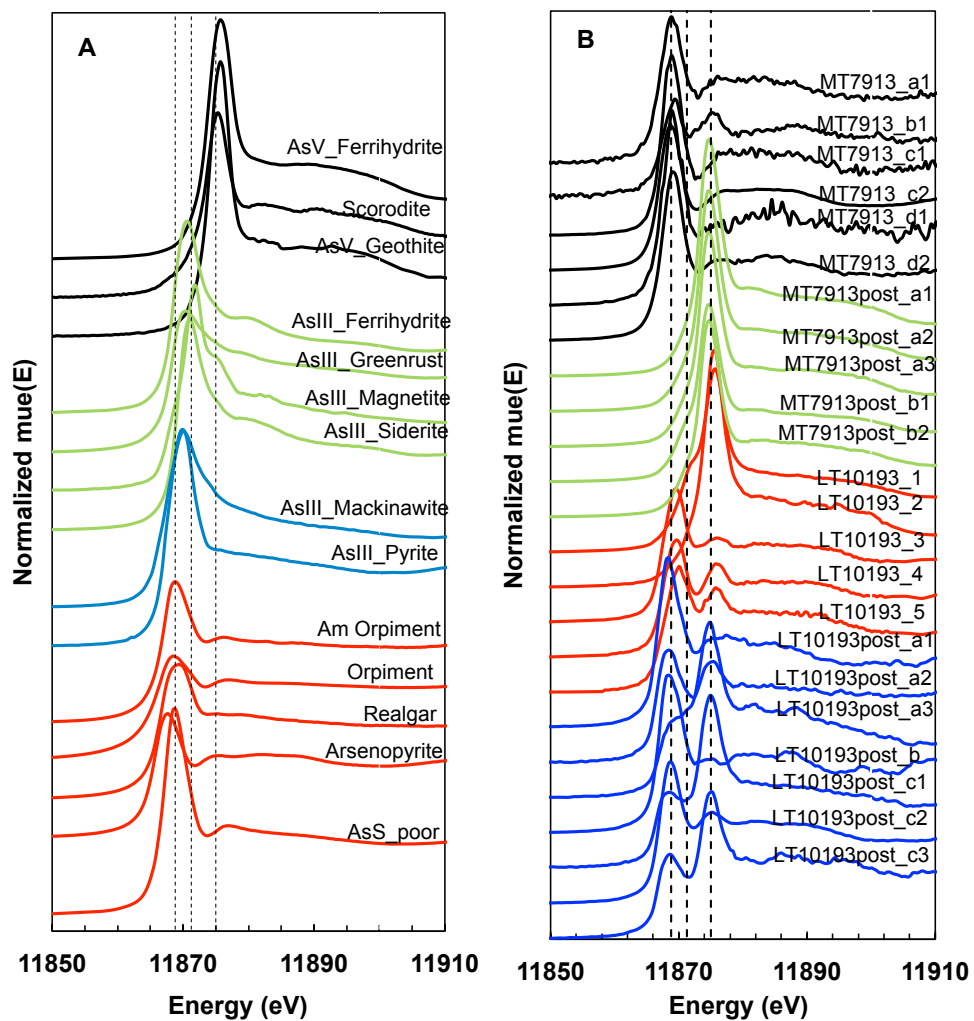


**Figure E1.** XANES spectra for (A) 14 As references and (B) all measured micro-spots in different samples. Dash vertical lines from right to left display energies at 11868.8eV, 11871.26eV, 11875eV, representing white line peaks for As<sup>V</sup>-FeOxide group, As<sup>III</sup>-FeOxide group and As<sup>III</sup> in Sulfide group, respectively. (Source: Lopano C. and Stuckman M.)

### E3. References

- Beak, D. G., & Wilkin, R. T. (2009). Performance of a zerovalent iron reactive barrier for the treatment of arsenic in groundwater: Part 2. Geochemical modeling and solid phase studies. *Journal of Contaminant Hydrology*, 106(1-2), 15-28.
- Bostick, B. C., & Fendorf, S. (2003). Arsenite sorption on troilite (FeS) and pyrite (FeS<sub>2</sub>). *Geochimica Et Cosmochimica Acta*, 67(5), 909-921.
- Drahota, P., Rohovec, J., Filippi, M., Mihaljevic, M., Rychlovsky, P., Cervený, V., & Pertold, Z. (2009). Mineralogical and geochemical controls of arsenic speciation and mobility under different redox conditions in soil, sediment and water at the Mokrsko-West gold deposit, Czech Republic. *Science of The Total Environment*, 407(10), 3372-3384.
- Farquhar, M. L., Charnock, J. M., Livens, F. R., & Vaughan, D. J. (2002). Mechanisms of arsenic uptake from aqueous solution by interaction with goethite, lepidocrocite, mackinawite, and pyrite: An x-ray absorption spectroscopy study. *Environmental Science & Technology*, 36(8), 1757-1762.
- Horneman, A., Van Geen, A., Kent, D. V., Mathe, P. E., Zheng, Y., Dhar, R. K., . . . Ahmed, K. M. (2004). Decoupling of As and Fe release to Bangladesh groundwater under reducing conditions. Part 1: Evidence from sediment profiles. *Geochimica Et Cosmochimica Acta*, 68(17), 3459-3473.
- Jones, R. A., & Nesbitt, H. W. (2002). XPS evidence for Fe and As oxidation states and electronic states in loellingite (FeAs<sub>2</sub>). *American Mineralogist*, 87(11-12), 1692-1698.
- Kachenko, A. G., Grafe, M., Singh, B., & Heald, S. M. (2010). Arsenic Speciation in Tissues of the Hyperaccumulator *P. calomelanos* var. *austroamericana* using X-ray Absorption Spectroscopy. *Environmental Science & Technology*, 44(12), 4735-4740.
- Lowers, H. A., Breit, G. N., Foster, A. L., Whitney, J., Yount, J., Uddin, N., & Muneem, A. (2007). Arsenic incorporation into authigenic pyrite, Bengal basin sediment, Bangladesh. *Geochimica Et Cosmochimica Acta*, 71(11), 2699-2717.
- Mayhew, L. E., Webb, S. M., & Templeton, A. S. (2011). Microscale Imaging and Identification of Fe Speciation and Distribution during Fluid-Mineral Reactions under Highly Reducing Conditions. *Environmental Science & Technology*, 45(10), 4468-4474.
- Neil, C. W., Yang, Y. J., & Jun, Y. S. (2012). Arsenic mobilization and attenuation by mineral-water interactions: implications for managed aquifer recharge. *Journal of Environmental Monitoring*, 14(7), 1772-1788.
- Newville, M. (2001). IFEFFIT: Interactive XAFS analysis and FEFF fitting. *Journal of Synchrotron Radiation*, 8, 322-324.

- O'Day, P. A., Vlassopoulos, D., Root, R., & Rivera, N. (2004). The influence of sulfur and iron on dissolved arsenic concentrations in the shallow subsurface under changing redox conditions. *Proceedings of the National Academy of Sciences of the United States of America*, 101(38), 13703-13708.
- Polizzotto, M. L., Harvey, C. F., Li, G. C., Badruzzman, B., Ali, A., Newville, M., Fendorf, S. (2006). Solid-phases and desorption processes of arsenic within Bangladesh sediments. *Chemical Geology*, 228(1-3), 97-111.
- Ravel, B., & Newville, M. (2005). ATHENA, ARTEMIS, HEPHAESTUS: data analysis for X-ray absorption spectroscopy using IFEFFIT. *Journal of Synchrotron Radiation*, 12, 537-541.
- Rochette, E. A., Bostick, B. C., Li, G. C., & Fendorf, S. (2000). Kinetics of arsenate reduction by dissolved sulfide. *Environmental Science & Technology*, 34(22), 4714-4720.
- Simon, G., Huang, H., Penner-Hahn, J. E., Kesler, S. E., & Kao, L. S. (1999). Oxidation state of gold and arsenic in gold-bearing arsenian pyrite. *American Mineralogist*, 84(7-8), 1071-1079.
- Smith, P. G., Koch, I., Gordon, R. A., Mandoli, D. F., Chapman, B. D., & Reimer, K. J. (2005). X-ray absorption near-edge structure analysis of arsenic species for application to biological environmental samples. *Environmental Science & Technology*, 39(1), 248-254.
- Wang, S. L., & Mulligan, C. N. (2008). Speciation and surface structure of inorganic arsenic in solid phases: A review. *Environment International*, 34(6), 867-879.
- Wilkin, R. T., & Ford, R. G. (2006). Arsenic solid-phase partitioning in reducing sediments of a contaminated wetland. *Chemical Geology*, 228(1-3), 156-174.

## **APPENDIX F**

### **Data Tables**

**Table F1.** Data for Figure 3.6

<b>Number of PV</b>	<b>Concentration (Mol/Liter)</b>
<b>1.1 ml/min</b>	
146.75	7.364E-04
587.01	1.352E-03
733.76	6.077E-04
1174.01	4.495E-04
1222.93	3.081E-04
1210.70	2.868E-05
1479.75	2.815E-05
<b>0.8 ml/min</b>	
105.66	2.122E-04
258.28	1.807E-04
409.93	1.545E-04
556.68	8.775E-05
683.86	8.775E-05
830.61	6.556E-05
977.37	6.465E-05
<b>0.4 ml/min</b>	
122.29	5.225E-04
269.04	3.685E-04
415.80	2.109E-04
562.55	2.519E-04
709.30	1.996E-04
1076.18	1.695E-04
1222.93	1.315E-04
1320.76	1.002E-04
1565.35	8.592E-05
<b>0.2ml/min</b>	
146.75	7.364E-04
587.01	1.352E-03
733.76	6.077E-04
1174.01	4.495E-04
1222.93	3.081E-04

**Table F2.** Data for Figure 3.7

<b>Number of PV</b>	<b>Concentration (ppm)</b>	<b>Concentration (Mol/Liter)</b>
<b>1 bar- Trial 1</b>		
293.50	9.525	1.270E-04
489.17	5.789	7.719E-05
684.84	4.4	5.867E-05
880.51	3.513	4.684E-05
1076.18	3.019	4.025E-05
1271.85	2.667	3.556E-05
1467.52	2.336	3.115E-05
1663.18	2.254	3.005E-05
1858.85	2.084	2.779E-05
<b>1 bar- Trial 2</b>		
293.50	7.08	9.440E-05
489.17	5.536	7.381E-05
684.84	4.798	6.397E-05
880.51	4.238	5.651E-05
1076.18	3.878	5.171E-05
1271.85	3.34	4.453E-05
1467.52	3.176	4.235E-05
1663.18	2.726	3.635E-05
1858.85	2.662	3.549E-05
<b>100 bar</b>		
342.4203822	6.288	8.384E-05
538.089172	5.526	7.368E-05
733.7579618	5.324	7.099E-05
929.4267516	4.733	6.311E-05
2103.43949	2.758	3.677E-05
2396.942675	2.492	3.32267E-05
2592.611465	2.482	3.30933E-05
2788.280255	2.4	0.000032
2983.949045	2.302	3.06933E-05
<b>1 bar- Trial 3</b>		
440.2547771	5.837	7.783E-05
733.7579618	5.189	6.919E-05
2201.273885	2.808	3.744E-05
2396.942675	2.79	3.720E-05
2592.611465	2.619	3.492E-05
2788.280255	2.674	3.565E-05
2983.949045	2.423	3.231E-05

**Table F3.** Data for Figure 4.3

<b>Element</b>	<b>% Oxidation</b>			
	<b>1N HCl</b>	<b>12 N HCl</b>	<b>50% Acetic acid (10 mins)</b>	<b>50% Acetic acid (20 mins)</b>
Fe	11.2	11.9	21.6	15.9
As	8.6	0	17.2	11.9
S	2.9	0	11	5.3

**Table F4.** Data for Figure 5.1

<b>Galena</b>			
<b>Solution</b>	<b>Chloride activity</b>	<b>Steady state Pb concentration (micro M)</b>	<b>Steady state S concentration (micro M)</b>
HCl	0.0028	1.42	3.93
NaCl 10mM	0.0115	1.246	2.12
CaCl <sub>2</sub> 10mM	0.0192	0.604	0.07
MgCl <sub>2</sub> 10mM	0.0192	0.98	0.25
<b>Pyrite</b>			
<b>Solution</b>	<b>Chloride activity</b>	<b>Steady state Fe concentration (micro M)</b>	<b>Steady state S concentration (micro M)</b>
HCl	0.0028	0.809830852	0.69
NaCl 10mM	0.0115	0.493266965	1.19
CaCl <sub>2</sub> 10mM	0.0192	0.080133267	0
MgCl <sub>2</sub> 10mM	0.0192	3.740347043	0

**Table F5.** Data for Figure 5.2

<b>Solution</b>	<b>Cation Activity</b>	<b>Chloride Activity</b>	<b>Steady state As concentration (micro M)</b>	<b>Steady state Fe concentration (micro M)</b>	<b>Steady state S concentration (micro M)</b>
HCl	0.0028	0.0028	0.091	0.558	3.89
NaCl 10mM	0.0089	0.0115	0.404	0.677	0.06
CaCl <sub>2</sub> 10mM	0.0053	0.0192	0.141	0.403	0
MgCl <sub>2</sub> 10mM	0.0056	0.0192	0.149	0.230	0
NaCl 5.6mM	0.0051	0.0076	0.154	0.268	0.653

**Table F6.** Data for Figure 6.1

	<b>NaCl</b>	<b>R=0.11</b>	<b>R=0.5</b>	<b>R=1</b>	<b>CaCl<sub>2</sub></b>
<b>Time</b>	<b>As (micro mol/m<sup>2</sup> mineral)</b>				
30	1.12E-03	2.84E-04	6.31E-04	7.02E-04	1.59E-03
28	1.03E-03	3.00E-04	4.40E-04	1.04E-03	2.70E-03
26	9.26E-04	3.45E-04	5.50E-04	6.99E-04	1.12E-03
24	1.15E-03	3.64E-04	6.03E-04	6.45E-04	1.09E-03
22	1.07E-03	4.09E-04	5.14E-04	7.77E-04	1.44E-03
20	1.11E-03	3.55E-04	6.88E-04	6.08E-04	1.05E-03
18	1.06E-03	3.73E-04	9.62E-04	7.84E-04	1.07E-03
16	9.78E-04	3.38E-04	1.13E-03	7.49E-04	1.49E-03
14	1.11E-03	3.44E-04	1.01E-03	8.96E-04	1.19E-03
12	1.14E-03	5.12E-04	7.00E-04	9.48E-04	1.36E-03
10	1.11E-03	3.26E-04	9.08E-04	1.00E-03	1.56E-03
8	1.34E-03	3.51E-04	1.43E-03	1.02E-03	1.50E-03
6	1.45E-03	3.90E-04	1.18E-03	1.22E-03	1.34E-03
4	1.65E-03	3.22E-04	1.43E-03	1.37E-03	1.57E-03
2	2.14E-03	1.34E-03	1.35E-03	1.59E-03	1.72E-03

**Table F7.** Data for Figure 6.3

	<b>NaCl</b>	<b>R=0.11</b>	<b>R=0.5</b>	<b>R=1</b>	<b>CaCl<sub>2</sub></b>
<b>Time</b>	<b>As (micro mol/m<sup>2</sup> mineral)</b>				
30	0.000509781	BDL	0.000830764	0.00025711	0.000129669
28	0.000445135	2.33842E-05	0.001342931	0.000248707	0.000731355
26	0.000537121	6.37693E-05	0.00017789	BDL	0.000264524
24	0.000314562	4.88792E-05	0.000189563	0.00070747	0.000191913
22	0.00065899	2.55077E-05	0.000221747	0.000441961	0.000155596
20	0.00064904	3.18783E-05	0.00026912	0.000531017	0.000840277
18	0.00042399	8.9277E-05	0.000266214	0.000470524	0.000394197
16	0.015799966	0.00026359	0.000230877	0.00059824	0.000513496
15.67	0.000814411	0.000199815	0.000238155	0.000761248	0.001042561
15.33	0.000798249	0.000242336	0.000236291	0.001015	0.001203362
15.17	0.001104108	0.000403889	0.000192909	0.001436813	0.000705413
15.08	0.003602273	0.001426398	0.000212096	0.001867028	0.000596486
15.03	0.000810673	0.000905568	0.00014647	0.000611684	0.000632784
14	0.000806953	0.000437904	0.000172268	0.000904092	0.001224113
12	0.00072862	0.000416643	0.000448146	0.001001551	0.00160274
10	0.000889007	0.00051868	0.000719032	0.000919215	0.002017754
8	0.000902694	0.000599457	0.000562341	0.001174651	0.002282296
6	0.001148889	0.000654726	0.000238536	0.001470416	0.003122634
4	0.001146397	0.000858813	0.000207649	0.00245019	0.003573941
2	0.001443569	0.001930226	0.00025619	0.005302264	0.004201592

**Table F8.** Data for Figure 6.5

	<b>298 K, 1 bar</b>	<b>333K, 100 bar</b>
<b>Time</b>	<b>As (micro mol/m<sup>2</sup> mineral)</b>	<b>As (micro mol/m<sup>2</sup> mineral)</b>
30	BDL	0.000352808
28	2.33842E-05	0.00041209
26	6.37693E-05	0.00049017
24	4.88792E-05	0.001610812
22	2.55077E-05	0.000624647
20	3.18783E-05	0.000815513
18	8.9277E-05	0.000600066
16	0.00026359	0.001078681
15.67	0.000199815	0.00124353
15.33	0.000242336	0.001149535
15.17	0.000403889	0.001250748
15.08	0.001426398	0.001519706
15.03	0.000905568	0.001093138
14	0.000437904	0.001609368
12	0.000416643	0.001171214
10	0.00051868	0.001369328
8	0.000599457	0.001694675
6	0.000654726	0.002284665
4	0.000858813	0.003580371
2	0.001930226	0.007114977

**Table F9.** Data for Figure 7.2

<b>7913.8 ft.</b>			<b>7930.1 ft.</b>			<b>10193 ft.</b>		
<b>Time</b>	<b>Fe (ppb)</b>	<b>As (ppb)</b>	<b>Time</b>	<b>Fe (ppb)</b>	<b>As (ppb)</b>	<b>Time</b>	<b>Fe (ppb)</b>	<b>As (ppb)</b>
2	250.00	50.10	2	1500.00	84.50	2	8.83	116.00
4	143.00	49.70	4	1380.00	70.80	4	7.17	73.80
6	139.00	25.20	6	971.00	62.30	6	10.80	59.10
8	114.00	49.00	8	890.00	34.10	8	13.80	53.90
10	124.00	44.50	10	527.00	57.00	10	20.20	47.90
12	203.00	45.40	12	397.00	65.40	12	18.30	43.80
14	105.00	49.20	14	269.00	57.50	14	15.10	44.10
16	186.00	90.90	16	220.00	59.50	16	13.20	42.50
18	88.60	53.00	18	181.00	62.40	18	14.60	40.80
20	138.00	54.20	20	172.00	67.30	20	17.90	41.40
20.5	5760.00	57.00	20.5	38100.00	62.00	20.5	2090.00	73.80
21	3700.00	57.20	21	12600.00	58.20	21	1380.00	61.30
21.5	2400.00	58.50	22	7070.00	67.60	21.5	1190.00	53.40
22	1860.00	59.10	24	4520.00	58.40			
24	1690.00	25.30	26	3270.00	61.10			
26	1190.00	57.00	28	2510.00	26.70			
28	1030.00	57.20	30	1990.00	59.60			
30	878.00	58.90	32	1570.00	59.40			
32	781.00	57.80	34	1320.00	61.60			
34	877.00	62.30	36	1150.00	64.40			
36	850.00	65.50	38	985.00	65.00			
38	674.00	59.40						
40	677.00	62.90						

**Table F10.** Data for Figure 7.4

CO <sub>2</sub>			HCl, pH 3.6		
Time	Fe (ppb)	As (ppb)	Time	Fe (ppb)	As (ppb)
2	1500.00	84.50	2	5.94	113.70
4	1380.00	70.80	4	26.82	BDL
6	971.00	62.30	6	191.10	79.48
8	890.00	34.10	8	346.10	53.77
10	527.00	57.00	10	403.30	56.90
12	397.00	65.40	12	413.90	23.75
14	269.00	57.50	14	418.90	77.21
16	220.00	59.50	16	394.80	BDL
18	181.00	62.40	18	375.30	107.00
20	172.00	67.30	20	319.60	87.40
20.5	38100.00	62.00	20.5	728.10	BDL
21	12600.00	58.20	21	1301.00	58.11
22	7070.00	67.60	21.5	1610.00	52.97
24	4520.00	58.40	22	1837.00	18.35
26	3270.00	61.10	24	2154.00	42.84
28	2510.00	26.70	26	2573.00	39.51
30	1990.00	59.60	28	2192.00	17.49
32	1570.00	59.40	30	2191.00	BDL
34	1320.00	61.60	32	2119.00	85.31
36	1150.00	64.40	34	2037.00	33.54
38	985.00	65.00	36	1946.00	34.87
			38	1807.00	BDL
			40	1717.00	21.66